THE FLUKA RADIATION TRANSPORT CODE AND ITS USE FOR SPACE PROBLEMS

1st International Workshop on Space Radiation Research
and
11th Annual NASA Space Radiation Health Investigators' Workshop

Alfredo Ferrari, Paola R. Sala

CERN, Geneva Switzerland (on leave from INFN-Milan)

Topics

- Generalities about FLUKA
- Reliability of calculation of particle production and transport in FLUKA:
  - Thin target benchmarks
  - Thick target benchmarks
  - More complex shielding benchmarks
- The production of fragments nuclei: the ultimate problem of hadron reaction modelling
- Cosmic rays and FLUKA: the atmospheric neutrino calculations:
  - The primary fluxes and the geomagnetic effects
  - Benchmarking FLUKA against measured data in the atmosphere
- Extending FLUKA to ions transport and interactions
- Conclusions

FLUKA: a long history

The beginning of the FLUKA *history is back to 1964 when Johannes Ranft started to develop MonteCarlo codes for high energy beams, as required at CERN for many accelerator related tasks.*

The name FLUKA *came around 1970, when first attempts were made to predict calorimeter fluctuations on an event-by-event basis (FLUKA = FLUctuating KASkades).*

The present code is mostly an effort of researchers of INFN-Milan (now at CERN) started in 1990, and has little or no remnants of older versions. The main link with the past is Johannes Ranft, mostly in the development of the high energy generator part.

The code is huge ($\approx 350,000$ lines of fortran code) and has the ability to treat with good accuracy a variety of problems.

It is a "private" effort, it has no official distribution and is in continuos evolution. It has been always meant as a tool where new ideas and models for radiation interactions and transport can be developed and tested rather than as general user tool. There is no "official" CERN support for it, even though presently A. Ferrari and P.R. Sala are CERN staff. The only "official" status is that it is the MonteCarlo of the ICARUS/ICANOE experiments, as well as for the spallation part of the Energy Amplifier studies (all activities chaired by C. Rubbia).

The code is in wide use at CERN and in other labs, and is THE tool used for all radiation calculations and for the neutrino beam studies at CERN.

FLUKA

Authors: **A. Fassò[†], A. Ferrari[&], J. Ranft[*], P.R. Sala[&]**
[†] SLAC , [&] INFN Milan and CERN, [*] Siegen University

Interaction and transport MonteCarlo code

- Hadron-hadron and hadron-nucleus interactions 0-100 TeV
- Nucleus-nucleus interactions 0-10000 TeV/n: *under development !!!*
- Electromagnetic and μ interactions 1 keV-100 TeV
- Charged particle transport - ionization energy loss
- Neutron multigroup transport and interactions 0-20 MeV
- Analogue or biased calculations

Structure: a fully integrated code

Four major radiation components:

- Hadrons (and now ions!)
- Muons
- Electrons and photons
- Low energy neutrons

FLUKA can deal with all components in a single run, without any interface between components.

It is not an assembly of different codes. All the secondaries issued from the same primary are transported before a new history is started.
Correlations are preserved as far as possible, also between different radiation components.

Memory for geometry, tables, etc. is dynamically allocated.

A multipurpose code

The program has been used successfully in different fields such as shielding, dosimetry, high energy experimental physics and engineering, cosmic ray studies, medical physics, etc.

- Each radiation component is treated as far as possible with the same level of accuracy
  (it's like having 4 different programs in one, for pure neutron, electron-photon or muon problems – and hadrons, of course!)
- FLUKA can be run in fully analog mode, for calorimetry. It can calculate coincidences and anticoincidences
- It can also be run in biased mode, for shielding design

  But also experimental high energy physicists need sometimes to make studies of deep penetration or rare events: hadron punchthrough, radiation background in underground experiments, muon production over short decay lengths

Energy limits

Approximate values

PARTICLES	transport limits	limits for primary particles
charged hadrons	1 keV – 20 TeV	100 keV – 20 TeV
neutrons	thermal – 20 TeV	thermal – 20 TeV
antineutrons	50 MeV – 20 TeV	100 MeV – 20 TeV
muons	1 keV – 1000 TeV	100 keV – 1000 TeV
electrons	1 keV – 1000 TeV	70 keV – 1000 TeV *(low-Z)*
		150 keV – 1000 TeV *(high-Z)*
photons	1 keV – 1000 TeV	7 keV – 1000 TeV
neutrinos (with NUX)	100 keV – 1 TeV	1 MeV – 400 GeV

The FLUKA hadron interaction models

Two models are used inside FLUKA to describe nonelastic interactions

- The "low-intermediate" energy one, PEANUT, which covers the energy range up to 5 GeV
- The high energy one which can be used up to several tens of TeV

The nuclear physics embedded in the two models is very much the same. The main differences are a coarser nuclear description (and no preequilibrium stage) for the high energy one, and the Gribov-Glauber cascade for the high energy one.

In the following the description will mostly concentrate on PEANUT PEANUT is a three step model:

1. (Generalized) IntraNuclear Cascade
2. Preequilibrium
3. Evaporation/Fission or Fermi break-up

(Generalized) IntraNuclear Cascade basic assumptions

1. Interaction probability from σ_{free} + Fermi motion $\times$ $\rho(r)$
2. Classical trajectories $(+)$ nuclear mean potential (resonant for π's!!)
3. Curvature from nuclear potential $\rightarrow$ refraction and reflection.
4. Interactions in projectile–target nucleon CMS $\rightarrow$ Lorentz boosts
5. Interactions are incoherent and uncorrelated
6. Multibody absorption for π, μ^-, K^-
7. Quantum effects
8. Glauber cascade at high energies
9. Secondaries treated $=$ primary
10. Exact conservation of energy, momenta and all additive quantum numbers, including nuclear recoil

Quantistic effects in (G)INC

1. Pauli blocking,
2. Formation time (inelastic),
3. Coherence length ((quasi)-elastic and charge exchange),
4. Nucleon antisymmetrization,
5. Hard core nucleon correlations

"Coherence length"

Coherence length $\equiv$ formation time for elastic or quasielastic interactions.

Given a two body interaction between with four-momentum transfer

$$q = p_{1i} - p_{1f}$$

the energy transfer seen in a frame where the particle 2 is at rest is given by

$$\Delta E_2 = \nu_2 = \frac{q \cdot p_{2i}}{m_2} \tag{1}$$

From the uncertainty principle this ΔE corresponds to a indetermination in proper time given by $\Delta\tau \cdot \Delta E_2 = \hbar$, that boosted to the lab frames gives a coherence length

$$\Delta x_{lab} = \frac{p_{2lab}}{m_2} \cdot \Delta\tau = \frac{p_{2lab}}{m_2}\frac{\hbar}{\nu_2} \tag{2}$$

And analogue for particle 1

Applied also to $\nu - h$ interactions

Formation Zone

Naively: "materialization" time. Qualitative estimate: in the frame where $p_{\|} = 0$

$$\bar{t} = \Delta t \approx \frac{\hbar}{E_T} = \frac{\hbar}{\sqrt{p_T^2 + M^2}} \tag{3}$$

particle proper time

$$\tau = \frac{M}{E_T}\bar{t} = \frac{\hbar M}{p_T^2 + M^2} \tag{4}$$

$$\tag{5}$$

Going to lab system

$$t_{lab} = \frac{E_{lab}}{E_T}\bar{t} = \frac{E_{lab}}{M}\tau = \frac{\hbar E_{lab}}{p_T^2 + M^2}$$

As a function of particle rapidity y

$$t_{lab} = \bar{t}\cosh y = \frac{\hbar}{\sqrt{p_T^2 + M^2}}\cosh y$$

Condition for possible reinteraction inside a nucleus:

$$v \cdot t \leq R_A \approx r_0 A^{\frac{1}{3}}$$

Preequilibrium : GDH

Preequilibrium emission probability:

$$P_{x,n}(\epsilon)d\epsilon = \sum n_{p_x} \frac{\rho_n(U,\epsilon) g d\epsilon}{\rho_n(E)} \frac{r_c(\epsilon)}{r_c(\epsilon) + r_+(\epsilon)}$$

where the density (MeV^{-1}) of exciton states is given by:

$$\rho_n(E) = \frac{g(gE)^{n-1}}{n!(n-1)!}$$

the emission rate in the continuum:

$$r_c = \sigma_{inv} \frac{\epsilon}{g_x} \frac{(2s+1)\, 8\pi m}{h^3}$$

and the reinteraction rate:

$$r_+(\epsilon) = f_{Pauli}(\epsilon, E_F) \left[\rho_p \sigma_{xp} + \rho_n \sigma_{xn}\right] \left[\frac{2(\epsilon + V)}{m}\right]^{1/2}$$

$$(or\ from\ optical\ potential)$$

GDH: ρ,E_F are "local" averages on the trajectory and constrained exciton state densities are used for the lowest lying exciton configurations.

Preequilibrium: modified GDH in PEANUT

- σ_{inv} from systematics
- Correlation/formation zone / hardcore effect on reinteractions:

$$\frac{r_c(\epsilon)}{r_c(\epsilon)+r_+(\epsilon)} \rightarrow P_c^{(h\tau)} + P_c^{(co)} + P_c^{(std)}$$

$$\begin{aligned} P_c^{(h\tau)} &= escape\ prob.\ in\ zone\ = max(\tau, hardcore) \equiv h\tau \\ P_c^{(co)} &= escape/total\ prob.\ in\ zone\ = (correlation\ -\ h\tau) \\ & \quad (here\ reinteraction\ only\ on\ \mathrm{non}-correlated\ nucleon\ specie\ ) \\ P_c^{(std)} &= \text{"}standard\text{"}\ escape/total\ in\ remaining\ zone. \end{aligned}$$

- Constrained exciton state densities configurations 1p-1h, 2p-1h, 1p-2h, 2p-2h, 3p-1h and 3p-2h

Preequilibrium: modified GDH in PEANUT

- Energy dependent form for g_x
- Position dependent parameters = point like values :
  - first step : n_h holes generated in the INC step at positions $\vec{x}_i$:

$$\rho^{loc}_{n_h} = \frac{\Sigma_{i=1}^{n_h} \rho(\vec{x}_i)}{n_h} \qquad E^{loc}_{F\ n_h} = \frac{\Sigma_{i=1}^{n_h} E_F(\vec{x}_i)}{n_h}$$

  - When looking at reinteraction: consider neighborhood:

$$\rho^{nei}_{n_h} = \frac{n_h \rho^{loc}_{n_h} + \rho^{ave}}{n_h + 1} \qquad E^{nei}_{F\ n_h} = \frac{n_h E^{loc}_{F\ n_h} + E^{ave}_F}{n_h + 1}$$

  - Subsequent steps: go towards *ave*rage quantities

$$\rho^{loc}_{n_h+1} = \rho^{nei}_{n_h} \qquad E^{loc}_{F\ n_h+1} = E^{nei}_{F\ n_h}$$

Preequilibrium/(G)INC transition

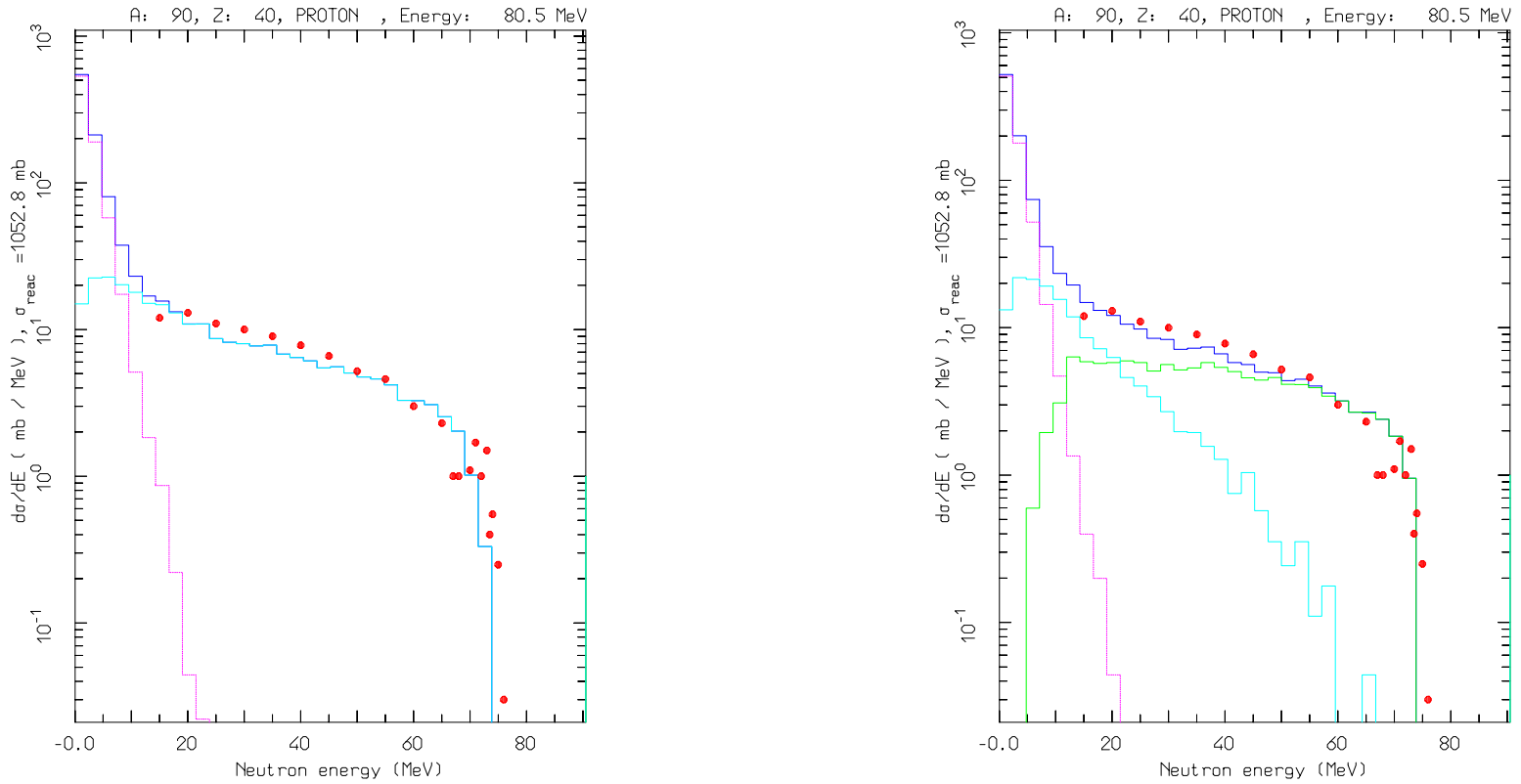

Example of angle integrated ^{90}Zr(p,xn) at 80.5 MeV calculations with the full algorithm (right), and without the INC stage (left). The various lines show the total, INC, preeq. and evaporation contributions, the exp. data have been taken from M.Trabandt et al. **PRC39** (1989) 452

Nucleon emission: thin target examples I

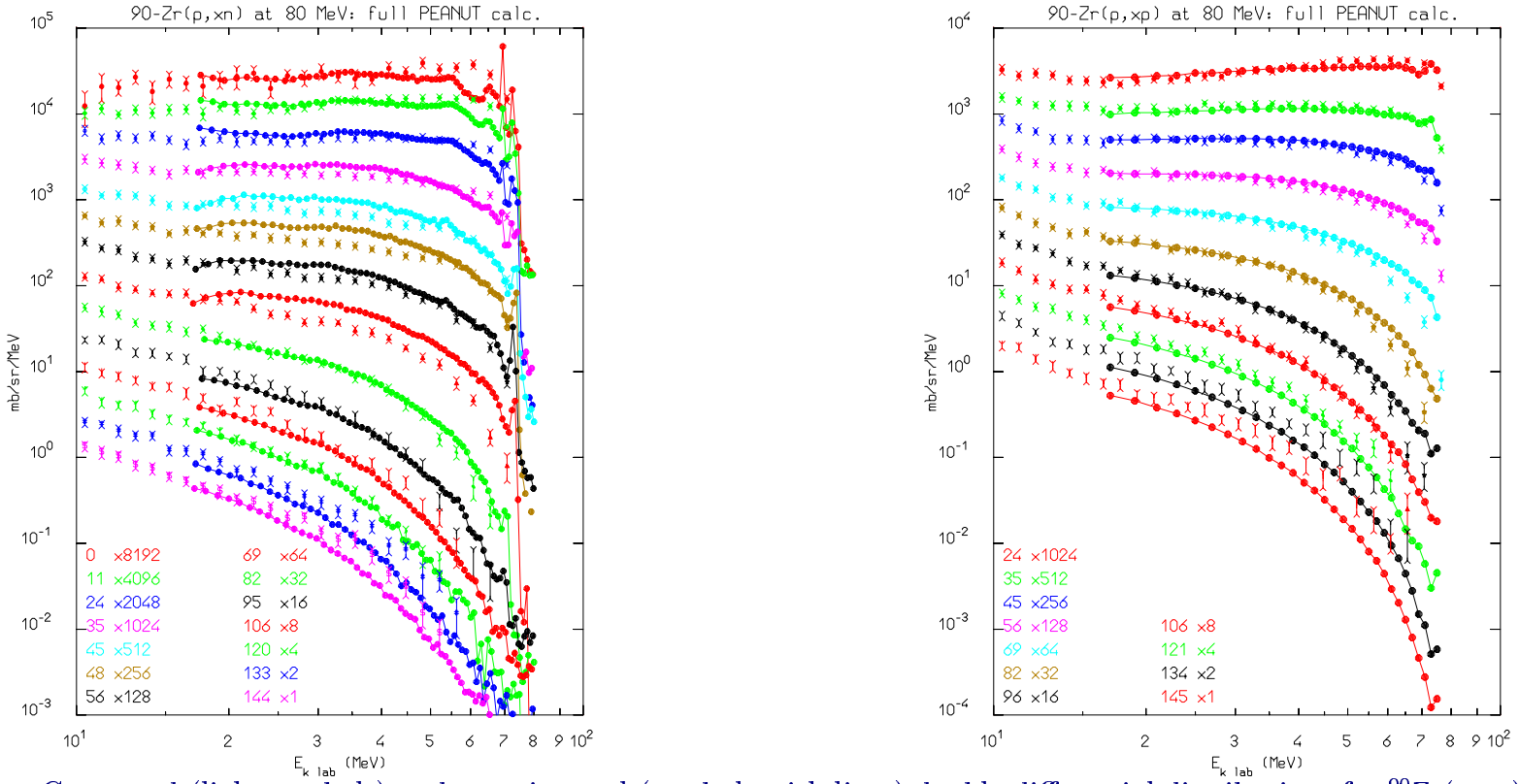

Computed (light symbols) and experimental (symbols with lines) double differential distributions for ^{90}Zr(p,xn) (left) and ^{90}Zr(p,xp) at 80.5 MeV. The exp. data have been taken from M.Trabandt et al. **PRC39** (1989) 452 and A.A. Cowley et al., **PRC43**, (1991) 678

Nucleon emission: thin target examples II

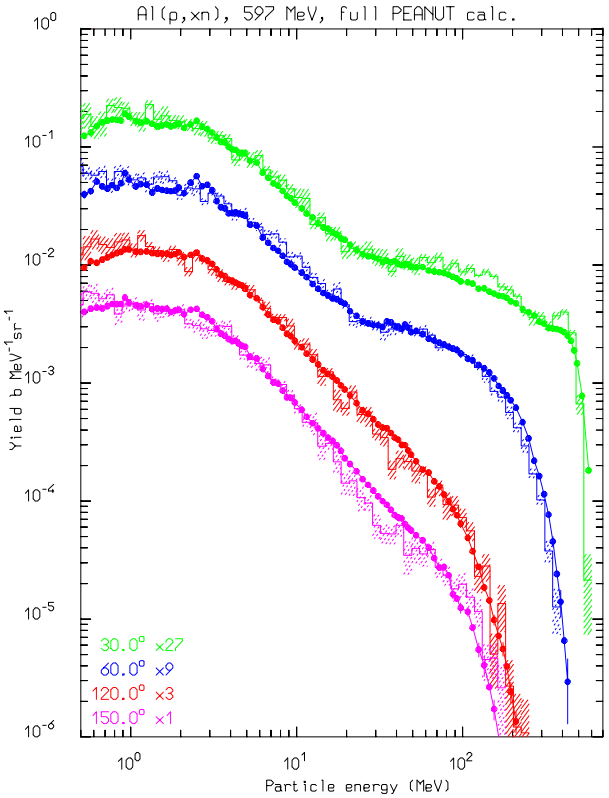

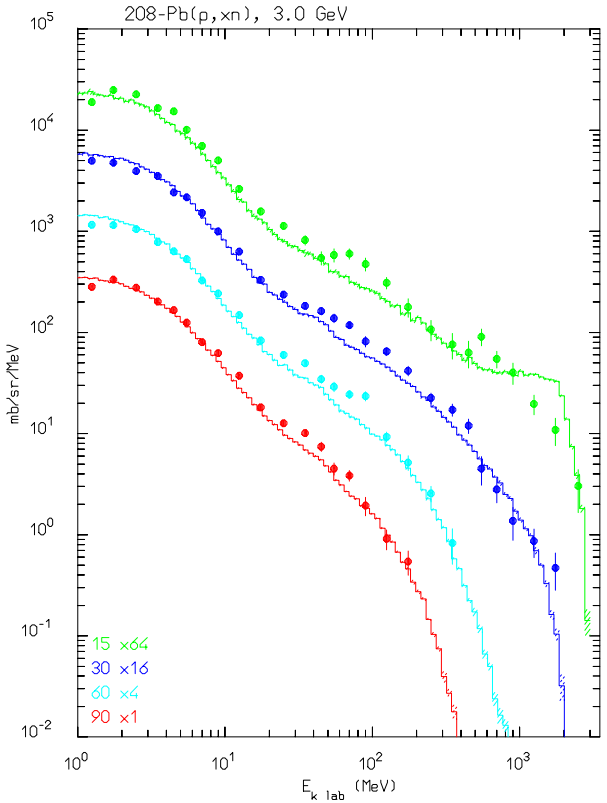

Computed (histograms) and experimental (symbols) double differential neutron distributions for Alr(p,xn) (left) at 597 MeV and Pb(p,xn) at 3 GeV. The exp. data have been taken from W.B. Amian et al., Nucl. Sci. Eng. **115**, (1993) 1, and K. Ishibashi et al, Nucl. Sci. Technol. **32** (1995) 827.

Pion interactions in nuclei

The description of pion interactions on nuclei in the sub-GeV energy range must take into account:

- The resonant nature of the $\pi - N$ interaction, mostly dominated by the $\Delta(1232)$.
- The effect of the nuclear medium on the $\pi - N$ interaction
- The possibility of absorption (both s-wave and p-wave) on two or more nucleons
- The resonant nature of the pion-nucleus potential, which is rapidly varying with the pion energy

Microscopic pion absorption cross sections

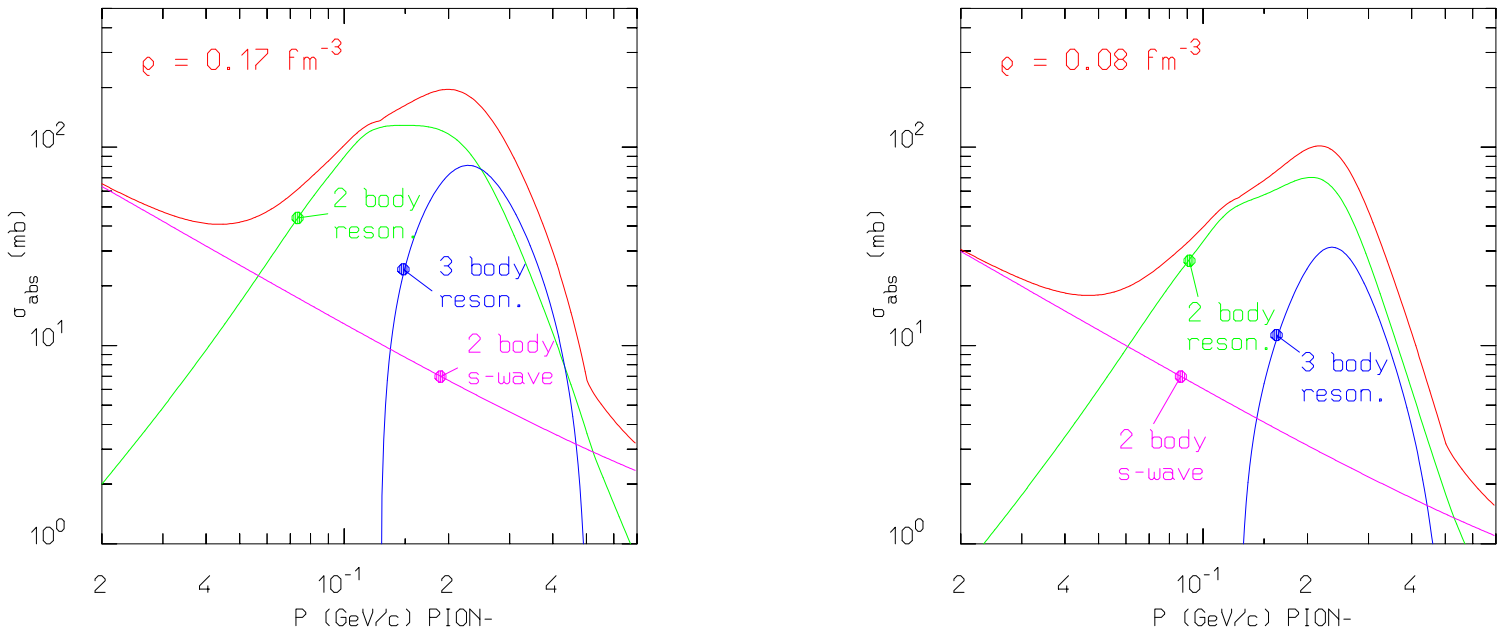

Charged pion absorption cross section for infinite symmetric nuclear matter at two different density values ($\lambda_{abs}^{-1} = \sigma_{abs} \cdot \frac{1}{2}\rho = \sigma_{abs} \cdot \rho_{pro} = \sigma_{abs} \cdot \rho_{neu}$)

Pion absorption cross sections: examples

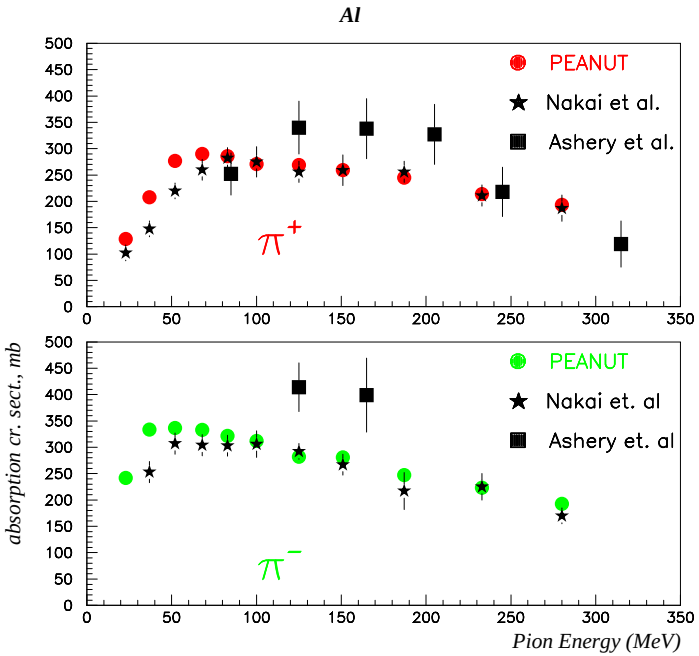

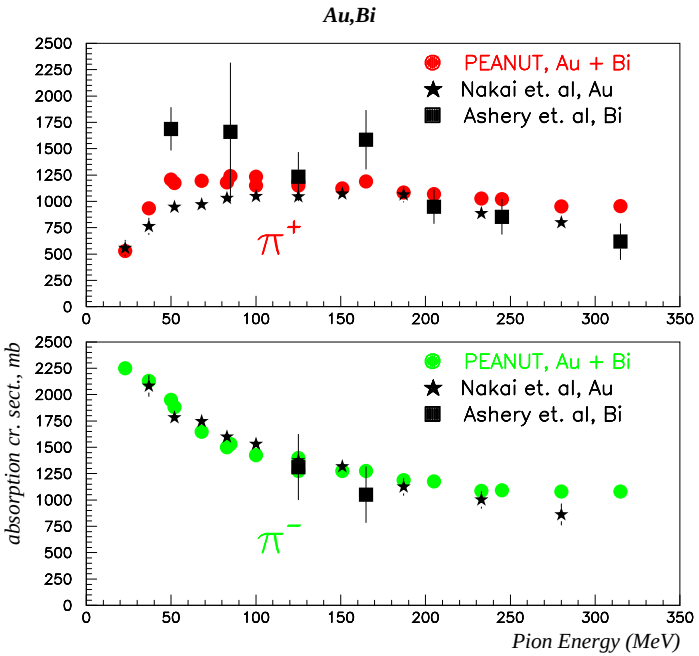

Computed and exp. pion absorption cross section on Aluminum as a function of energy

Computed and exp. pion absorption cross section on Gold or Bismuth as a function of energy

(Exp. data: D. Ashery et al., **PRC23**, (1981) 2173 and K. Nakai et. al., **PRL44**, (1979) 1446)

Pion interactions: examples

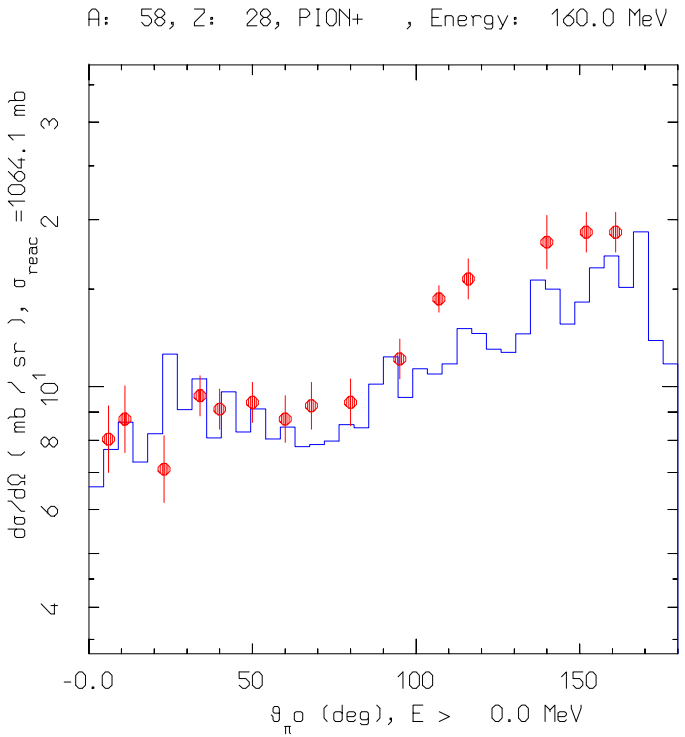

Computed and exp. pion charge exchange angular distribution for ^{58}Ni(π^+, π^0) at 160 MeV

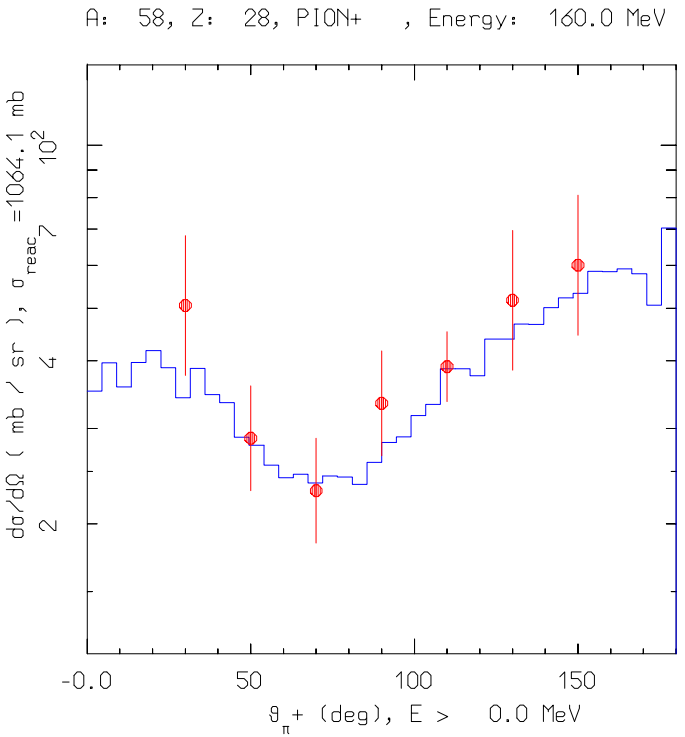

Computed and exp. pion inelastic angular distribution for ^{58}Ni$(\pi^+, \pi^{+\prime})$ at 160 MeV

(Exp. data: W.J. Burger et al., **PRC41**, (1990) 2215, R.D. McKeown et al.,**PRC24**, (1981) 211

Nonelastic hN interactions at intermediate energies

For energies in excess of few hundreds MeV the inelastic channels (pion production channels) start to play a major role.

- $N_1 + N_2 \rightarrow N_1' + N_2' + \pi$ has its threshold around 290 MeV, and it starts to be important around 700,
- $\pi + N \rightarrow \pi' + \pi'' + N'$ opens at 170 MeV.
- Dominance of the Δ resonance and of the N^* resonances at higher energies, in the π N channel $\rightarrow$ reactions treated in the framework of the isobar model $\rightarrow$ all reactions proceed through an intermediate state containing at least one resonance.

N-N nonelastic interactions at intermediate energies

Examples of N-N nonelastic interactions:

$$N_1 + N_2 \rightarrow N_1' + \Delta(1232) \rightarrow N_1' + N_2' + \pi$$
$$N_1 + N_2 \rightarrow N_1' + N^*(1440) \rightarrow N_1' + N_2' + \pi$$

where the $N^*(1440)$ is a T(J^P)=$\frac{1}{2}\left(\frac{1}{2}^+\right)$ baryon resonance with sizeable decay channels into one or two pions plus one nucleon.

π-N Nonelastic interactions at intermediate energies

Possibility of direct production of s-channel resonances (that is π N going into one resonance, like the Δ), which are not possible in the N N system since no dibaryon resonance has ever been discovered.

Examples:

$$\begin{aligned}
\pi + N &\rightarrow N^*(1440) \rightarrow \rho(770) + N' \rightarrow \pi' + \pi'' + N' \\
\pi + N &\rightarrow \Delta(1600) \rightarrow \pi' + \Delta(1232) \rightarrow \pi' + \pi'' + N' \\
\pi + N &\rightarrow \rho(770) + N' \rightarrow \pi' + \pi'' + N' \\
\pi + N &\rightarrow \pi' + \Delta(1232) \rightarrow \pi' + \pi'' + N'
\end{aligned}$$

where the first two reactions are examples of s-channel direct resonance production. $\rho(770)$ is a T(J^P)=1 (1^+) meson resonance with 100% decay branching into $\pi\pi$.

Multiple pion production at intermediate energies

The isobar model easily accommodates multiple pion production, for example allowing the presence of more than one resonance in the intermediate state (double pion production opens already at 600 MeV in nucleon-nucleon reactions, and at about 350 MeV in pion-nucleon ones).

Examples of two pion production for $N - N$:

$$N_1 + N_2 \rightarrow \Delta_1(1232) + \Delta_2(1232) \rightarrow N_1' + \pi_1 + N_2' + \pi_2$$
$$N_1 + N_2 \rightarrow N_1' + N^*(1440) \rightarrow N_1' + \pi_1 + \Delta(1232) \rightarrow N_1' + \pi_1 + N_2' + \pi_2$$
$$N_1 + N_2 \rightarrow N_1' + \Delta(1600) \rightarrow N_1' + \pi_1 + N^*(1440) \rightarrow N_1' + \pi_1 + N_2' + \pi_2$$

and for pion-nucleon:

$$\begin{aligned} \pi + N &\rightarrow \Delta(1600) \rightarrow \pi' + N^*(1440) \rightarrow \pi' + \pi'' + \Delta(1232) \\ &\rightarrow \pi' + \pi'' + \pi''' + N' \\ \pi + N &\rightarrow \omega(782) + N' \rightarrow \pi' + \pi'' + \pi''' + N' \\ \pi + N &\rightarrow \rho(770) + \Delta(1232) \rightarrow \pi' + \pi''' + \pi'' + N' \end{aligned}$$

Pion production at intermediate energies: summary

Summarizing, all reactions can be thought to proceed through channels like:

$$h + N \rightarrow X \rightarrow x_1 + ... + x_n \quad (6)$$

$$h + N \rightarrow X + Y \rightarrow x_1 + ... + x_n + y_1 + ... + y_m \quad (7)$$

where X and Y can be real resonances, or stable particles (n, p, π) directly.

Resonances which appear in the intermediate states can be treated as real particles, that is, in a MonteCarlo code they can be transported and then transformed into secondaries according to their lifetimes and decay branching ratios.

Reactions described by eq. 6 are examples of s-channel direct resonance production $\rightarrow$ **bumps** in the corresponding isospin cross section around the centre-of-mass energy corresponding to the resonance mass.

The reactions proceeding like in 7, due to the presence of two particles in the intermediate state with the associated extra degree of freedom of their relative motion, do not exhibit a resonant behaviour, but rather a relatively fast increase starting from a centre-of-mass energy, $\sqrt{s} \approx M_X + M_Y$, followed by a smooth behaviour. $N\ N$ reactions are all of this latter type and therefore no resonant structure can be find in $N\ N$ cross sections.

Nonelastic interactions at intermediate energies: Δ mass distribution

The actual Δ mass distribution can be represented by:

$$P(M_\Delta^2)\mathrm{d}M_\Delta^2 \propto \frac{\Gamma(k_\pi)M_0}{(M_\Delta^2 - M_0^2) + \Gamma^2(k_\pi)M_0^2}\frac{k_{\Delta cms}}{k_{\Delta max}}\mathrm{d}M_\Delta^2$$

$$\Gamma(k_\pi) = \Gamma_0\left(\frac{k_{\pi\Delta}}{k_{\pi 0}}\right)^3 \frac{1 + (0.83k_{\pi\Delta})^2 + (0.62k_{\pi\Delta})^4}{1 + (0.83k_{\pi 0})^2 + (0.62k_{\pi 0})^4}$$

Suitable momentum dependent widths have been implemented also for all other baryon and meson resonances, following general rules.

Nonelastic interactions at intermediate energies: examples

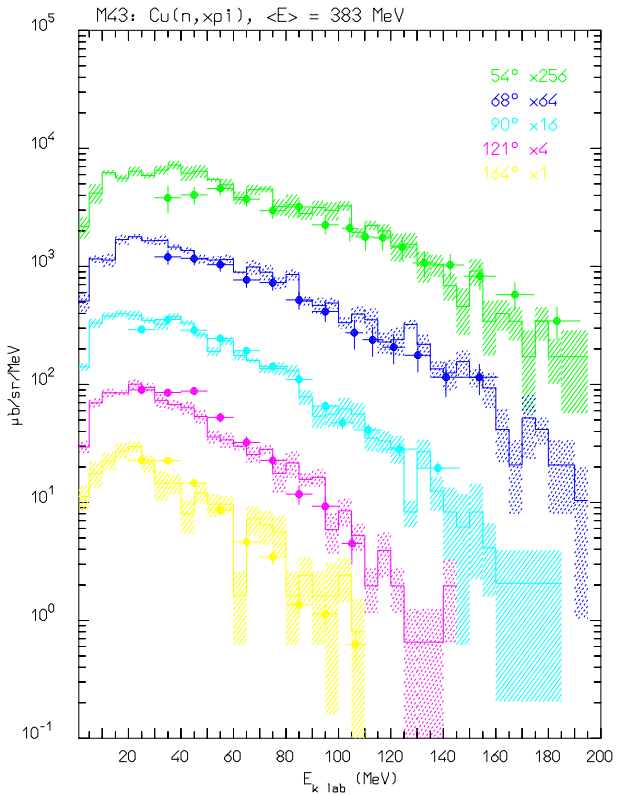

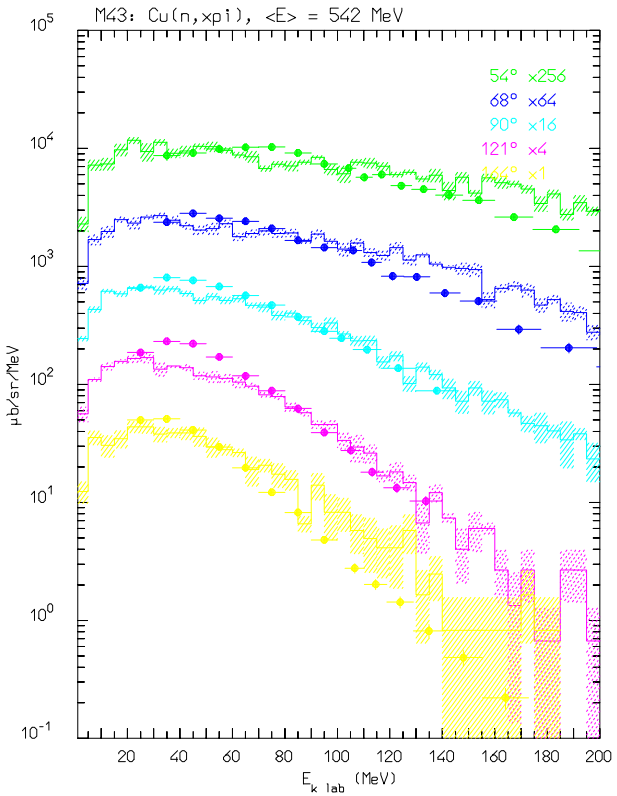

Double differential distributions of charged pions produced by neutrons of $< E_n >$=383 (left) and 542 MeV (right). Exp. data have been taken from Buchle et al. **NPA515**, (1990) 541

Nonelastic interactions at intermediate energies: examples II

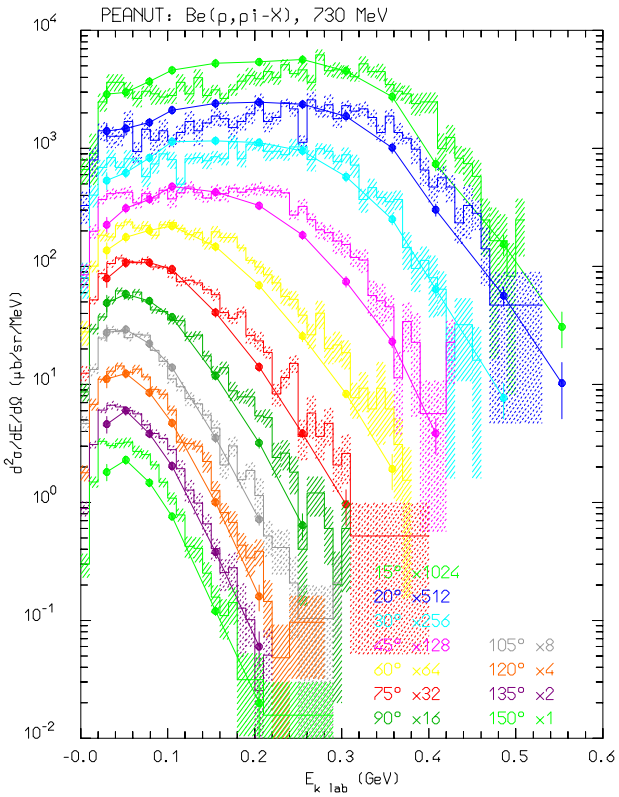

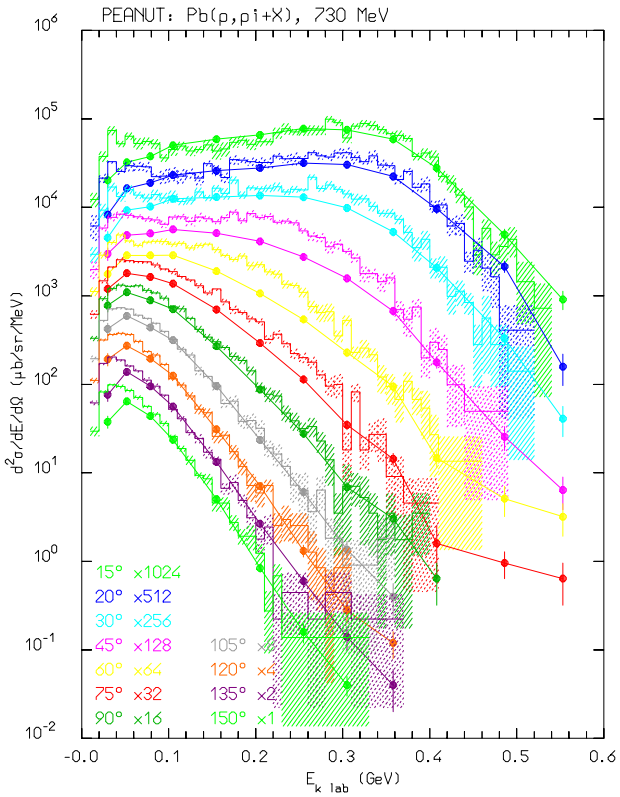

Double differential distributions of pions produced by 730 MeV protons. π^-'s from Be (left) and π^+ frpm Pb (right). Exp. data (symbols) have been taken from D.R.F. Cochran et al., **PRD6**, (1972)

Nonelastic interactions at intermediate energies: examples III

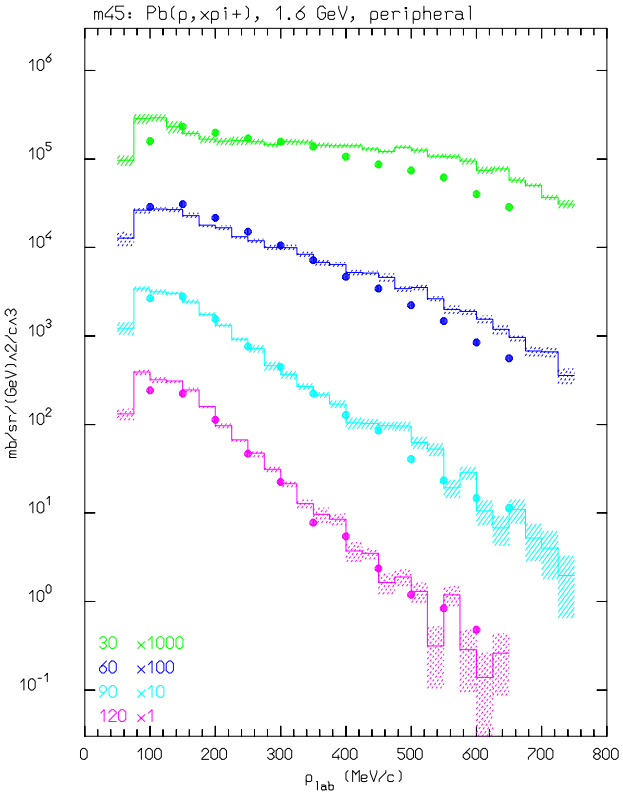

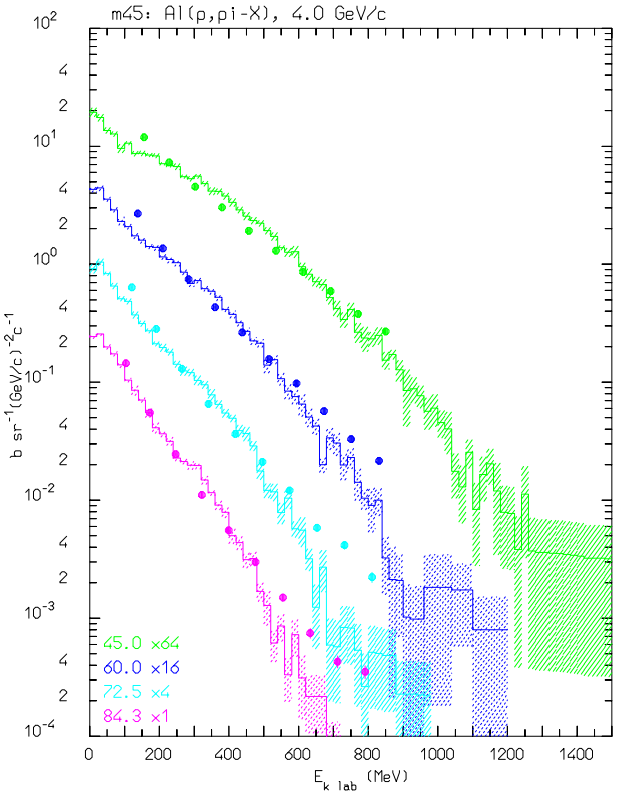

Double differential distributions of π^+'s produced by 1.6 GeV protons on Pb (left, exp. data from M.C.Lemaire et. al., CEA-N-2670) and π^- produced by 4 GeV/c protons on Al (right, exp data from H. En'yo et al, PL 159B, 1 (1985)).

Nonelastic hN interactions at high energies

Above a few GeV a DPM based model is used for the description of individual hN interactions. The model includes:

- main chain diagrams for all combinations of h-h. Well tested up to strange meson/(anti)baryons, not really for charm
- Diffraction including low mass diffraction to individual resonances
- Chain hadronization with p_t and mass effects particularly tuned for (relatively) low mass quark chains

Nonelastic hN interactions at high energies: examples

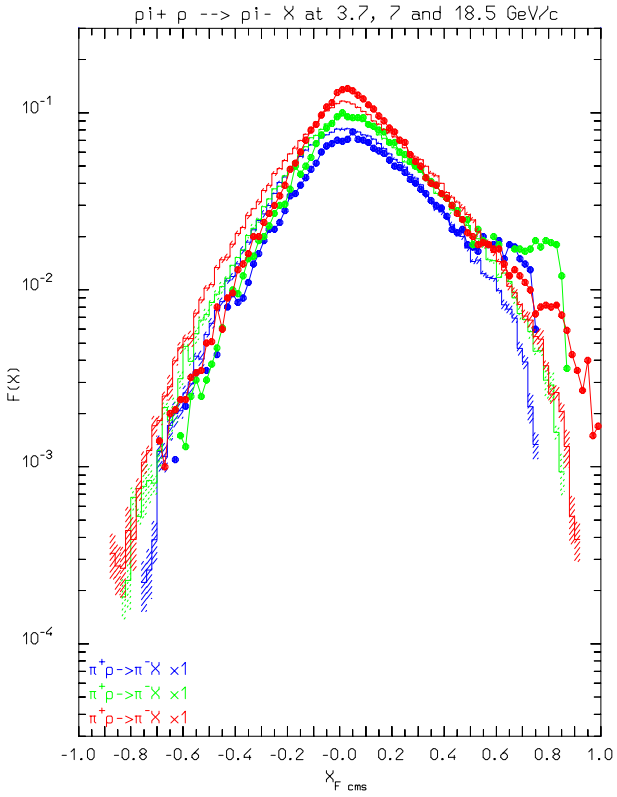

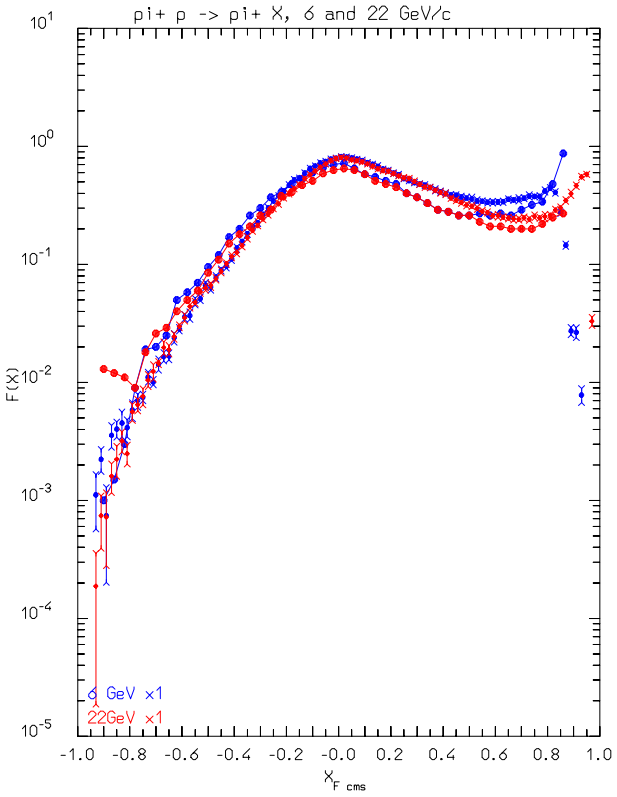

Invariant cross section spectra, as a function of Feynman x_F^* of negative (left), and positive (right) pions emitted for π^+ on protons at various momenta. Data from M.E Law et al. LBL80 (1972).

Nonelastic hN interactions at high energies: examples II

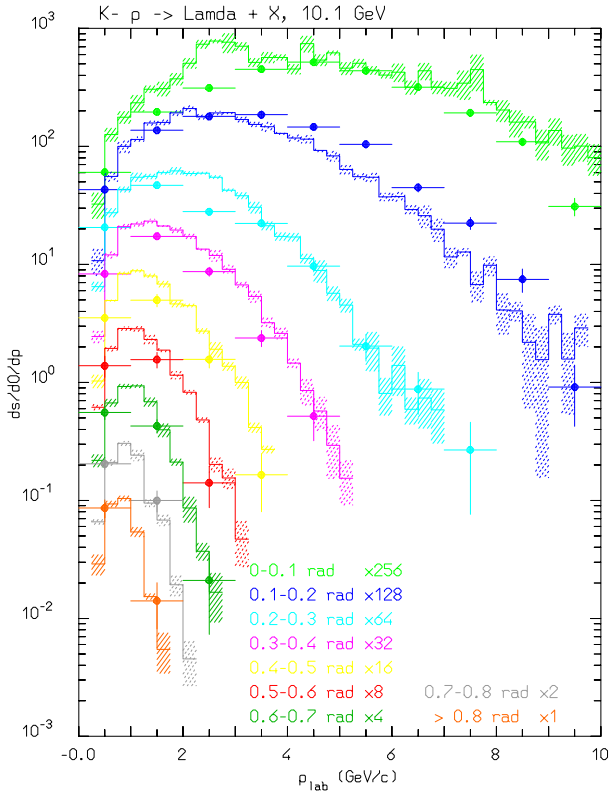

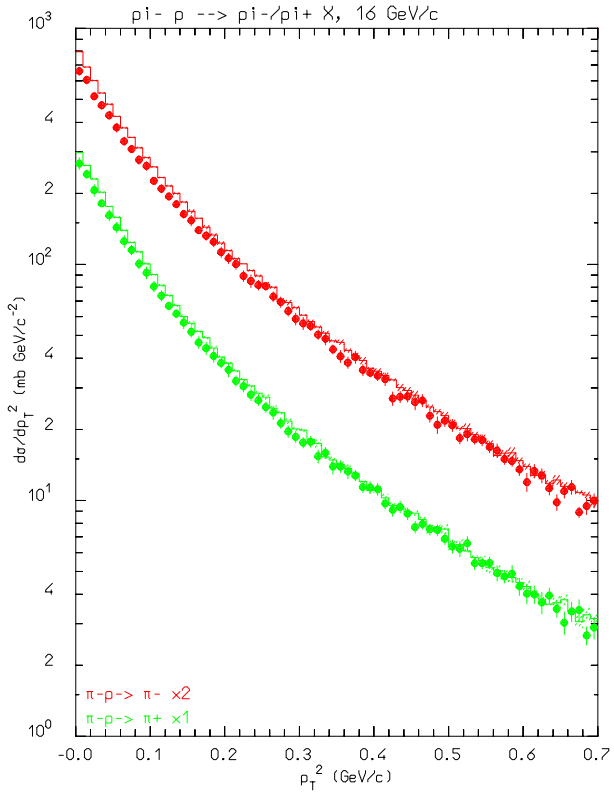

Double differential cross section for $K^- p \to \Lambda X$ at 10 GeV/c (left), p_T spectra of π^+ and π^- produced by 16 GeV/c π^- incident on an hydrogen target. Data from M.E Law et al. LBL80 (1972).

Nonelastic hN interactions at high energies: examples III

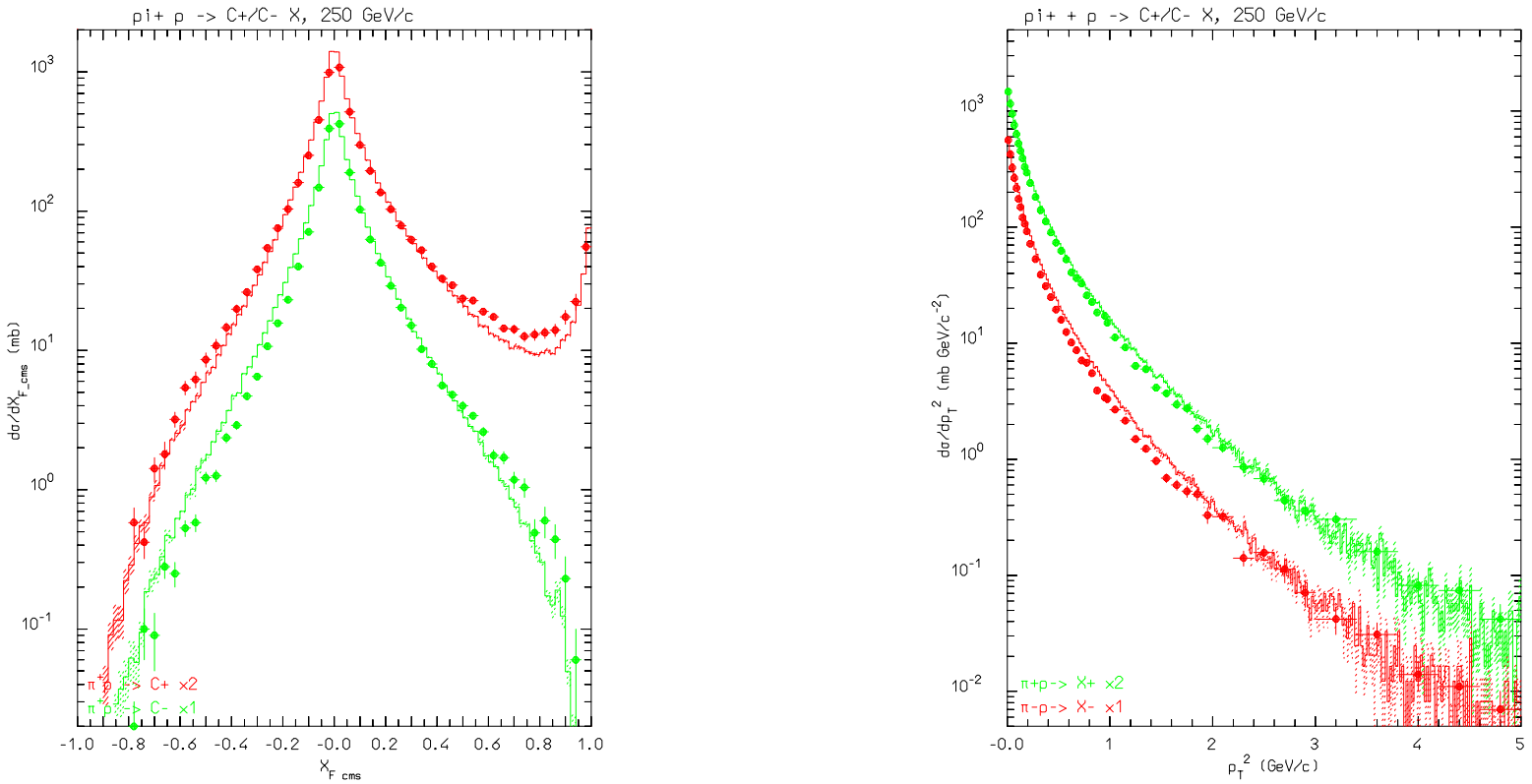

Feynman x_F^* (left) and p_t (right) spectra of positive particles and π^- produced by 250 GeV/c π^+ incident on an hydrogen target. Exp. data (symbols) have been taken from M. Adamus et al. ZPC39, 311 (1988).

Nonelastic hA interactions at high energies: examples

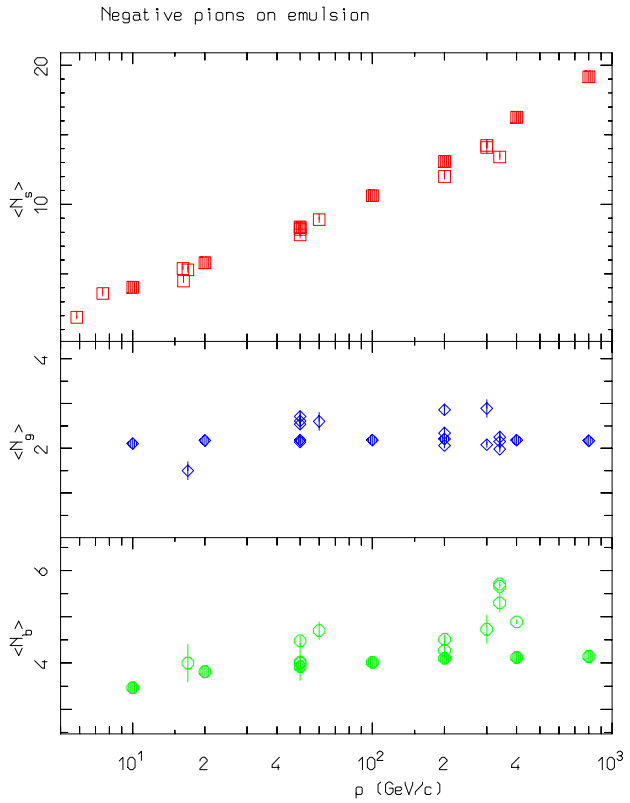

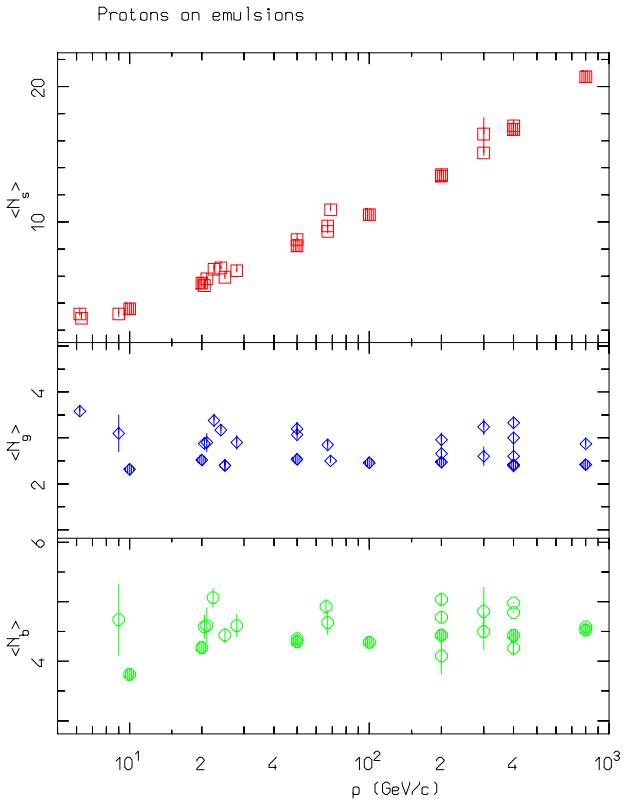

Shower, grey, and black tracks multiplicities for π^- (left) and protons (right) incident on emulsion, as a function of the projectile momentum. Open symbols are experimental data from various sources, full symbols are FLUKA results.

Nonelastic hA interactions at high energies: examples II

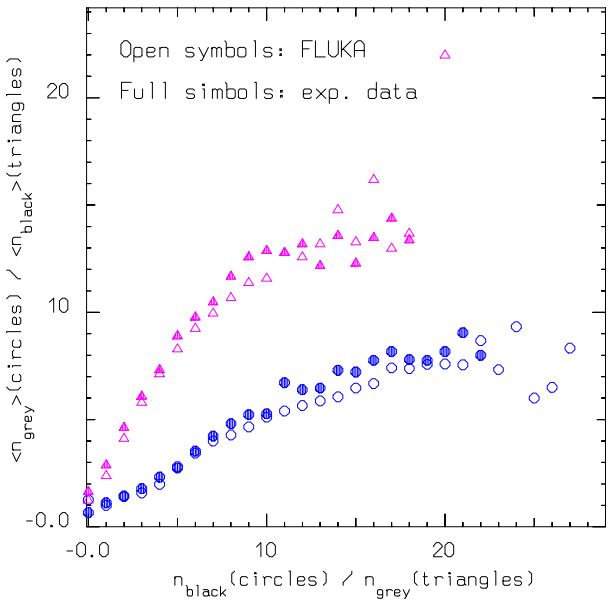

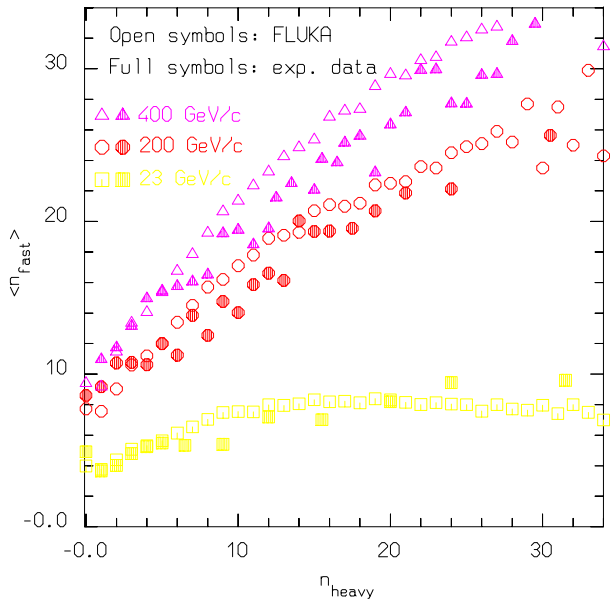

Correlation between the number of heavy prongs and fast particle multiplicity for protons on emulsion at various momenta, and mutual correlations ($< n_g >$ vs n_b and $< n_b >$ vs n_g) between black and grey charged tracks for 400 GeV/c p on emulsion. Open symbols are experimental data from various sources, full symbols are FLUKA results.

Nonelastic hA interactions at high energies: examples III

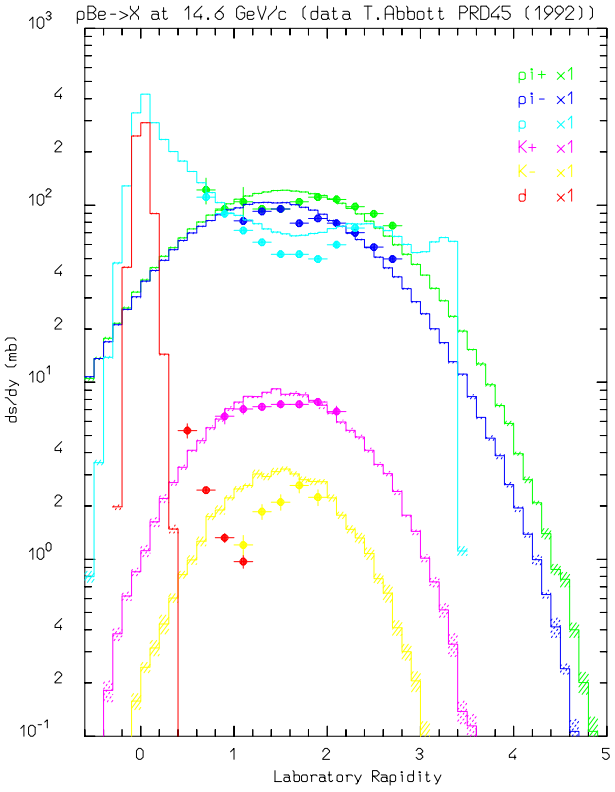

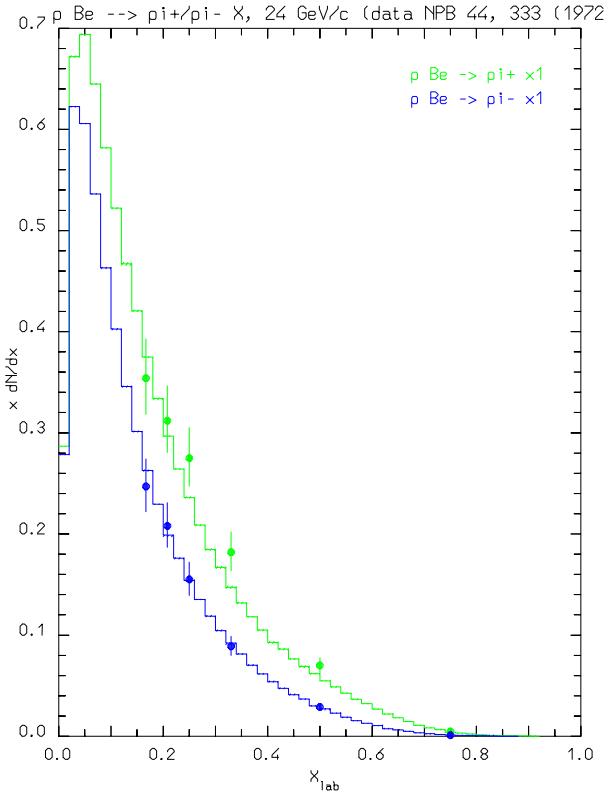

Rapidity distribution of $pi^{+/-}$, $K^{+/-}$, protons and deuterons for 14.6 GeV/c protons on Be (left, data from T.Abbott et al PRD45(11), 3906 1992), and X_{lab} distribution for $pi^{+/-}$ for 24 GeV/c protons on Be (right, symbols extrapolated from the DDCS reported in T.Eichten et al. NPB 44, 333 (1972)).

Nonelastic hA interactions at high energies: examples IV

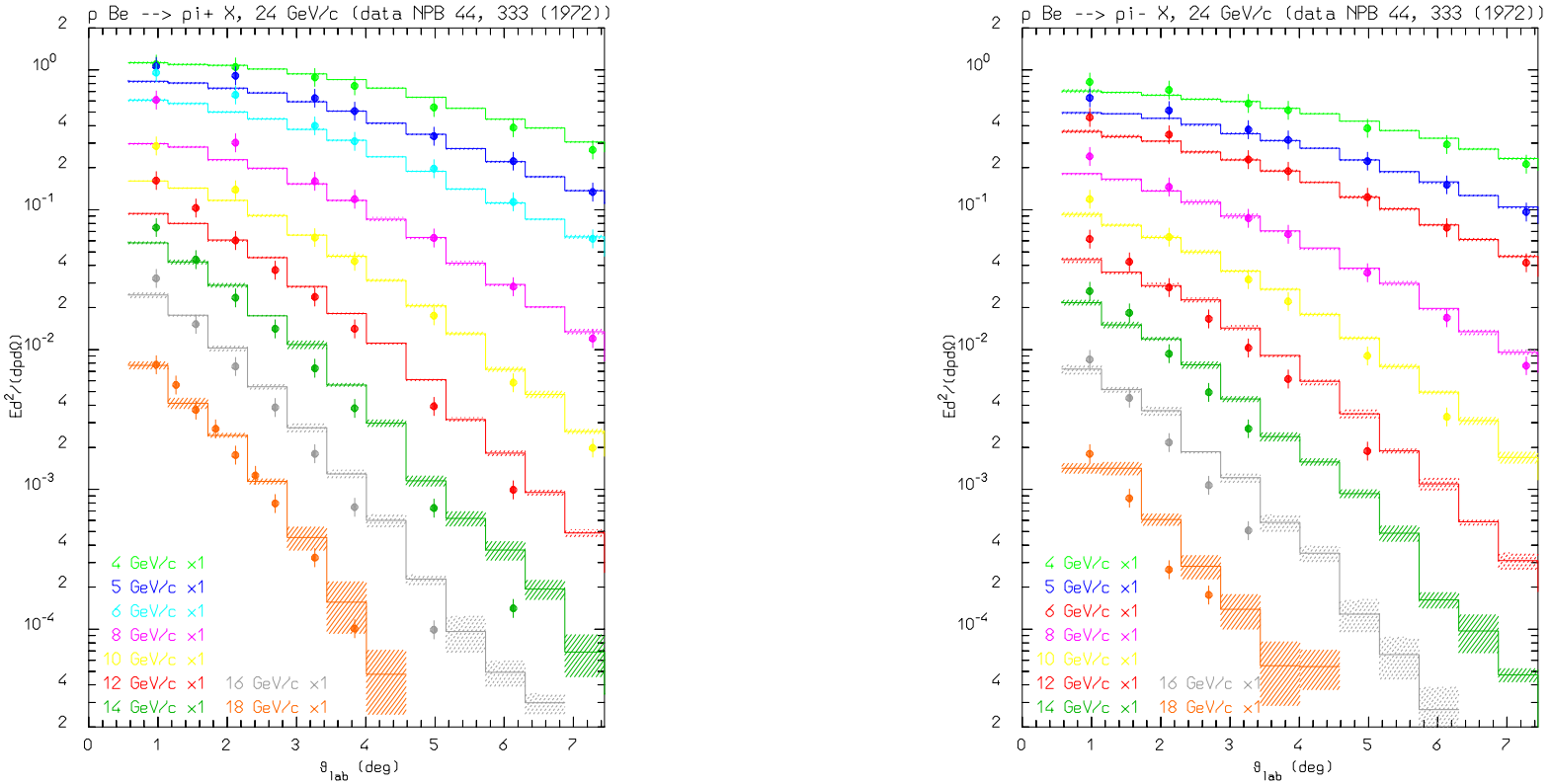

Invariant cross section distribution for pi^+ (left) and π^- for 24 GeV/c protons on Be (data from T.Eichten et al. NPB 44, 333 (1972)).

Nonelastic hA interactions at high energies: examples V

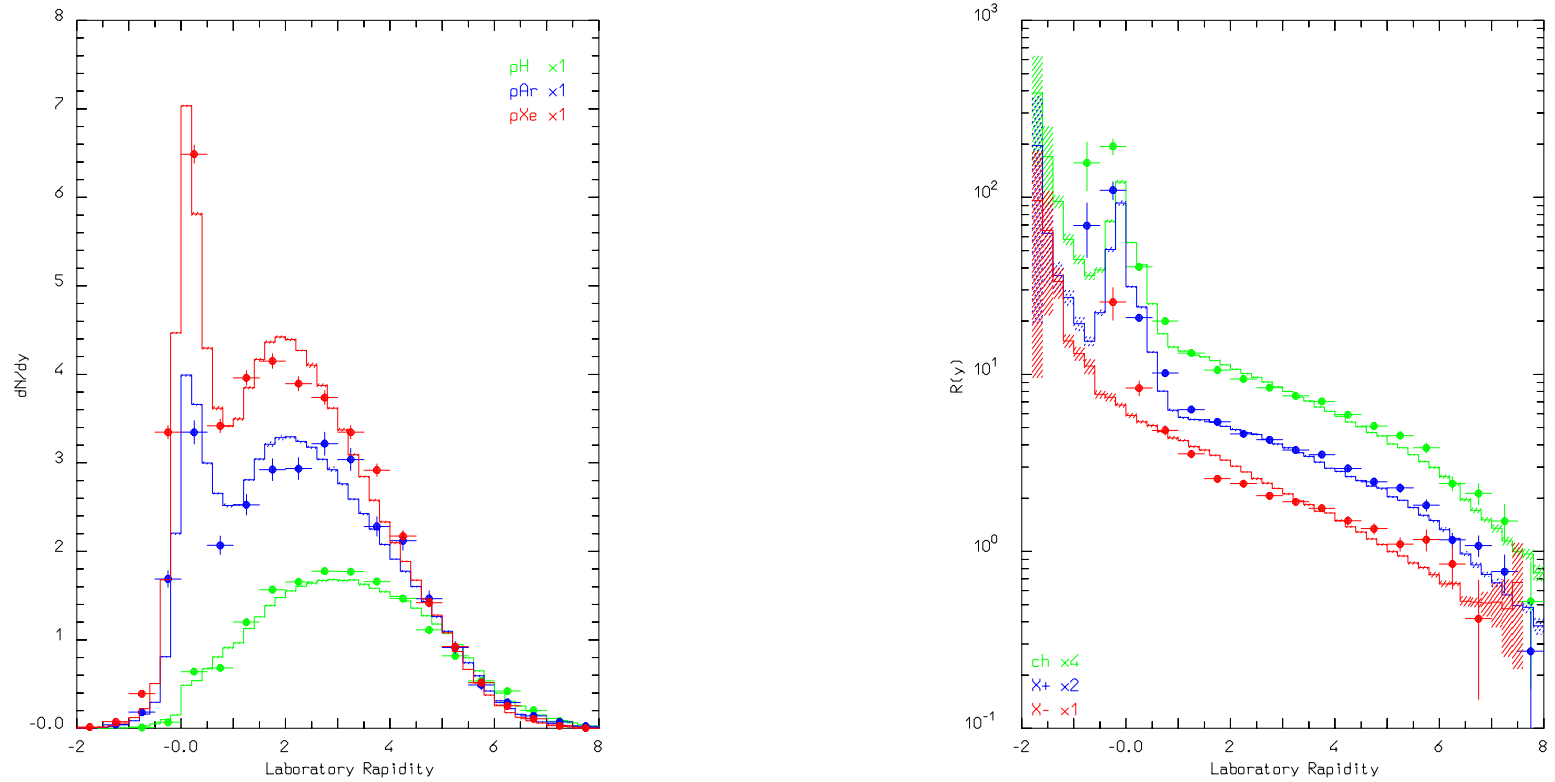

Rapidity distribution of charged particles produced in 200 GeV proton collisions on Hydrogen, Argon, and Xenon target (left) and ratio of rapidity distribution of charged, positive, and negative particles produced in 200 GeV proton collisions on Xenon and Hydrogen (right). Data from C. De Marzo et al., PRD26, 1019 (1982).

Nonelastic hA interactions at high energies: examples VI

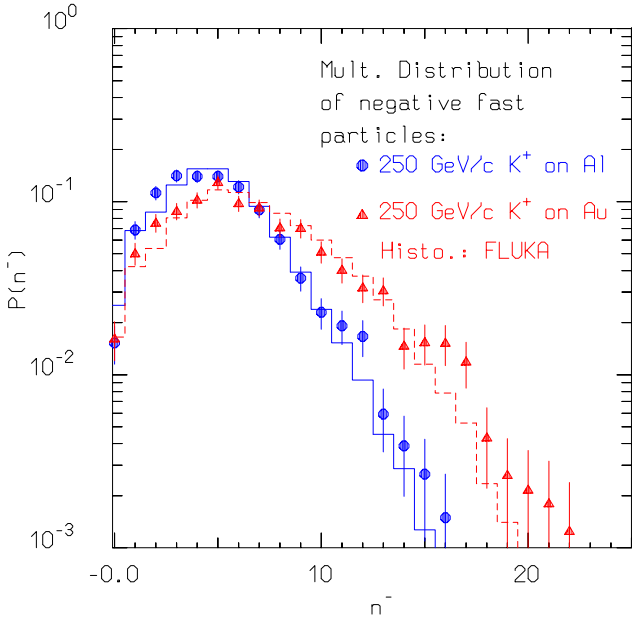

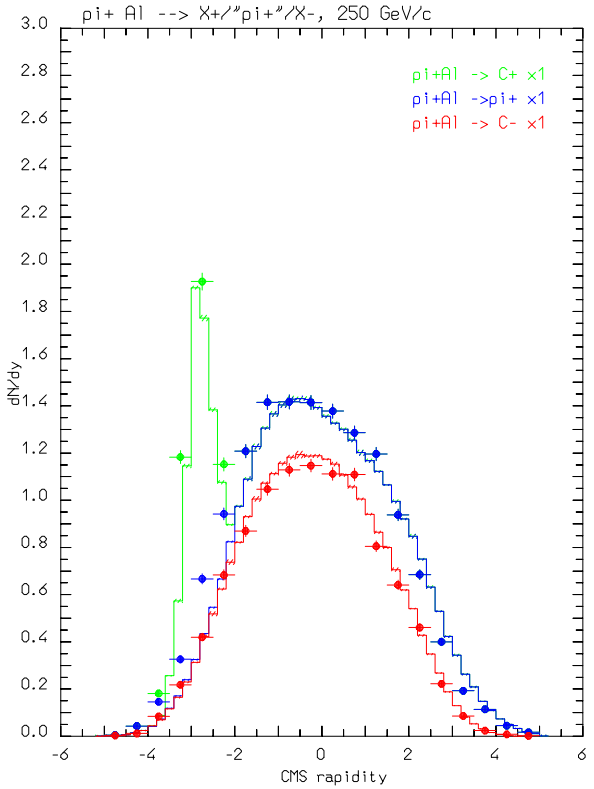

Multiplicity distribution of negative shower particles for 250 GeV/c K^+ on Aluminium and Gold targets (left), and rapidity distribution of positive, negative, and "π^+" particle for 250 GeV/c π^+ on Aluminium (right). Data from I.V. Ajinenko et al. ZPC42 377 (1989) and N.M. Agababyan et al. ZPC50 361 (1991).

Nonelastic hA interactions at high energies: examples VII

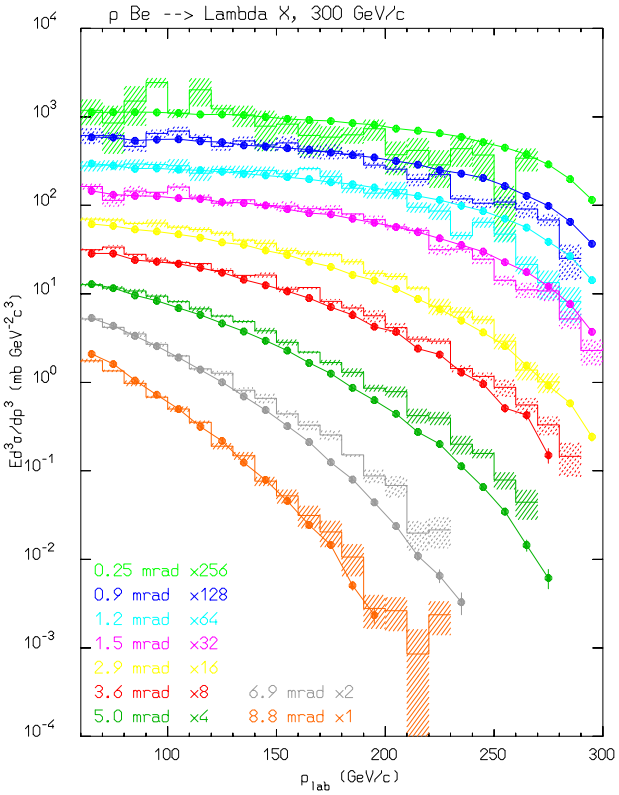

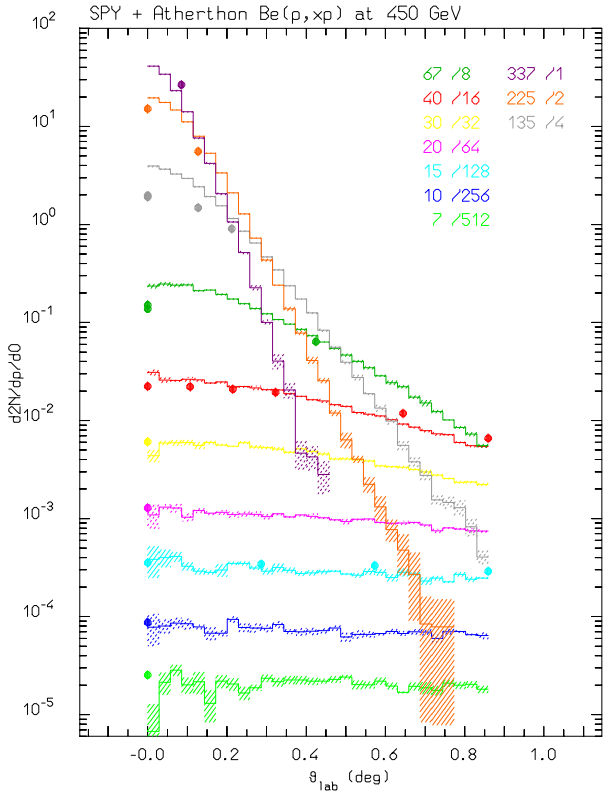

Invariant cross section for Λ production from 300 GeV protons on Be (left, data from P. Skubic et al. PRD 18 3115 (1978)), and double differential cross section for proton production (right) for 450 GeV/c protons on a 10 cm thick Be target (data from H.W. Atherton CERN 80–07, G. Ambrosini et al. PL B425 208 (1988)).

Nonelastic hA interactions at high energies: examples VIII

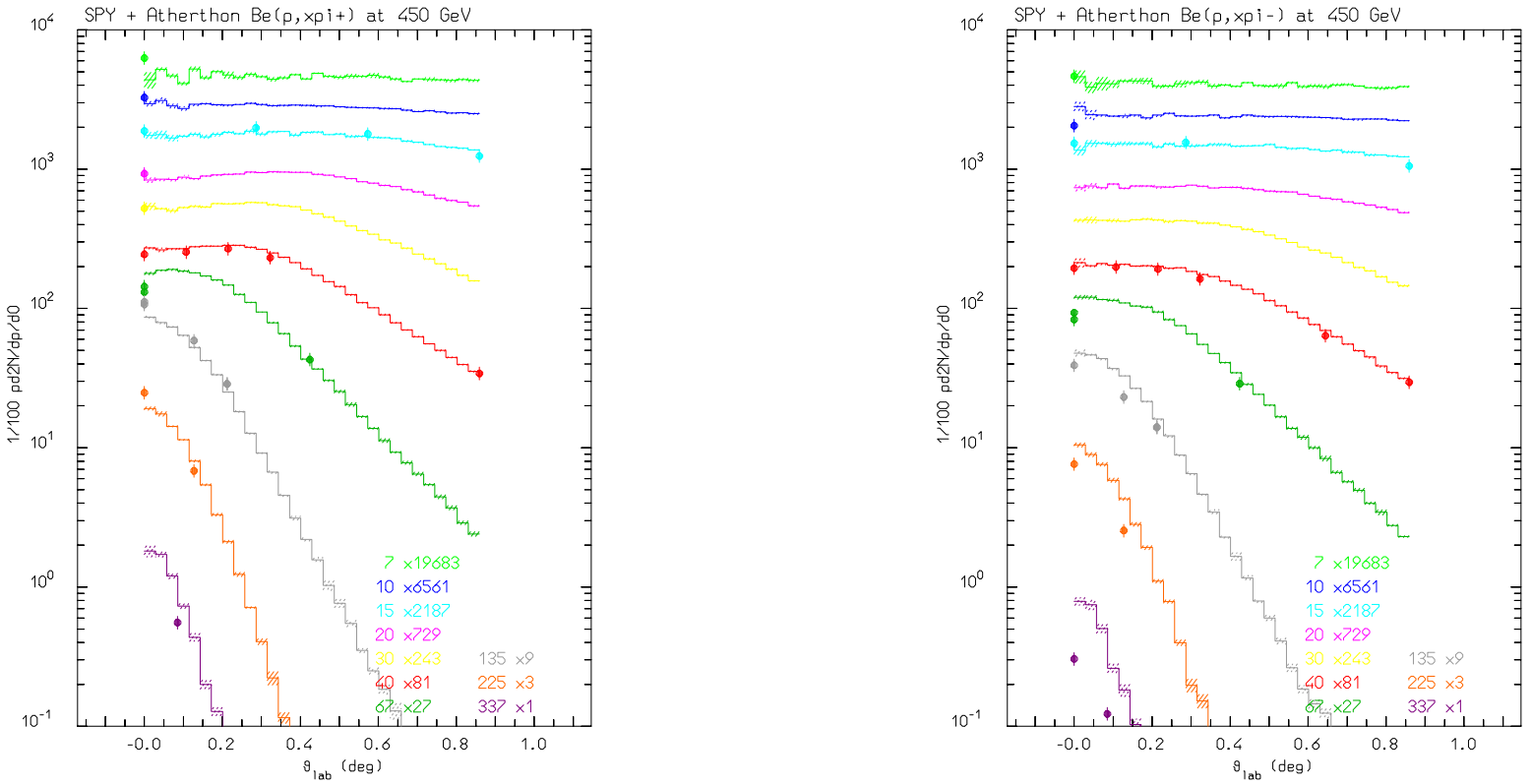

Double differential cross section for pi^+ (left) and π^- (right) production for 450 GeV/c protons on a 10 cm thick Be target (data from H.W. Atherton CERN 80–07, G. Ambrosini et al. PL B425 208 (1988)).

Nonelastic hA interactions at high energies: examples IX

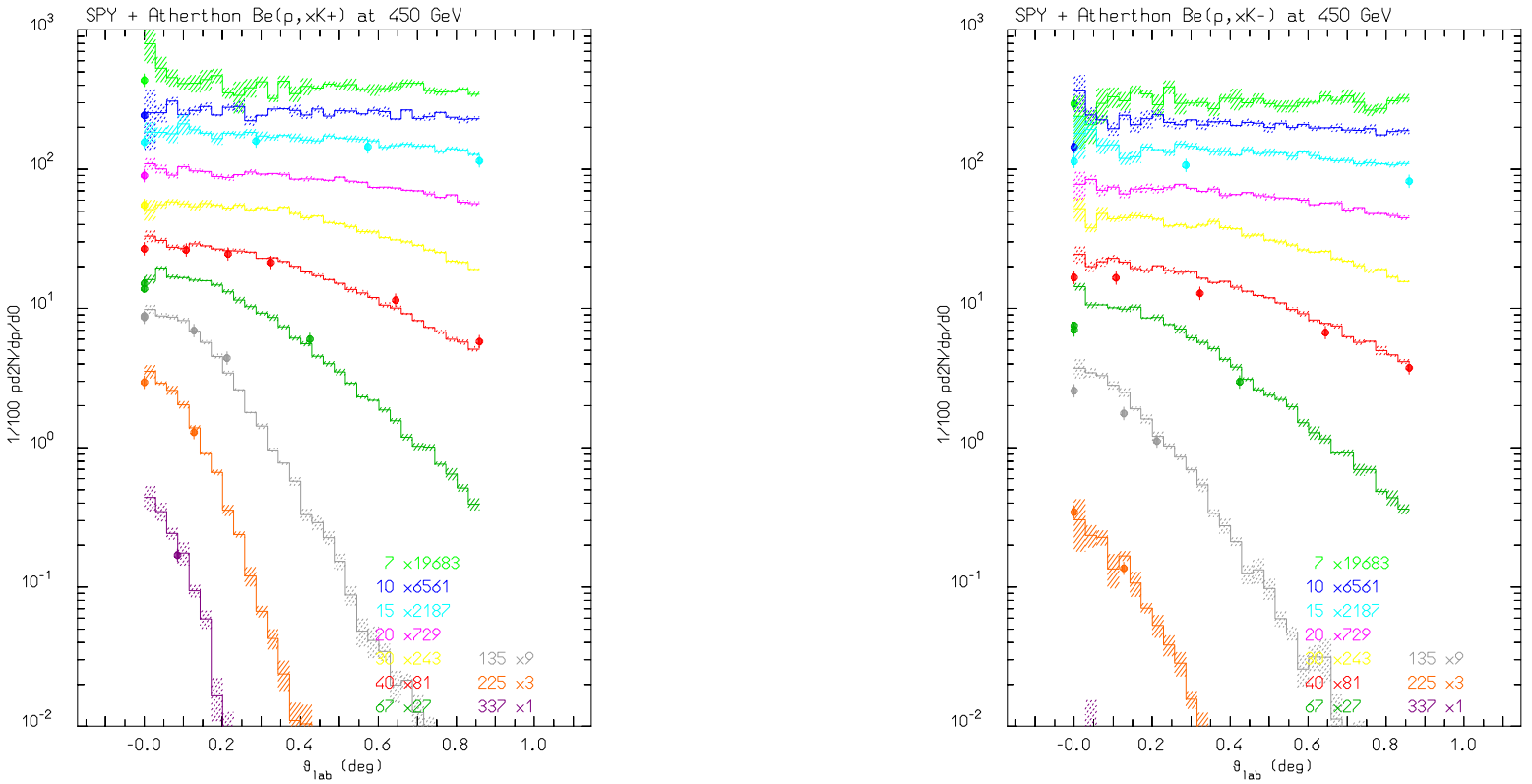

Double differential cross section for K^+ (left) and K^- (right) production for 450 GeV/c protons on a 10 cm thick Be target (data from H.W. Atherton CERN 80–07, G. Ambrosini et al. PL B425 208 (1988)).

Thick target neutron production: examples

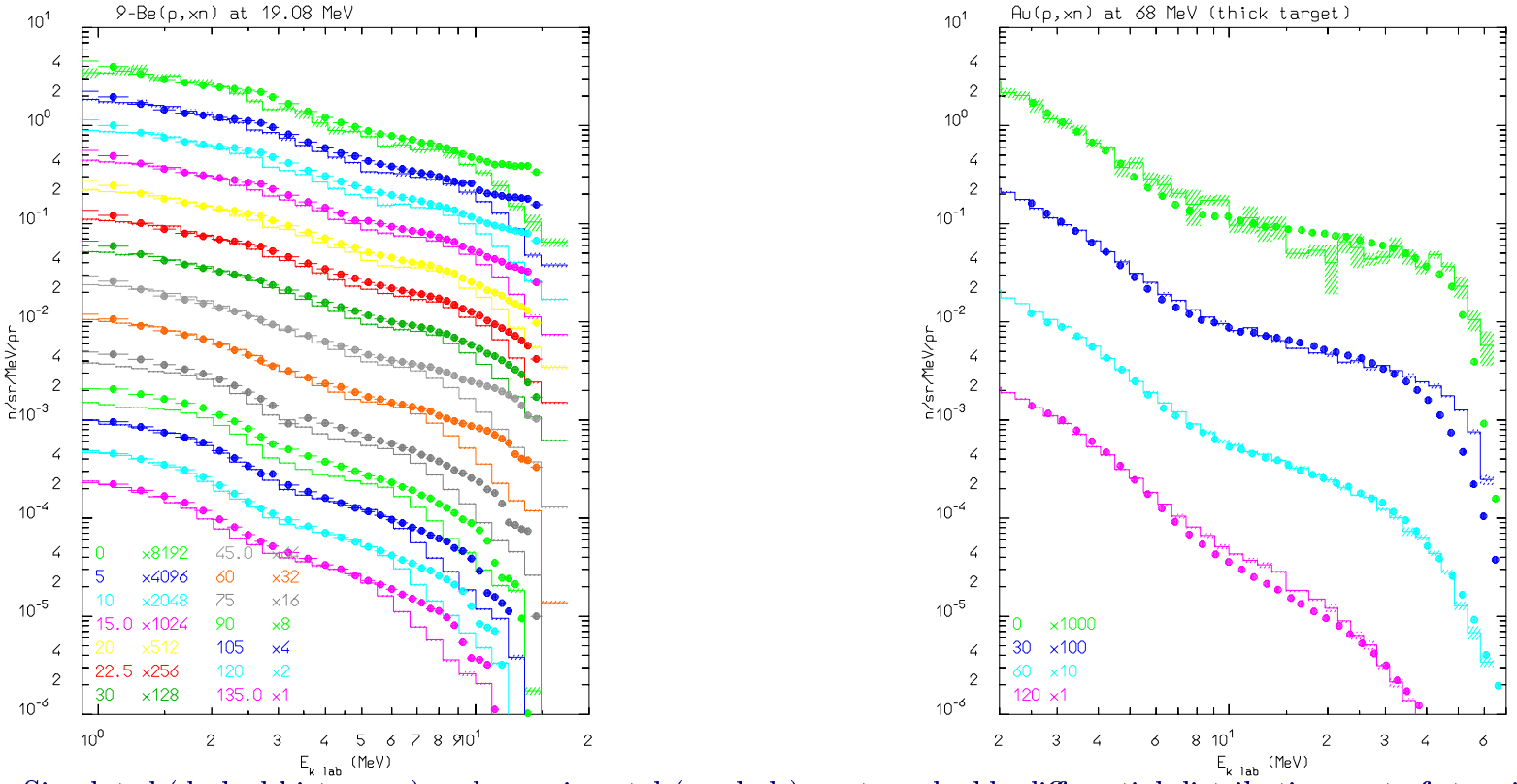

Simulated (dashed histogram) and experimental (symbols) neutron double differential distributions out of stopping length targets for 19.08 MeV protons on beryllium (left, H.J. Brede et. al., **NIMA274** (1989) 332) and 68 MeV protons on gold (right, S. Meigo et al., NDST97)

Thick target neutron production: examples II

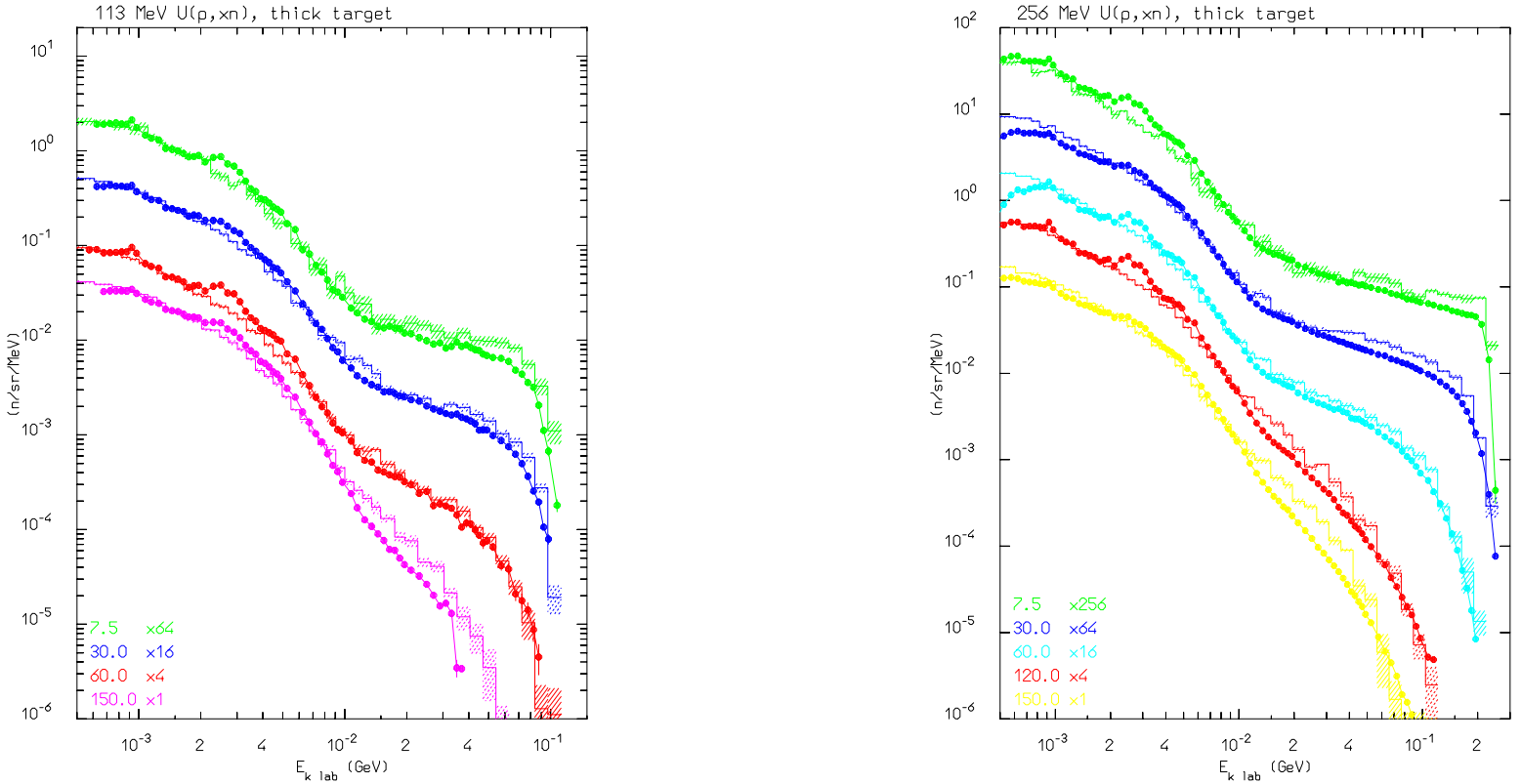

Simulated (dashed histogram) and experimental (symbols) neutron double differential distributions out of stopping length targets for 113 (left, M.M. Meier et al., Nucl. Sci. Eng. **110**, (1992) 299) and 256 MeV protons on uranium (right, M.M. Meier et al., Nucl. Sci. Eng. **102**, (1989) 310)

Thick target neutron production: examples III

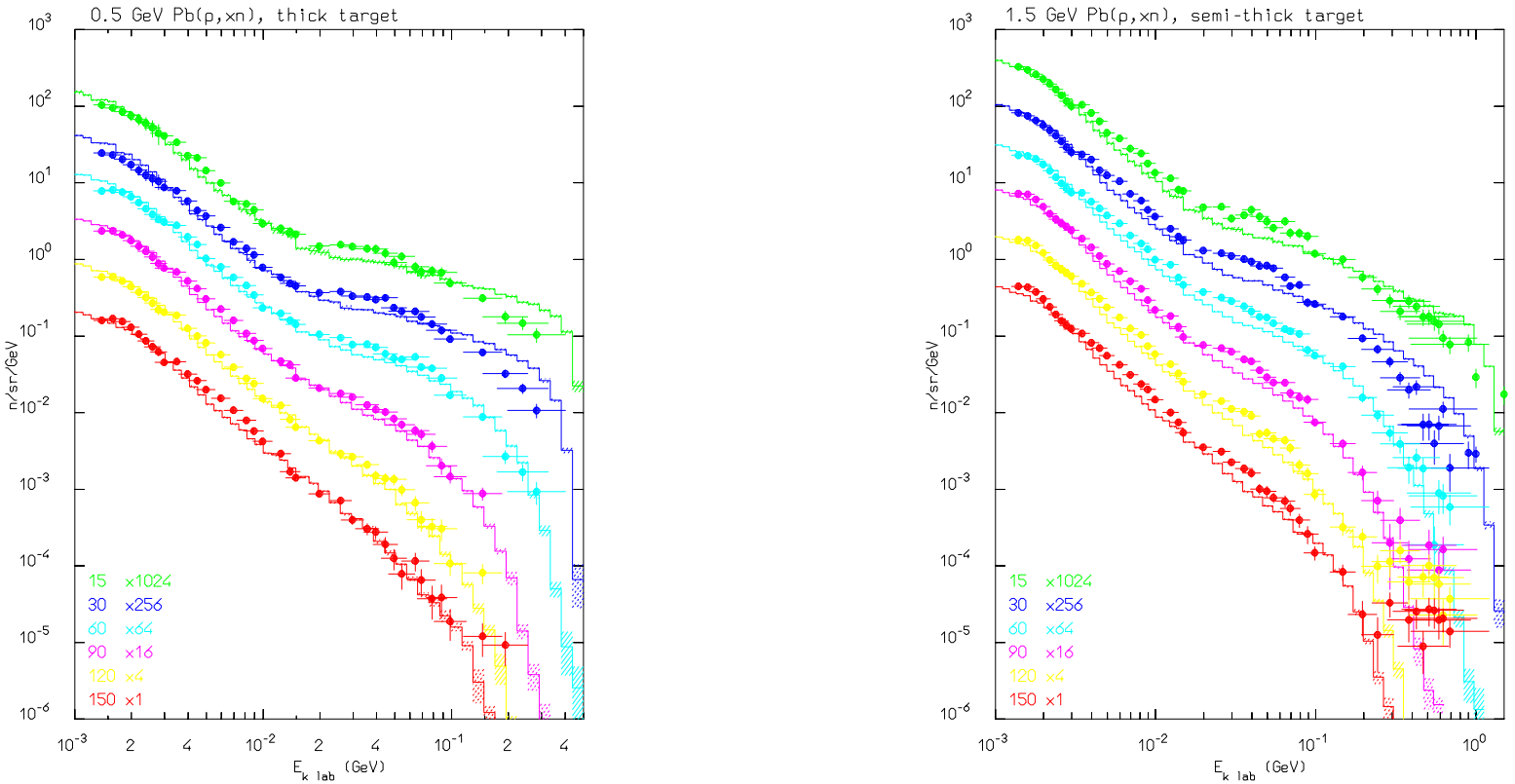

Simulated (dashed histogram) and experimental (symbols) neutron double differential distributions out of (semi)stopping length targets for 500 (left) and 1500 MeV protons on lead (right). Exp. data from S. Meigo et al., JAERI-Conf 95-008, (1995), 213

Residual nuclei predictions: the ultimate problem

Many problems require a reasonable knowledge of the identity and energy of the heavy fragments (residuals) produced in h-A and A-A interactions, both on the target and the projectile side. In particular, reliable estimates are important for

- Activation of irradiated components
- Environmental impact (activation of ground, water etc.)
- Radiation damage to sensitive components (SEU etc.)
- Radiobiological effects due to highly ionizing fragments

Evaporation/Fission and Fermi break-up

Main features of the FLUKA evaporation/fission/break-up model: Weisskopf-Ewing evaporation including

- Level densities from Gilbert-Cameron + Ignatyuk energy dependence
- Competition with fission
- Competition with γ ray emission
- Fermi Break-up for A$\leq$17 nuclei, with optional spin-parity effects
- Sampling from emission widths without Maxwellian approximation
- Rough sub-barrier emission
- Rough spin-parity effects for low excitations

Residual nuclei predictions: generalities

The predictions about production of specific isotopes have additional problems wrt the calculation of emission spectra *(this applies to both target and projectile ions)*:

- Small changes in the final evaporation steps can lead to fairly different residuals with little or no impact on the emitted spectra
- Nuclear structure effects play a major role which cannot be easily accounted for
- The lack of spin-parity dependent calculations in most MonteCarlo models limits their accuracy
- Fragmentation processes are known to populate the mass range A<20-30 for medium/heavy target nuclei. These processes are difficult to model in MonteCarlo codes.
- Isomer production: an open question
- The range of interesting cross section values typically spans *four* order of magnitudes

Residual nuclei: the mass distribution at high energies

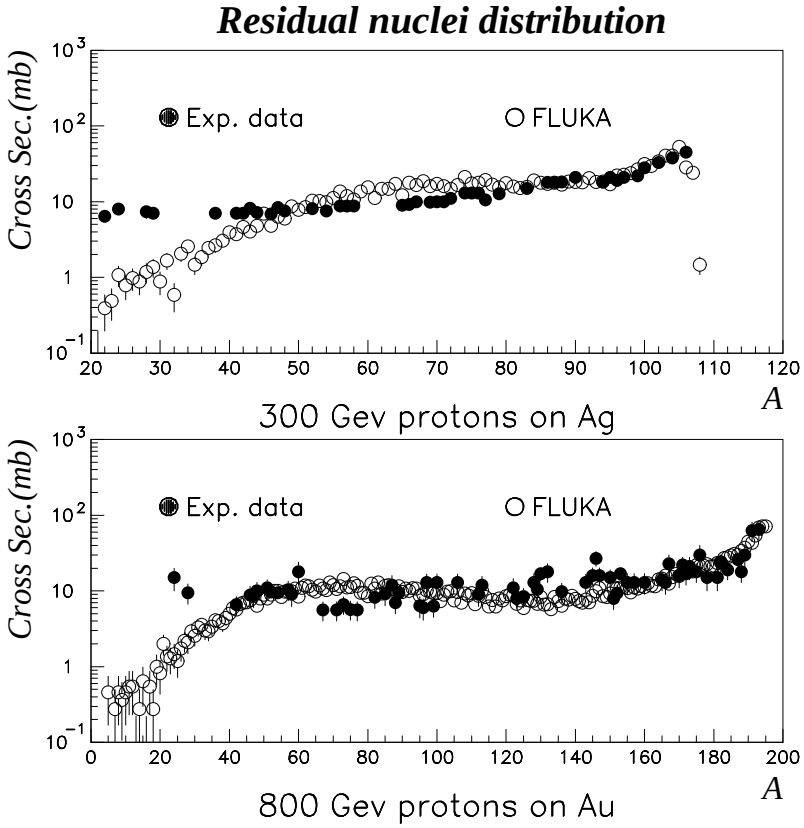

Experimental and computed residual nuclei mass distribution following for Ag(p,x)X at 300 GeV (top) and Au(p,x)X at 800 GeV (bottom).

Mass distribution for Gold at 300 MeV

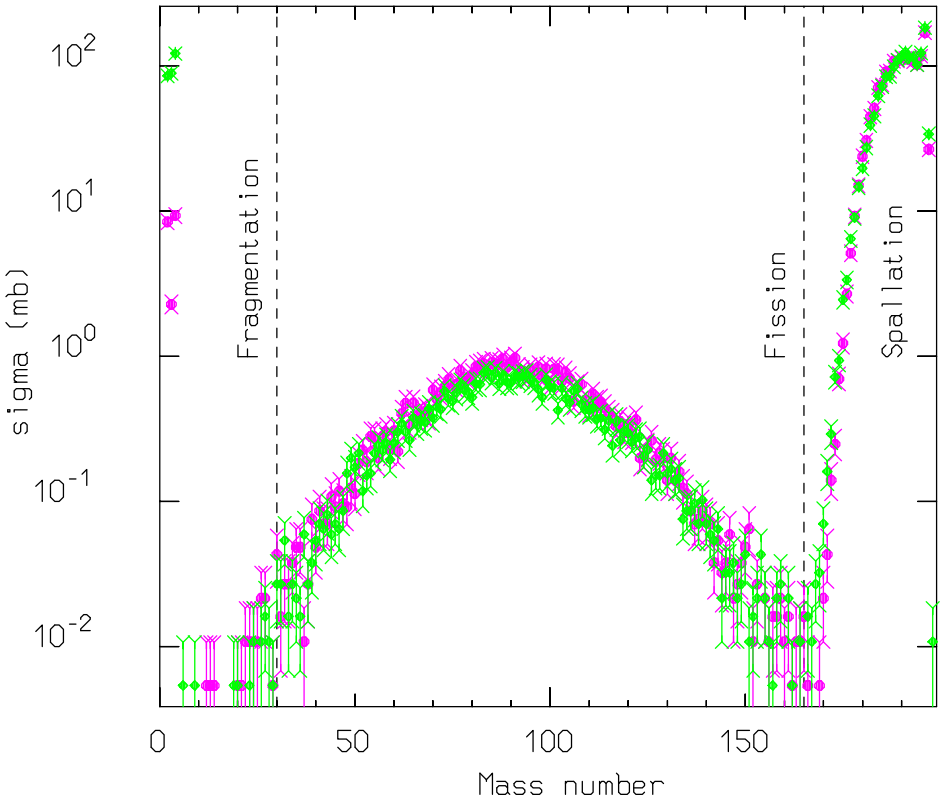

Computed mass yield distributions for 300 MeV protons on Gold using the old "a la EVAP" evaporation (purple) and the new FLUKA evaporation model (green)

Residual nuclei predictions: a look at the isotope table

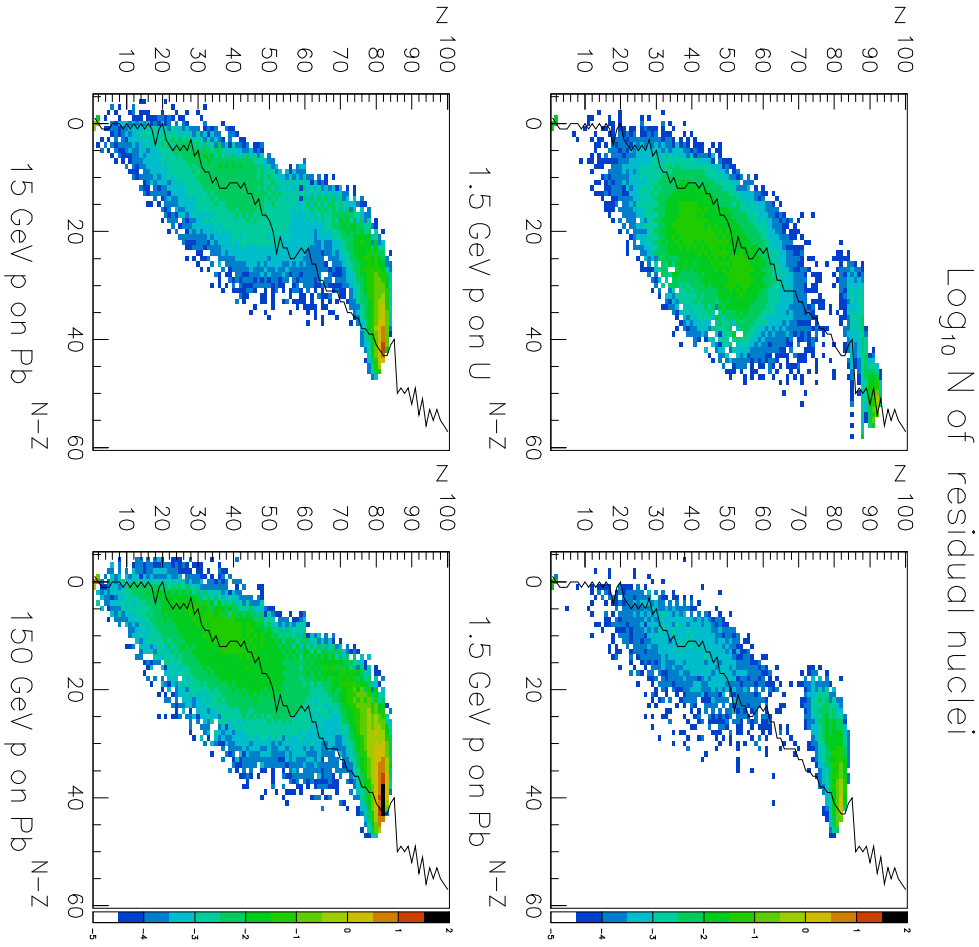

Residual nuclei predictions: examples

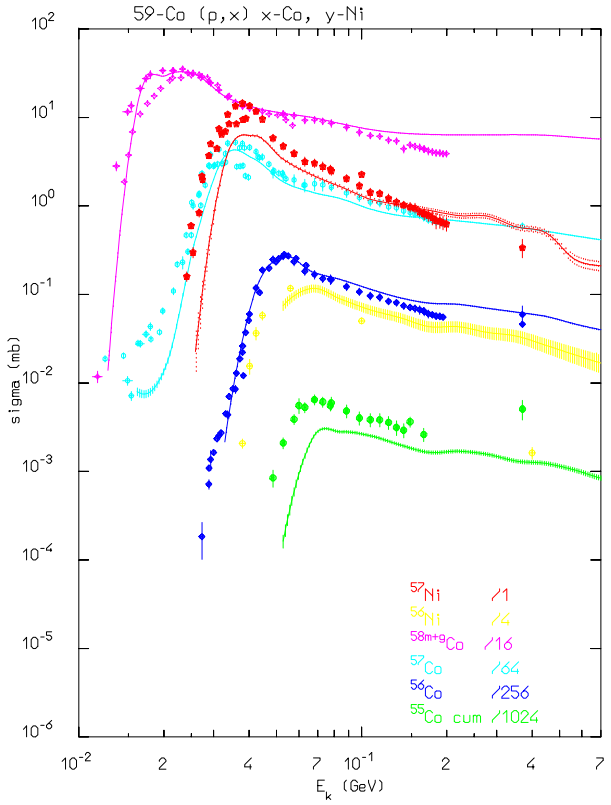

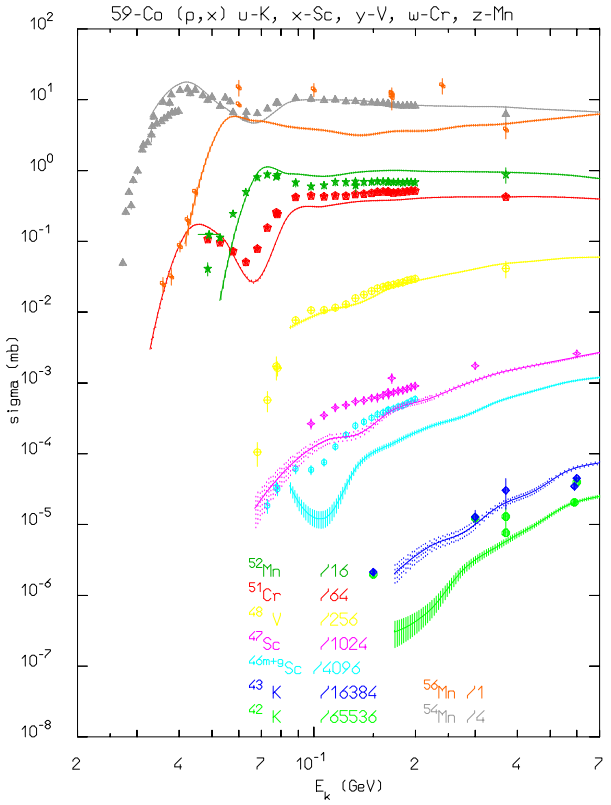

Comparison between computed and measured (A.S. Iljinov et al., Landolt-Börnstein, **Vol. 13a** (1991)) isotope production by protons on natural Cobalt

Residual nuclei predictions: "new" vs "old" evap.

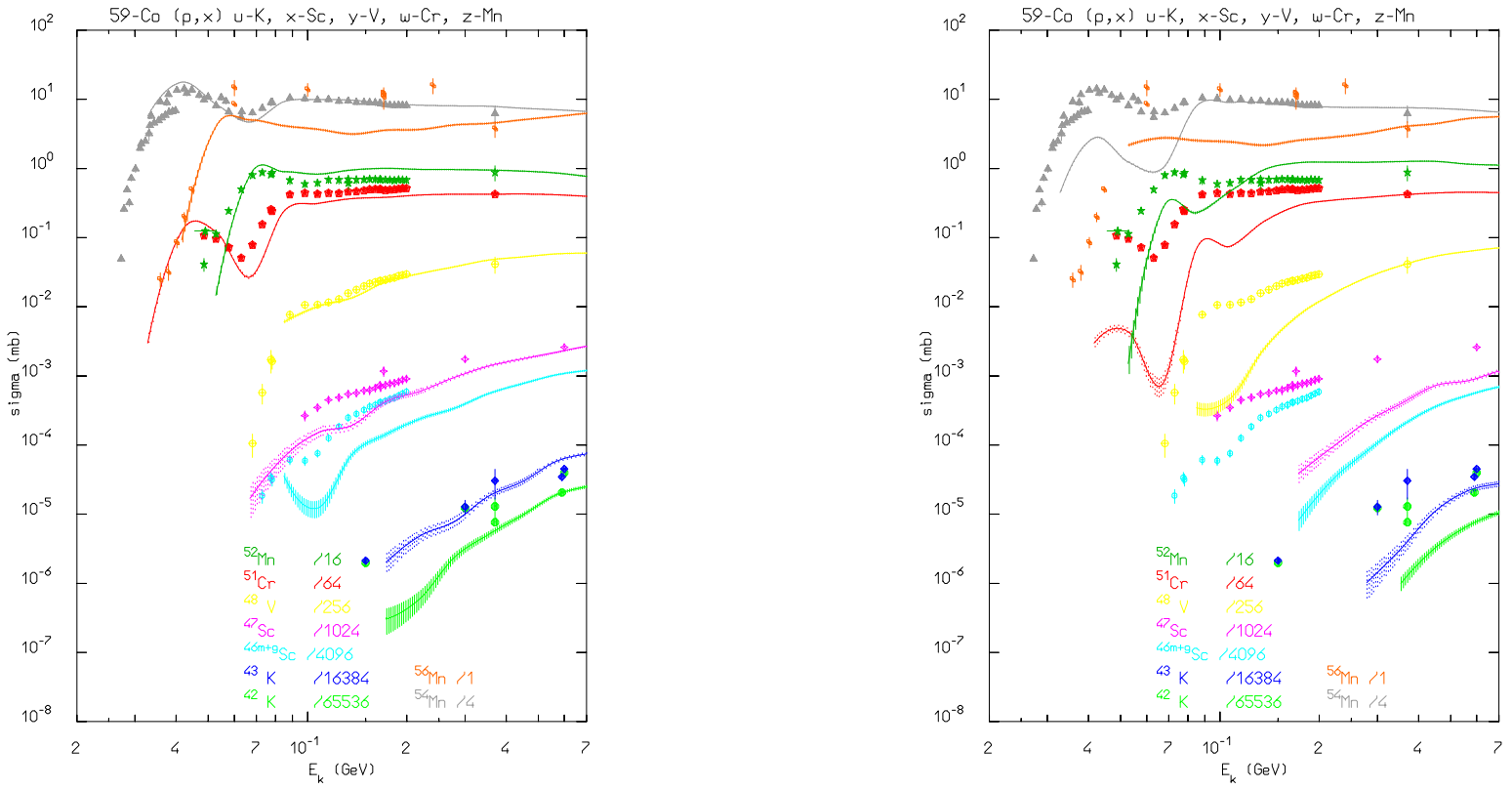

Comparison between isotope yields computed with the new (left) and (right) evaporation model in FLUKA

Residual nuclei predictions: examples II

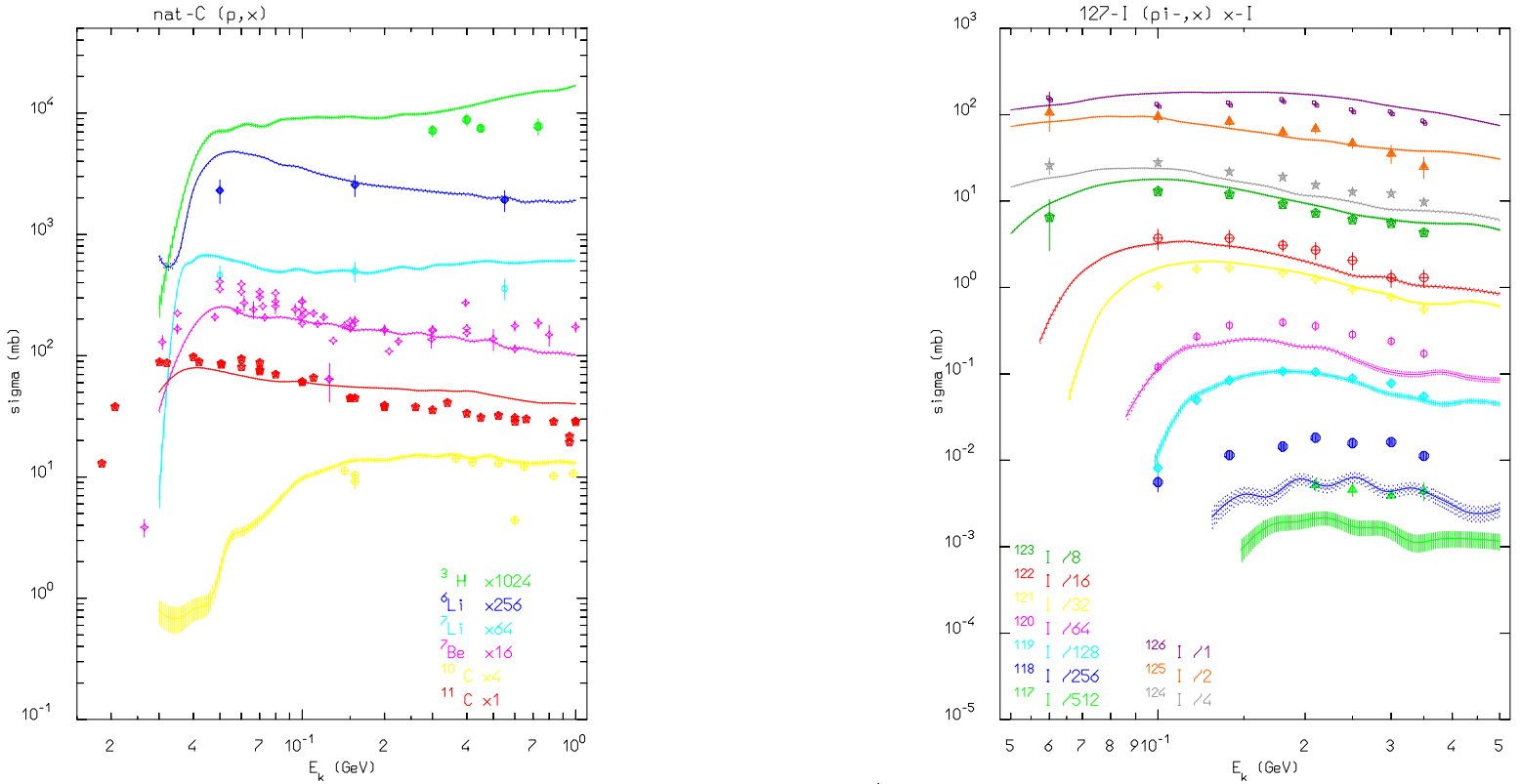

Comparison between computed and measured (A.S. Iljinov et al., Landolt-Börnstein, **Vol. 13a** (1991)) isotope production by protons on natural carbon (left) and by negative pions on Iodine (right)

Residual nuclei predictions: the example of Gold

In the following a few examples of ^{197}Au(p,x)X reactions will be shown comparing the experimental data and several model predictions.

The model predictions but the one of FLUKA, have been taken from

International Codes and Model Intercomparison for Intermediate Energy Activation Yields, NSC/DOC(97)-1 NEA/P&T No 14 (1997)

The references for the experimental data can be found in the same report

Residual nuclei predictions: the example of Gold I

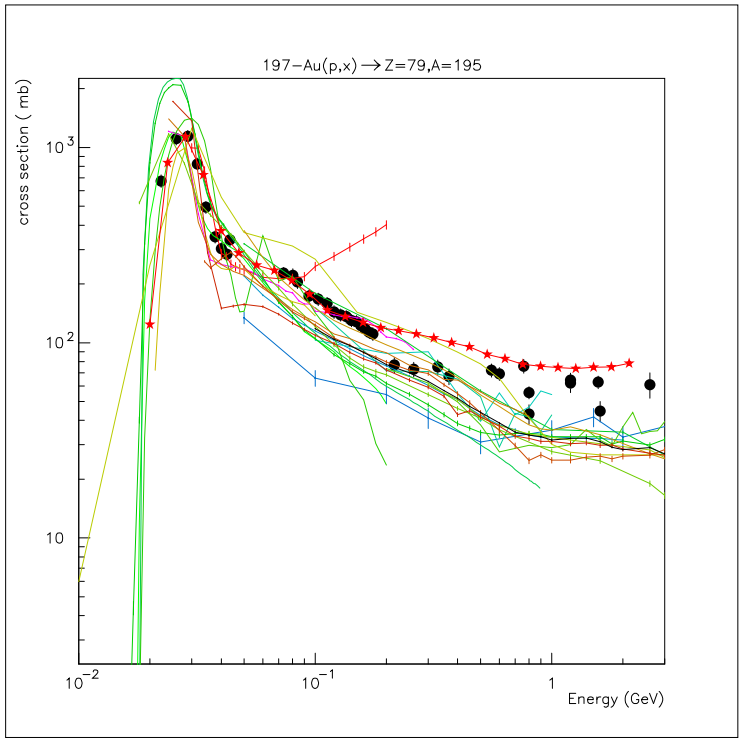

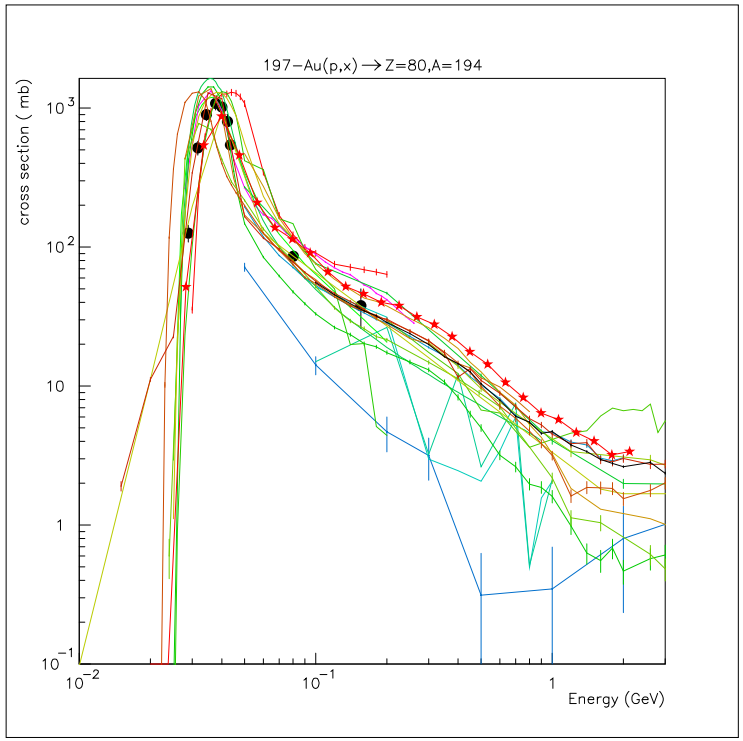

Comparison between computed (symbols with lines, FLUKA red line with stars) and measured cross sections (black symbols) for ^{197}Au(p,x)^{195}Au (left) and ^{197}Au(p,x)^{194}Hg (right) as a function of the proton energy

Residual nuclei predictions: the example of Gold II

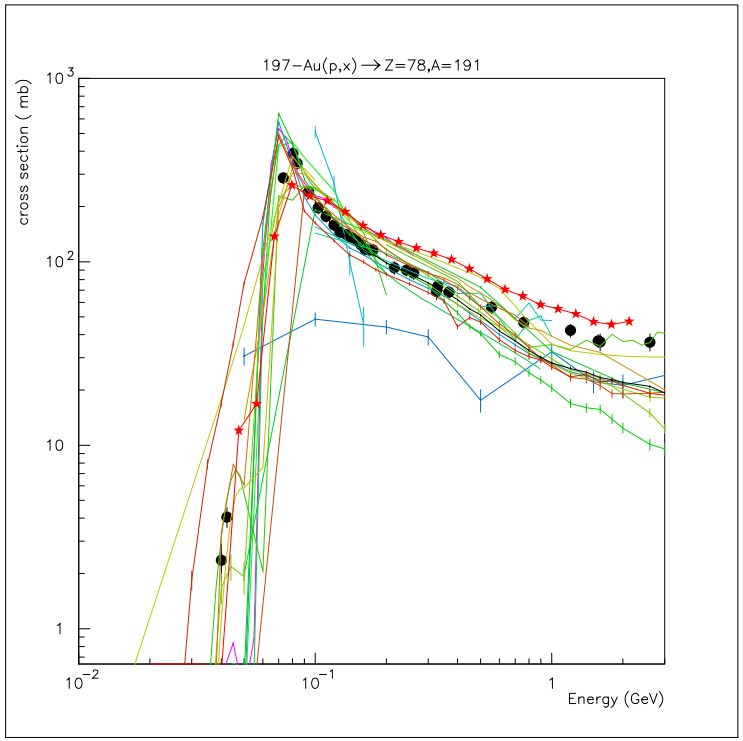

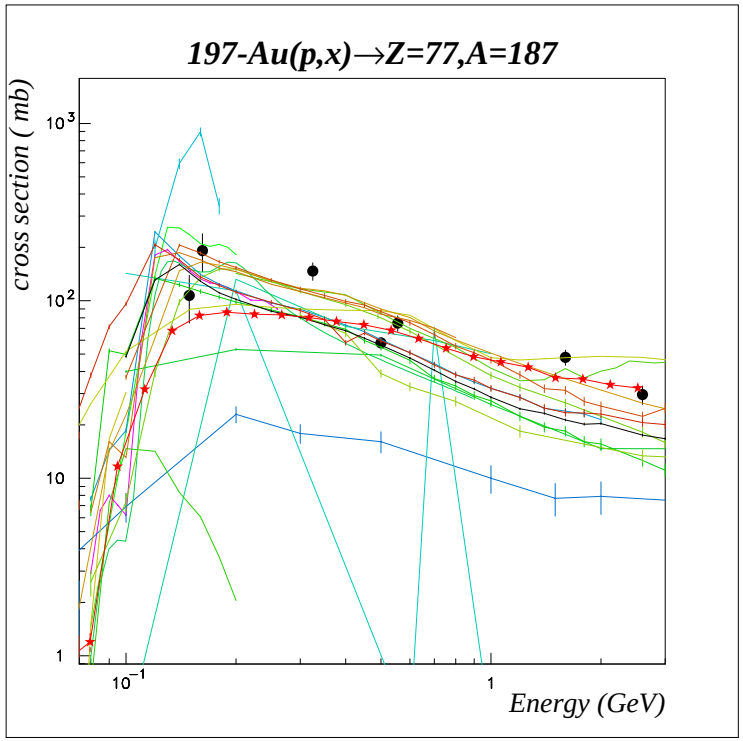

Comparison between computed (symbols with lines, FLUKA red line with stars) and measured cross sections (black symbols) for ^{197}Au(p,x)^{191}Pt (left) and ^{197}Au(p,x)^{187}Ir (right) as a function of the proton energy

Residual nuclei predictions: the example of Gold III

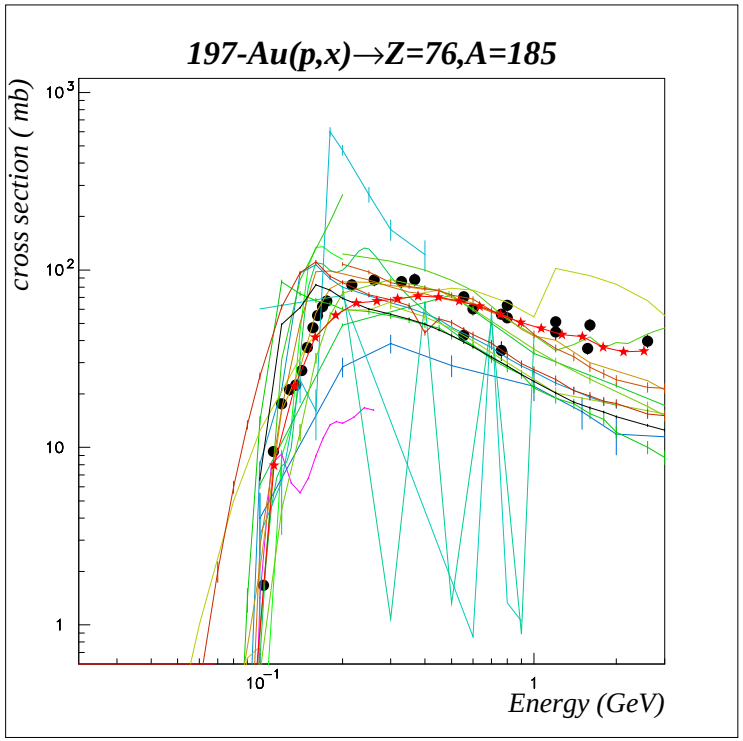

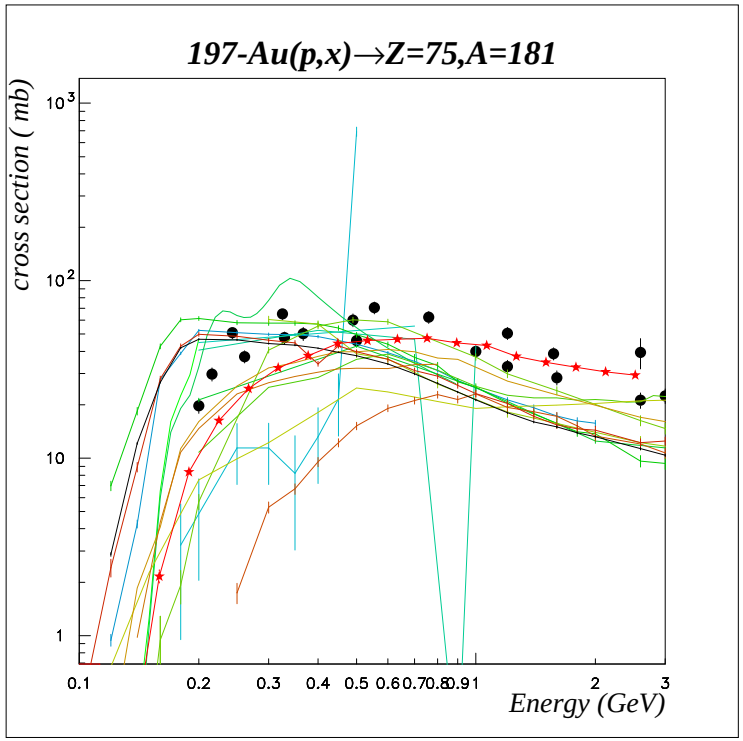

Comparison between computed (symbols with lines, FLUKA red line with stars) and measured cross sections (black symbols) for ^{197}Au(p,x)^{185}Os (left) and ^{197}Au(p,x)^{181}Re (right) as a function of the proton energy

Residual nuclei predictions: the example of Gold IV

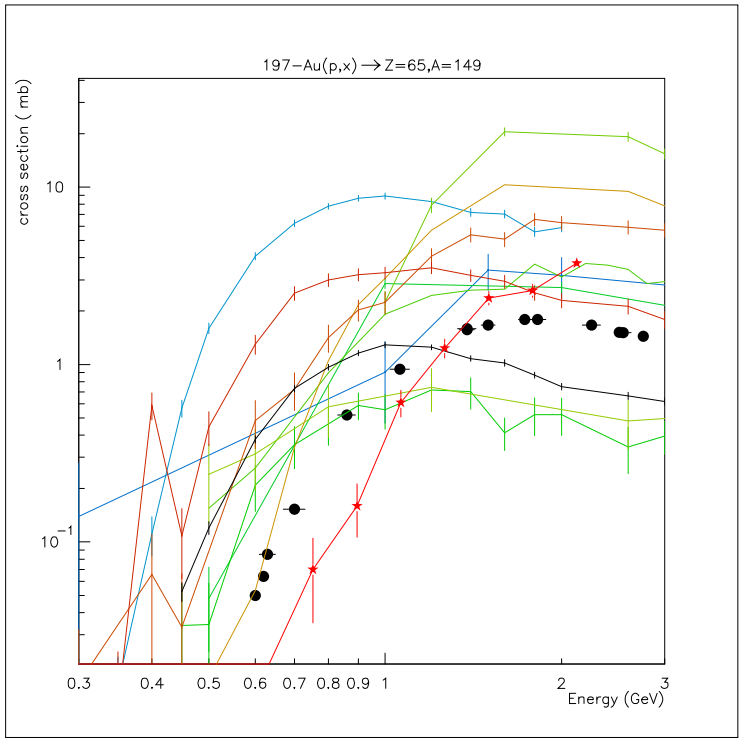

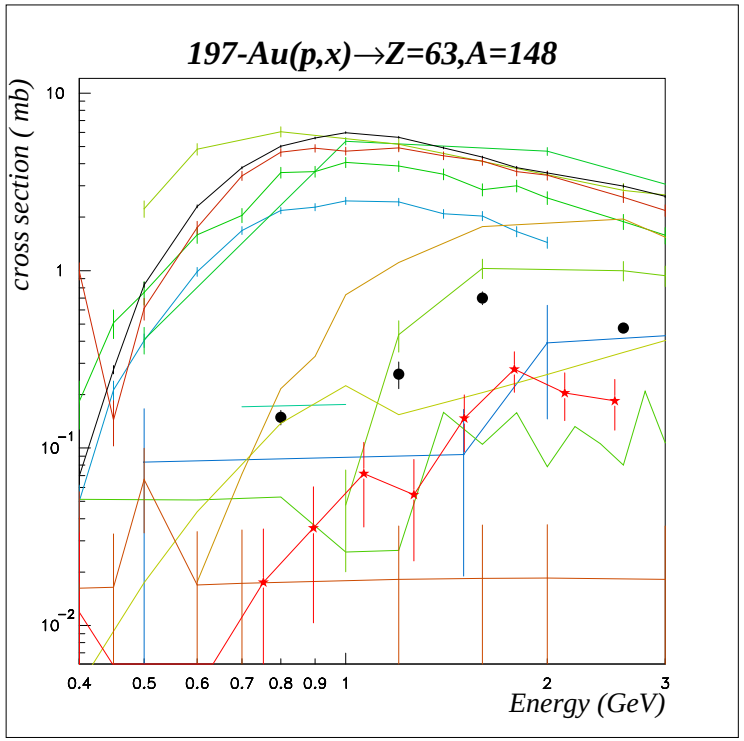

Comparison between computed (symbols with lines, FLUKA red line with stars) and measured cross sections (black symbols) for ^{197}Au(p,x)^{149}Tb (left) and ^{197}Au(p,x)^{148}Eu (right) as a function of the proton energy

Residual nuclei predictions: the example of Gold V

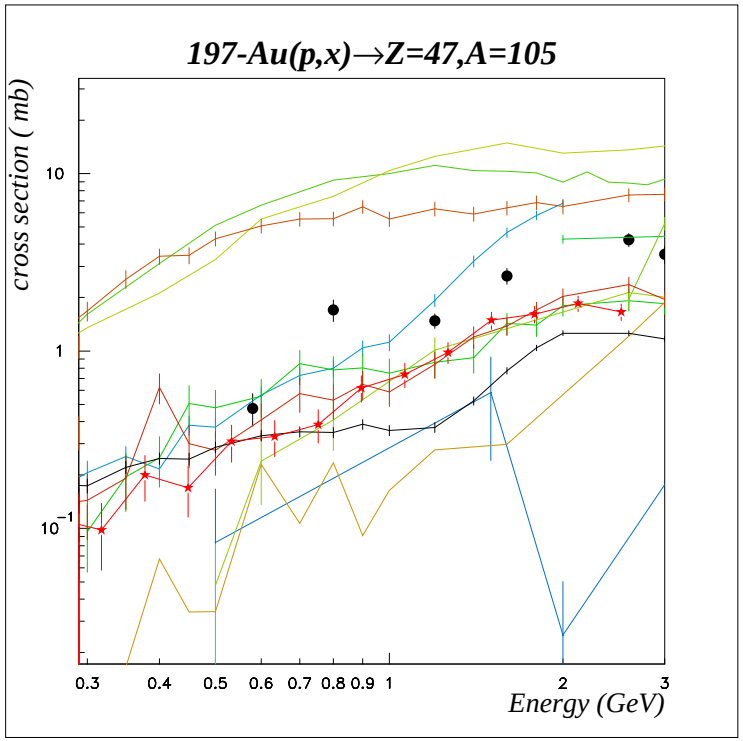

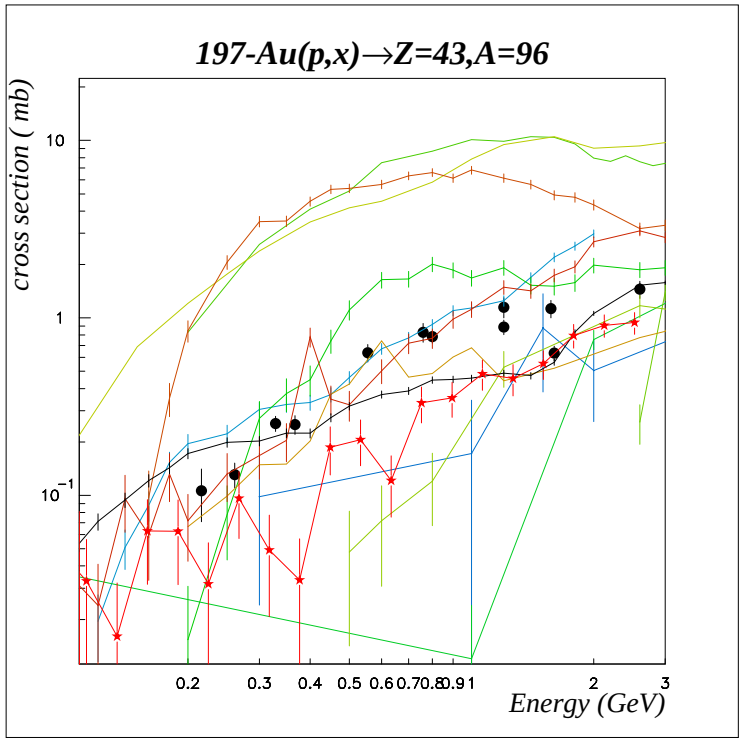

Comparison between computed (symbols with lines, FLUKA red line with stars) and measured cross sections (black symbols) for ^{197}Au(p,x)^{105}Ag (left) and ^{197}Au(p,x)^{96}Tc (right) as a function of the proton energy

Residual nuclei predictions: the example of Gold VI

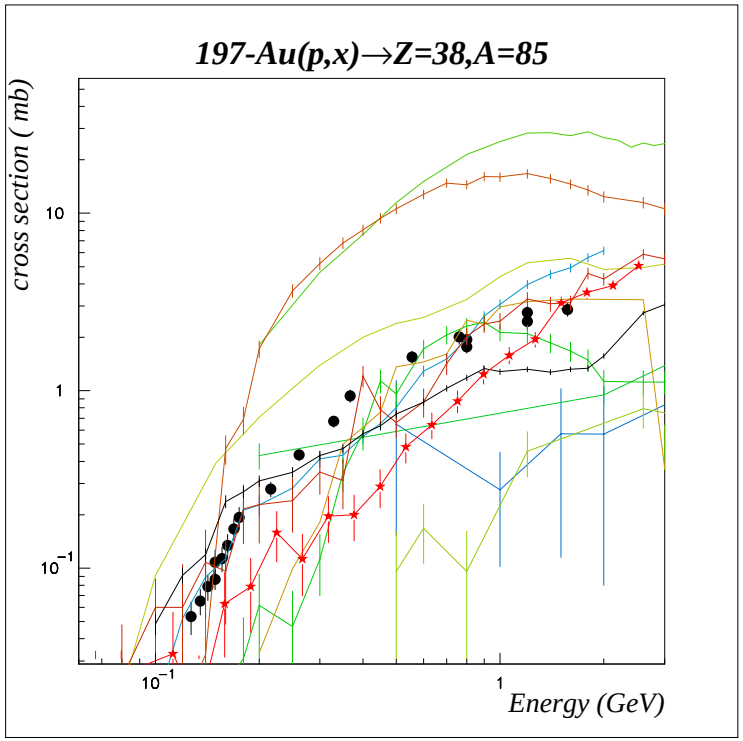

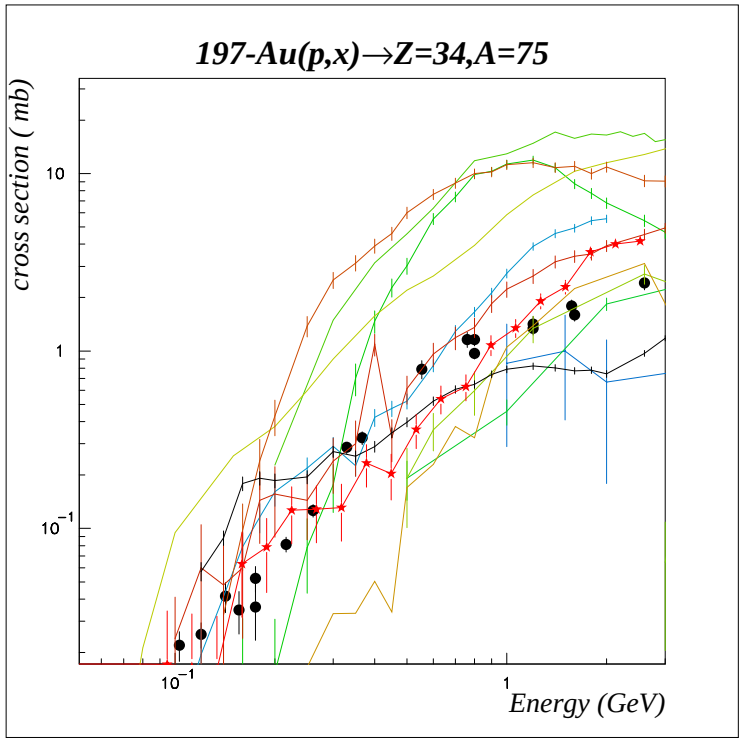

Comparison between computed (symbols with lines, FLUKA red line with stars) and measured cross sections (black symbols) for ^{197}Au(p,x)^{85}Sr (left) and ^{197}Au(p,x)^{75}Se (right) as a function of the proton energy

Residual nuclei predictions: the example of Gold VII

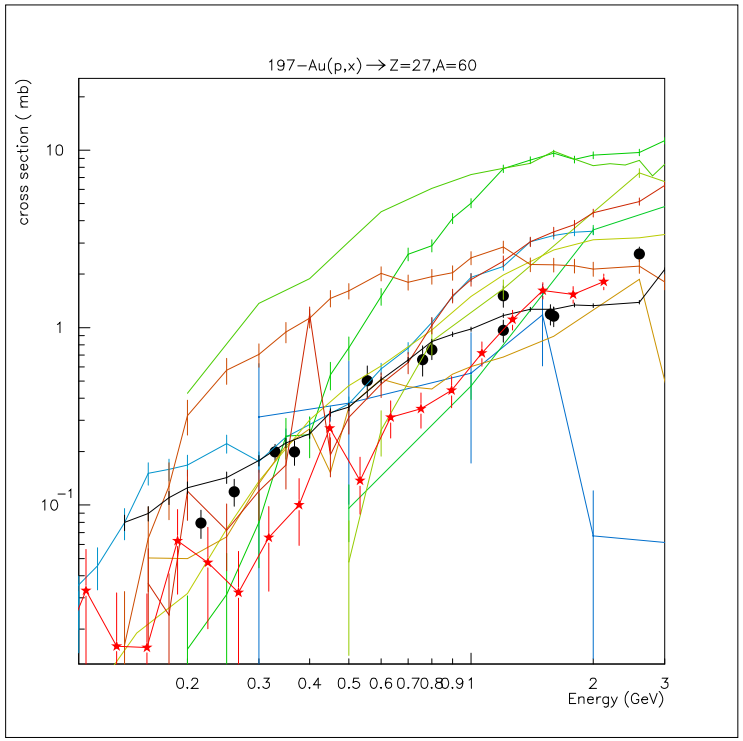

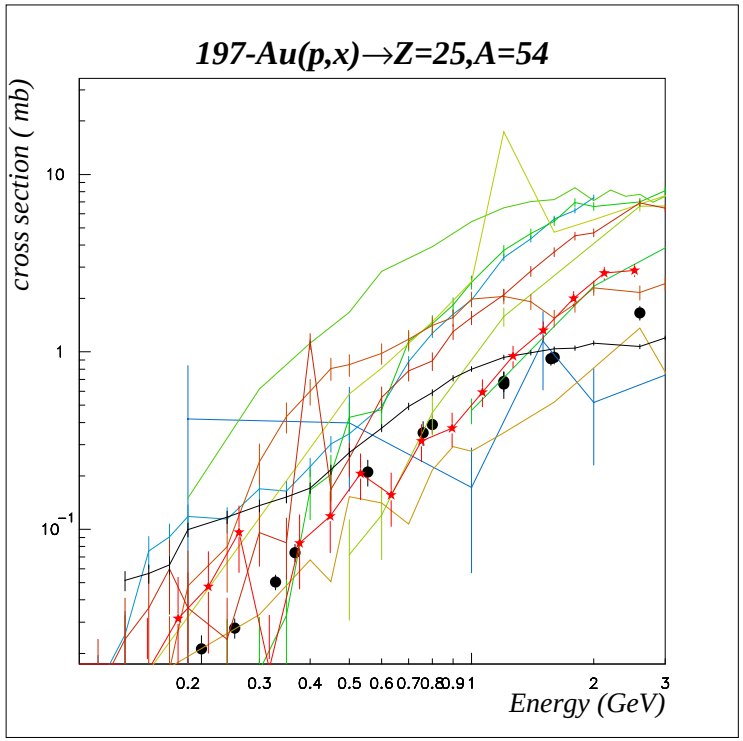

Comparison between computed (symbols with lines, FLUKA red line with stars) and measured cross sections (black symbols) for ^{197}Au(p,x)^{60}Co (left) and ^{197}Au(p,x)^{54}Mn (right) as a function of the proton energy

Residual nuclei predictions: summary

The present status of the residual nuclei predictions can be summarized as follows:

- Isotopes in the spallation peak can be predicted reasonably well (within a factor 2-3)
- Isotopes in the fission region can be predicted within a factor of a few
- Isotopes in between the spallation peak and the fission region are subject to large errors (heavy nuclei only)
- Isotopes in the fragmentation region (left of the fission region) are difficult to predict when the fragmenting target is a medium/heavy mass one
- The split between ground state and isomer production is still missing

The uncertainties in the predicted isotope production can be *greatly mitigated* in all practical situations when the production is dominated by *interactions of neutrons below 20 MeV*, where extensive and reasonably precise collections of evaluated data exist, i.e. for bulky fissionable targets

LEP dismantling: a calculational nightmare

Request : demonstrate that ALL activities are below 1/10 of the 1996 European Directive limits (around 10 Bq/g) after 10 year operation

An almost unaffordable task for a MC :
Starting from an electron beam,
simulate the extremely rare photon induced nuclear interactions
with such an accuracy as to determine the residual nuclei.

EXPERIMENT: samples of different materials (Al, Cu, stainless steel, Pb and iron-laminated concrete) were irradiated on LEP beam dumps.

- Irradiation time: 5 months, at about 20 cm from the beam axis
- Saturated specific activity of the radionuclides detected in the samples were compared with FLUKA calculations
- The measured activities are so low (few Bq/g) that even the experimental measurement is difficult

LEP activation: some experimental results

Radio nuclide	$T_{1/2}$	Specific Activity (Bq/g)			Ratio
		Exp.	FLUKA	(%)	F/E
^{46}Sc	83.8 d	0.13	0.065	12	0.5
^{48}V	15.97 d	0.31	0.52	7	1.7
^{51}Cr	27.7 d	4.12	2.7	5	0.65
^{52}Mn	5.6 d	0.17	0.74	6	4.3
^{54}Mn	312.2 d	3.54	2.9	2	0.82
^{59}Fe	44.5 d	0.028	0.0088	27	0.31
^{56}Co	77.7 d	0.29	0.46	7	1.6
^{57}Co	271.8 d	1.3	1.1	4	0.85
^{58}Co	70.9 d	2.65	1.4	3	0.52
^{60}Co	5.27 y	0.18	0.085	21	0.47
^{95}Nb	34.9 d	0.038	0.013	27	0.34

Stainless Steel sample on the LEP electron dump. The exp. points have a systematic error of ≈20%(A.Fassò et al. CERN-TIS-99-011-RP-CF/SLAC-PUB-8214 and CERN-TIS-99-012-RP-CF/SLAC-PUB-8215)

Cross sections: examples

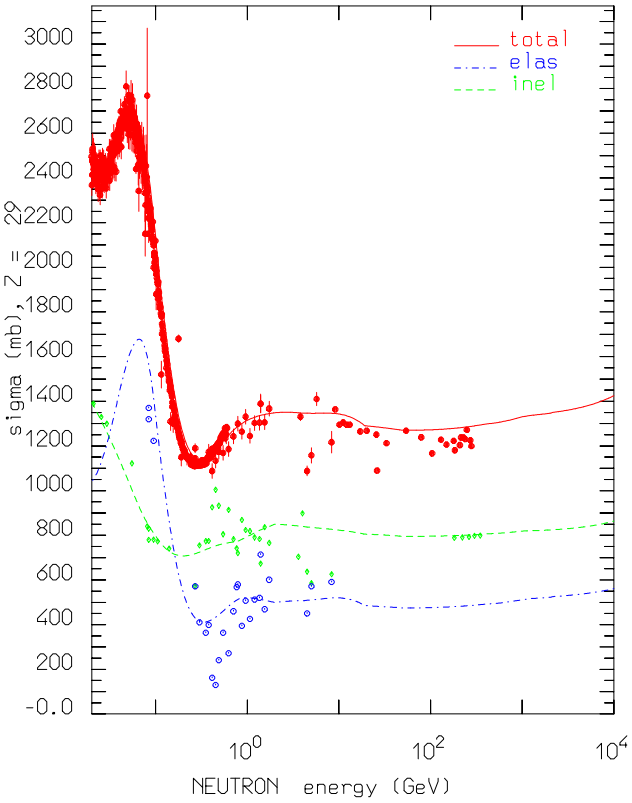

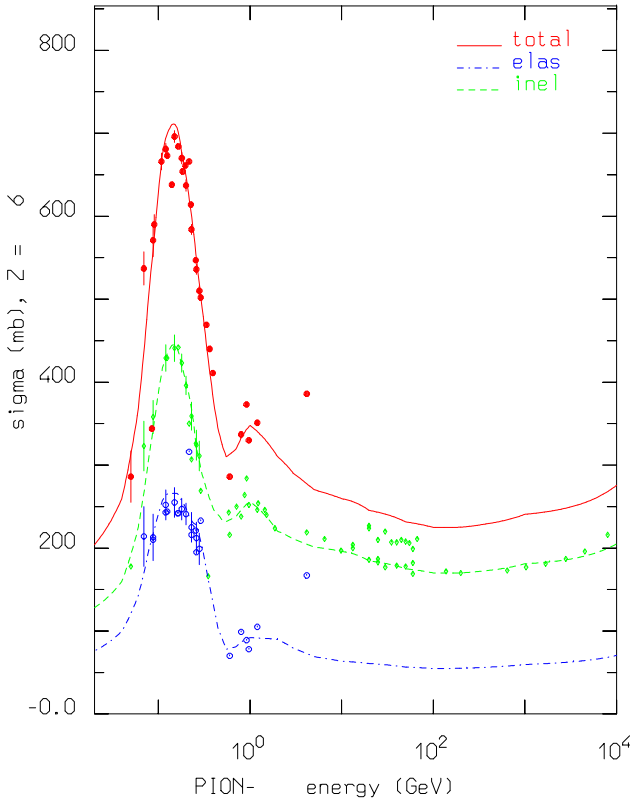

MonteCarlo (FLUKA) and experimental cross sections for neutrons on copper (left) and negative pions on carbon (right)

Cross sections: examples II

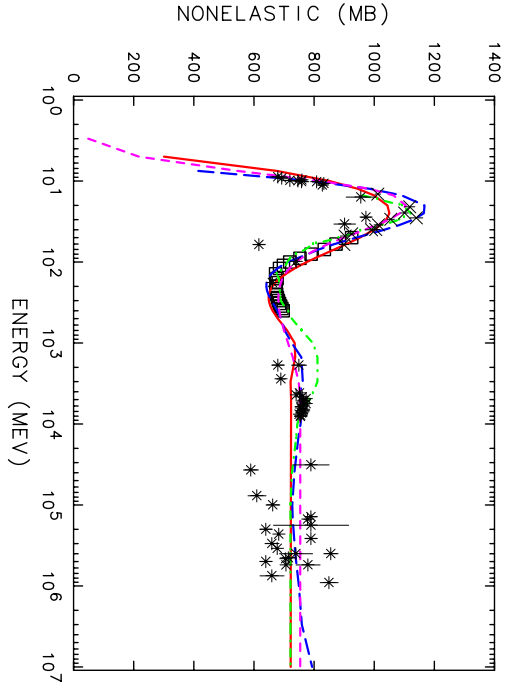

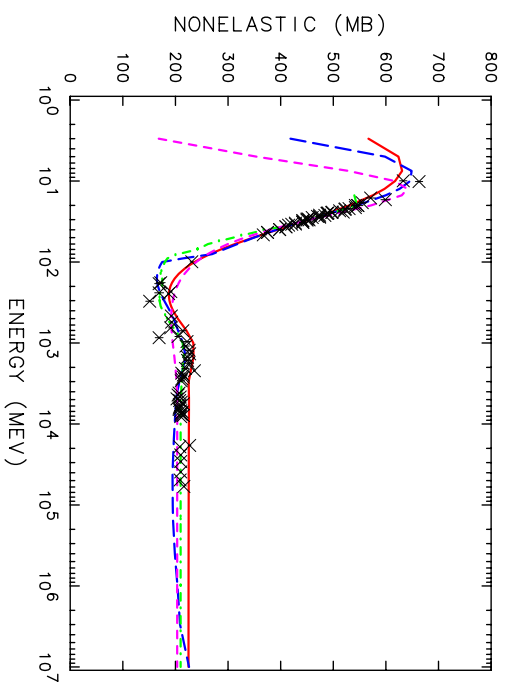

Complex benchmarks

Full cascade or neutron propagation benchmarks:

- The TIARA [1] neutron propagation experiment
- The TARC [2] experiment at CERN: the ultimate neutronic benchmark
- The Rösti [3] experiments at CERN
- The CERF [4] dosimetry facility at CERN
- The OPTIS beam at PSI: an attempt of merging biophysical and physical models [5]

[1] H. Nakashima et al. Nucl. Sci. Eng. **124** (1996) and N. Nakao et al. Nucl. Sci. Eng. **124** (1996) 228

[2] H. Arnould et al., **PLB458** (1999) 167

[3] J.S. Russ et al, CERN/TIS **RP/89-02**, (1989) and A. Fassò et al., CERN/TIS **RP/90-19**, (1990)

[4] A. Esposito et al, Rad. Prot. Dos. **76**, (1998) 135

[5] M. Biaggi et al., Nucl. Instr. Meth, **B159**, (199) 89

The TIARA neutron propagation experiment

Main features [6]:

- Source term: semi-monoenergetic neutron spectra generated by 43 and 68 MeV protons on a ^{7}Li target, carefully measured with TOF tecniques
- Attenuation of the neutron beam at different depths in concrete and iron shields, both on axis and off-axis (*critical for elastic scattering!!*)
- Emerging neutron spectra measured with liquid scintillator detectors (the high energy component) and Bonner spheres (the low energy component)

[6] H. Nakashima et al. Nucl. Sci. Eng. **124** (1996) and N. Nakao et al. Nucl. Sci. Eng. **124** (1996) 228

The TIARA exp.: FLUKA vs exp. data (concrete on axis)

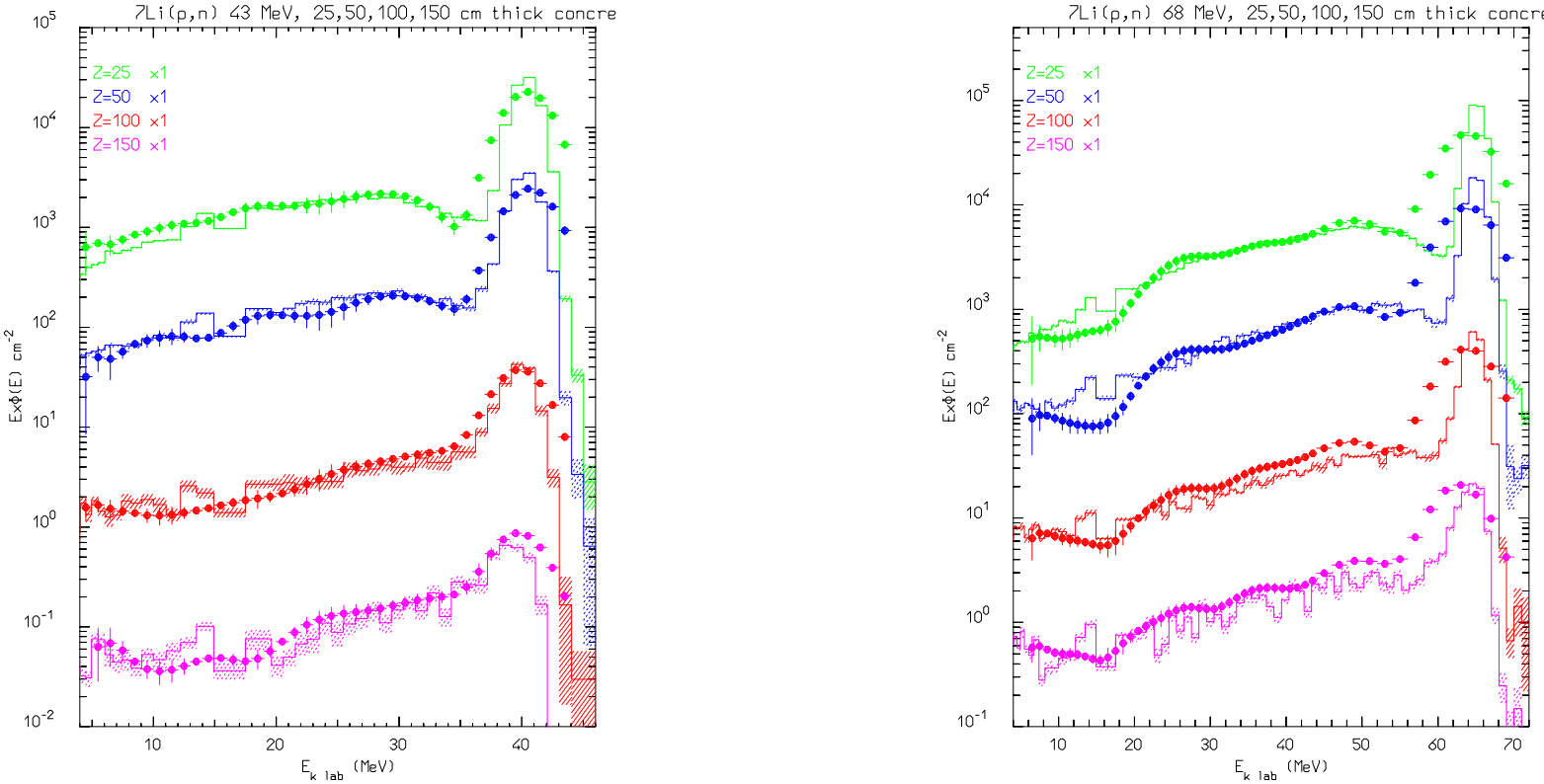

Comparison of simulated (dashed histogram) and measured (symbols) neutron spectra after different concrete thicknesses (from 25 to 150 cm), on axis. The neutrons are generated by ^{7}Li(p,n) at 43 (left) and 68 MeV (right)

The TIARA exp.: FLUKA vs exp. data (iron on axis)

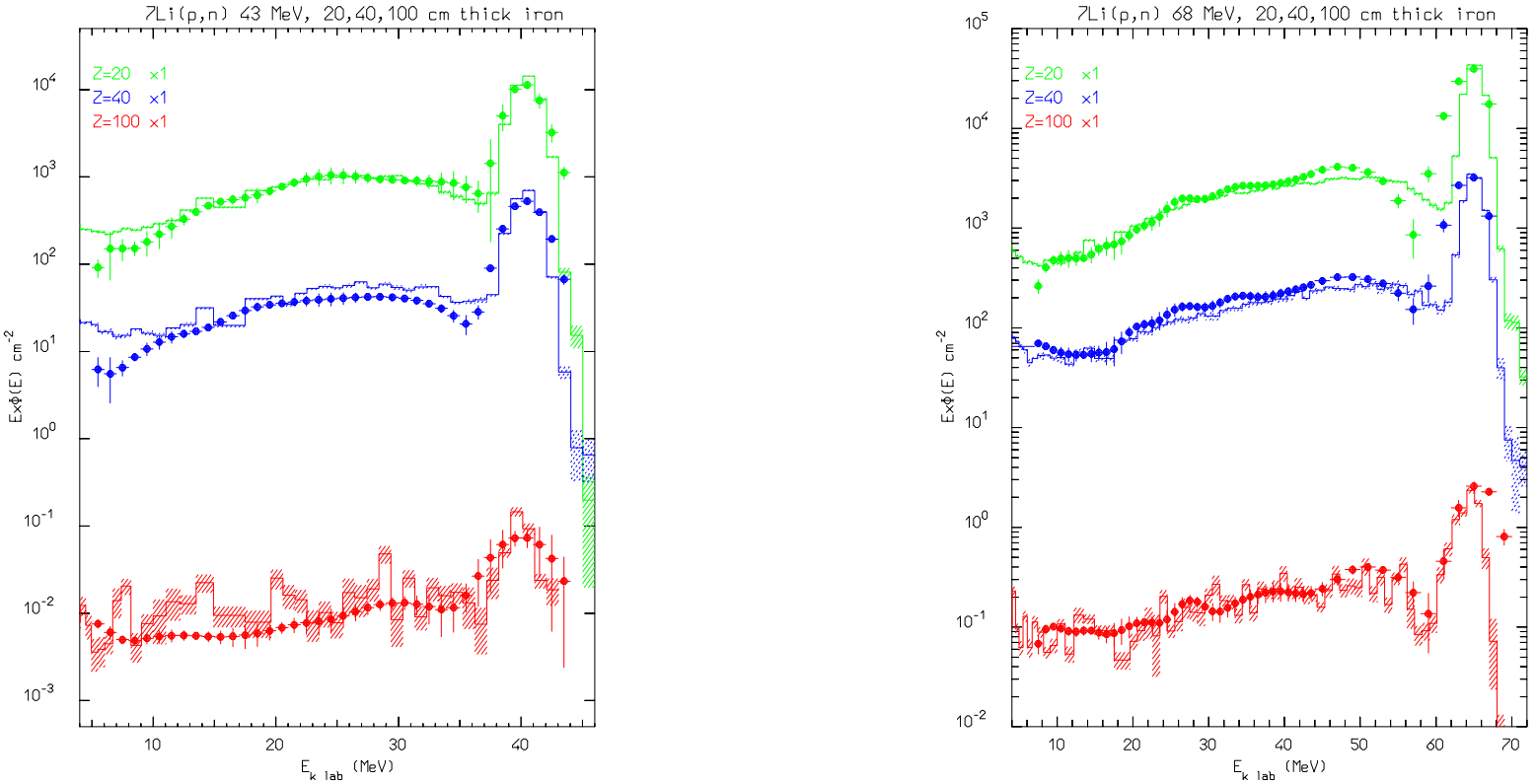

Comparison of simulated (dashed histogram) and measured (symbols) neutron spectra after different iron thicknesses (from 20 to 100 cm), on axis. The neutrons are generated by ^{7}Li(p,n) at 43 (left) and 68 MeV (right)

The TIARA exp.: FLUKA vs exp. data (concrete off axis)

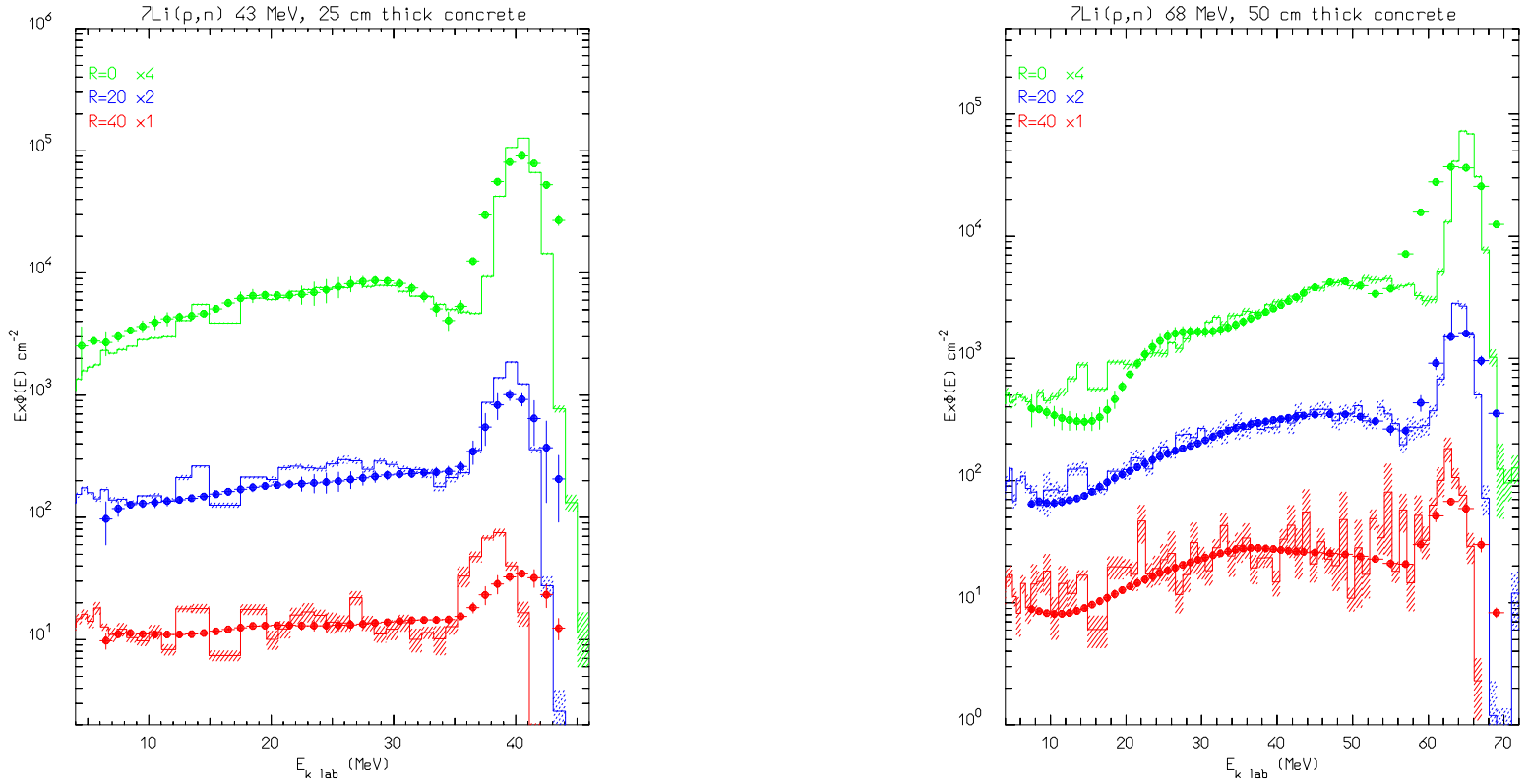

Comparison of simulated (dashed histogram) and measured (symbols) neutron spectra off axis (from 0 to 40 cm) after 25 (left) and 50 cm thick concrete shields. The neutrons are generated by ^{7}Li(p,n) at 43 (left) and 68 MeV (right)

The TIARA exp.: FLUKA vs exp. data (iron off axis)

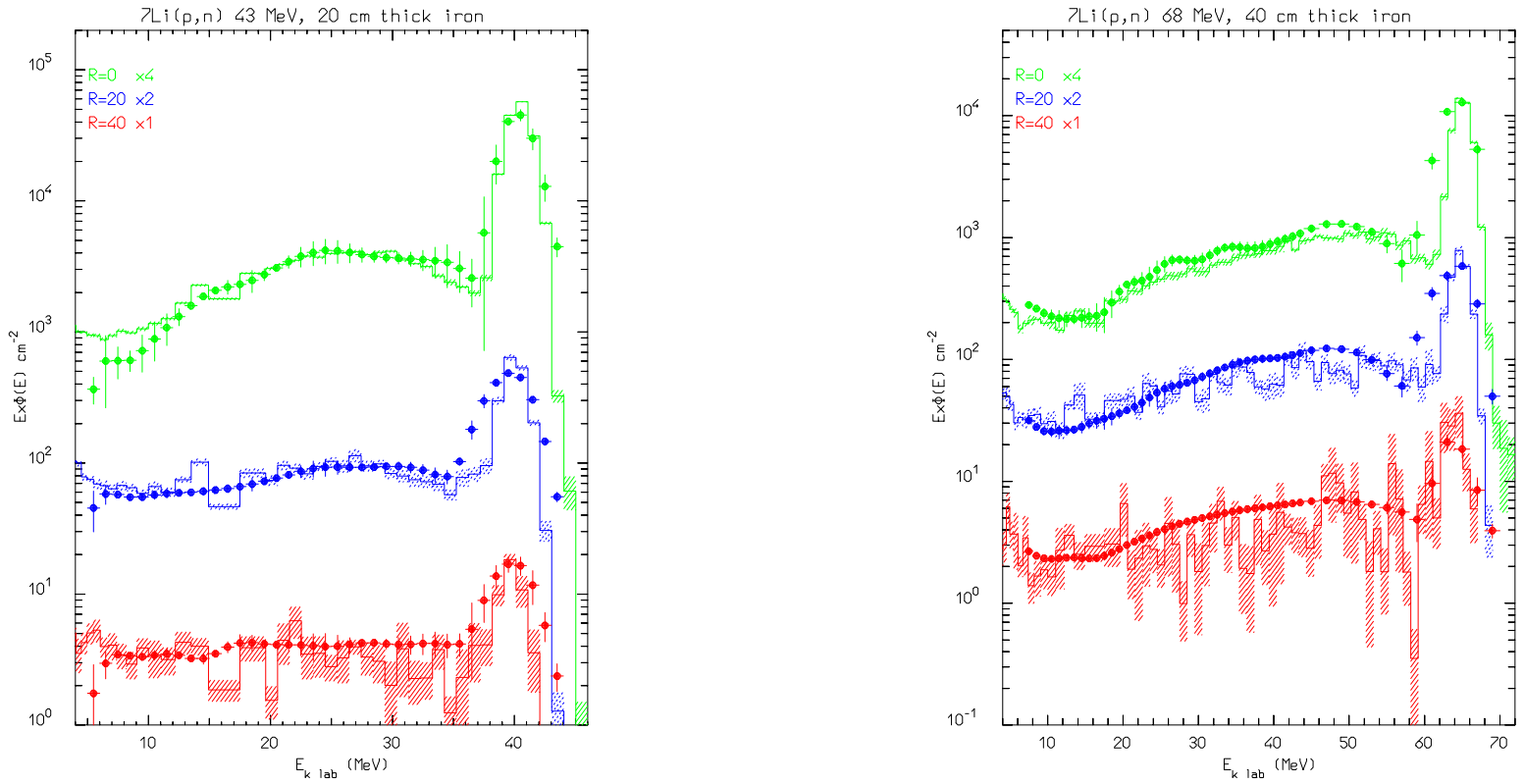

Comparison of simulated (dashed histogram) and measured (symbols) neutron spectra off axis (from 0 to 40 cm) after 20 (left) and 40 cm thick iron shields. The neutrons are generated by ^{7}Li(p,n) at 43 (left) and 68 MeV (right)

The CERN reference radiation facility – CERF

- A reference radiation facility (called CERF) for the calibration and intercomparison of dosimetric devices in high energy stray radiation fields is available at CERN since 1993, on the H6 beam line in the North Area.
- Hadron beams with momentum of either 120 or 205 GeV/c are stopped in a copper target, which can be installed in two different positions. On top and on side of these two positions, the secondary particles produced in the target are filtered by a shielding made up of either concrete or iron.
- The facility is partially supported by the European Commission in the framework of a research program for the assessment of radiation exposure at civil flight altitudes.
- The composition of the CERF field is accurately known by means both of FLUKA calculations and measurements with several instruments which nicely agree each other. Some examples of comparisons of computed vs measured data are presented in the following.

Neutron detector calibration

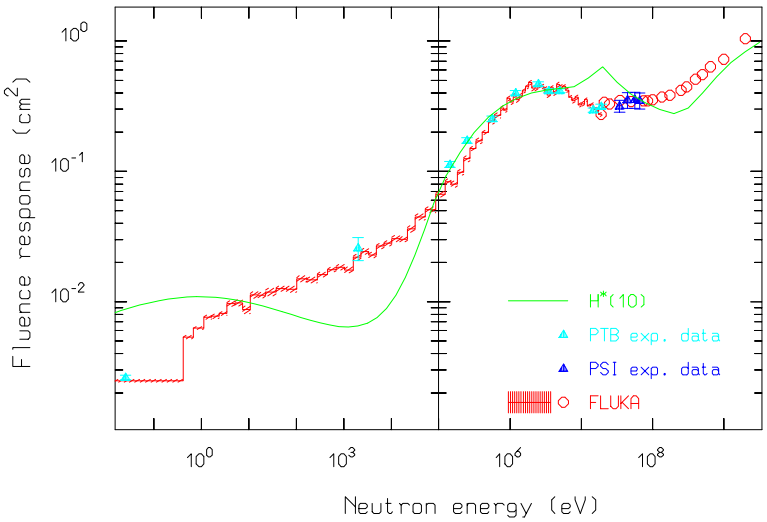

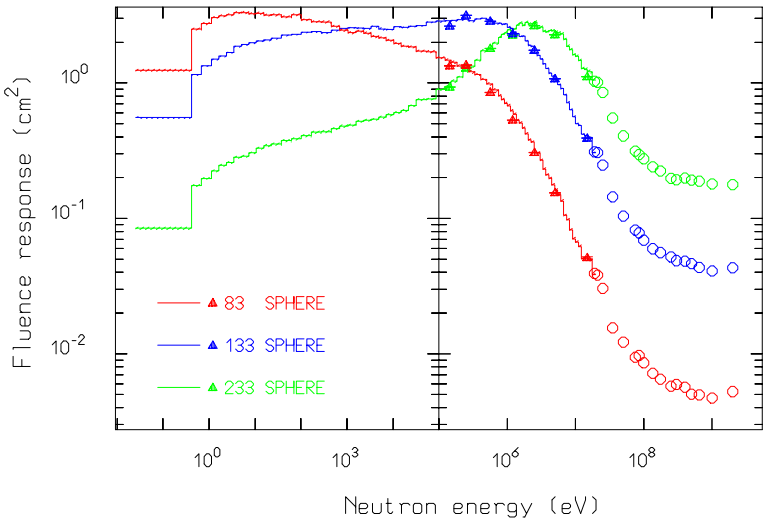

Calibration of the LINUS rem counter (left) and of three Bonner spheres (right) with monoenergetic neutron beams at PTB–Braunschweig and with semi–monoergetic neutron beams at PSI (full symbols), compared with simulations (dashed histos and open circles)

CERF: layout

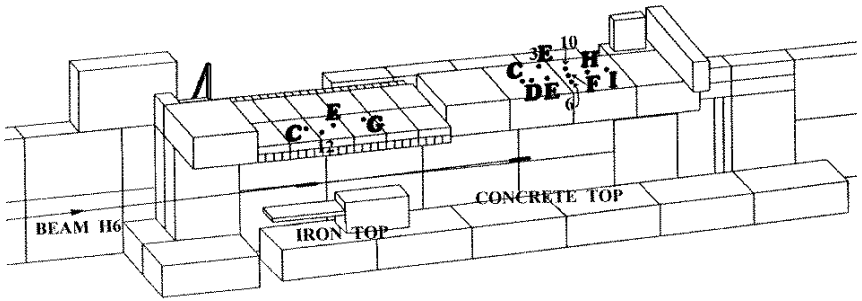

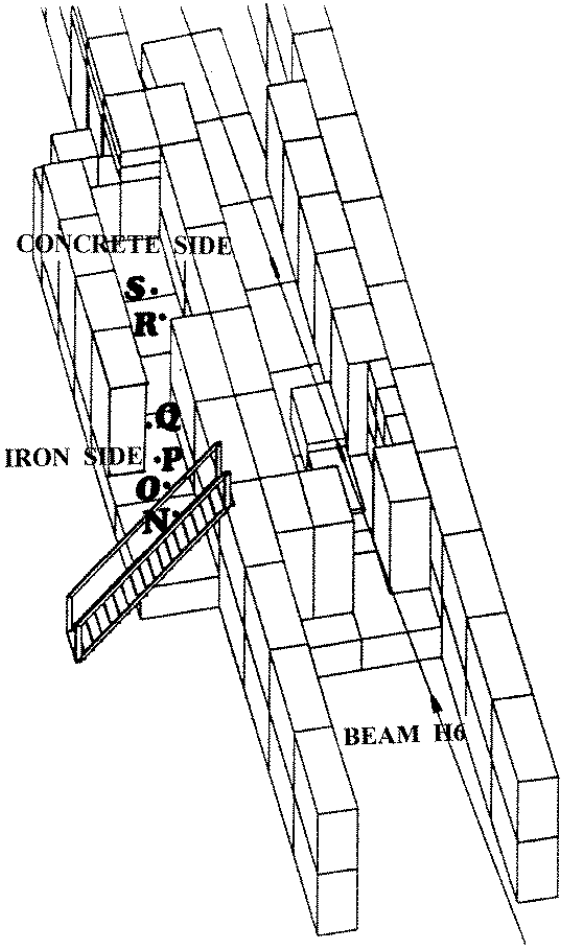

Top (left, one side removed) and side (right, roof removed) views of the CERF facility with the measuring positions.

CERF: some results

	experimental		FLUKA		experimental		FLUKA	
	cts/PIC	%	cts/PIC	%	cts/PIC	%	cts/PIC	%
	CONCRETE TOP "E"				IRON TOP "C"			
LINUS rem counter*	0.364	0.36	0.409	2.2	1.78	0.30	1.68	2.1
SNOOPY rem counter*	0.200	0.59	0.207	3.3	1.83	0.75	1.71	2.0
233 sphere	0.788	0.33	0.899	3.7	9.28	0.28	9.23	2.0
178 sphere	0.989	0.36	1.01	3.4	16.1	0.24	16.9	1.9
133 sphere	1.02	0.30	0.981	3.2	19.2	0.19	21.2	1.9
108 sphere	0.942	0.35	0.883	3.1	17.7	0.20	19.2	1.9
83 sphere	0.704	0.30	0.717	3.1	11.2	0.26	12.1	1.9

Comparison between the FLUKA predictions and the experimental response of the various detectors in stray radiation fields at CERN [7]. The percent statistical uncertainty (%) is indicated.

[7] C.Birattari et al., Rad.Prot.Dos.**76** (1998) 135

From atmospheric neutrinos to aircrew doses

Ultimate goal: exploit the FLUKA interaction models to compute atmospheric neutrino fluxes for ICARUS with unprecedented accuracy within a full 3D calculation

- Primary cosmic ray spectra and interplanetary modulation according to measured solar activity on a day-to-day basis have been implemented
- Geomagnetic effects implemented with full multipole expansion of the field or with a simplified offset dipole model (much faster...)
- Extensive benchmarking against available experimental muon and hadron

A natural byproduct: a powerful tool for computing radiation fluxes in the earth (and Mars...) atmosphere as well as for spacecrafts or satellites

The code is now used in several labs (Frascati, Siegen, Bartol, Houston, GSF...) for simulating the radiation fields generated by cosmic rays in the atmosphere and/or inside spacecrafts.

Hadron/muon fluxes in the atmosphere: examples

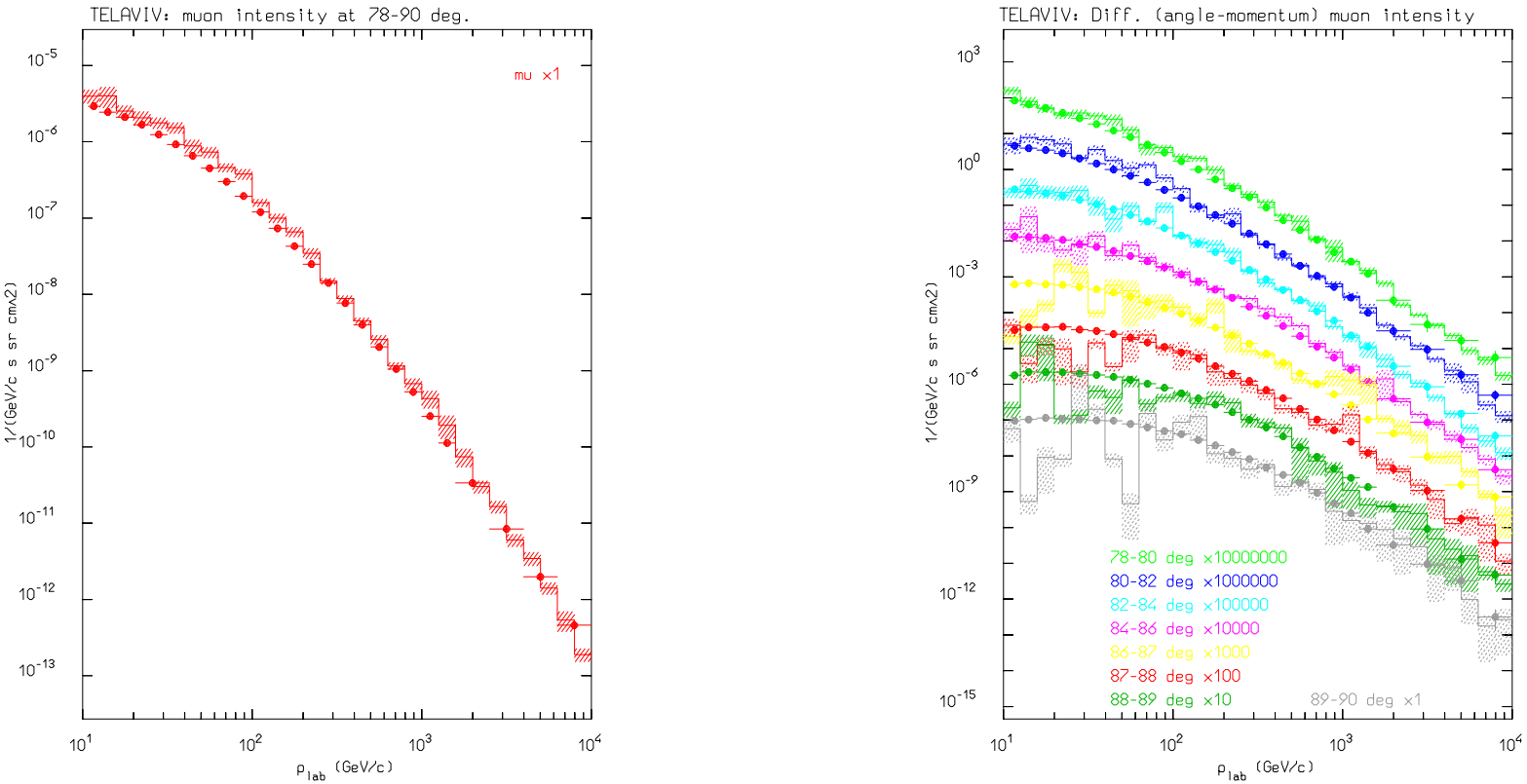

Angle integrated (78-90 deg, left) and double differential muon fluxes, measured close to the horizontal in Tel Aviv. Data from O.C. Allkofer et al. NPB 259, 1, (1985).

Hadron/muon fluxes in the atmosphere: examples II

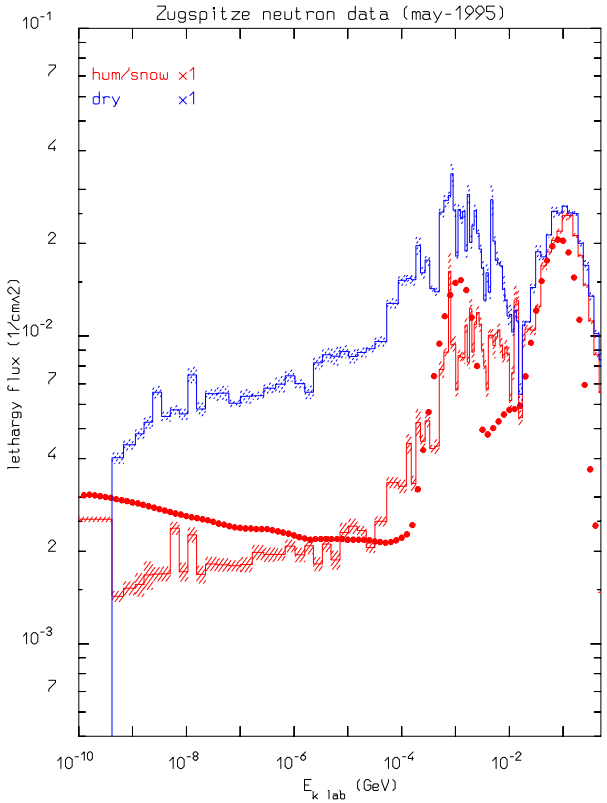

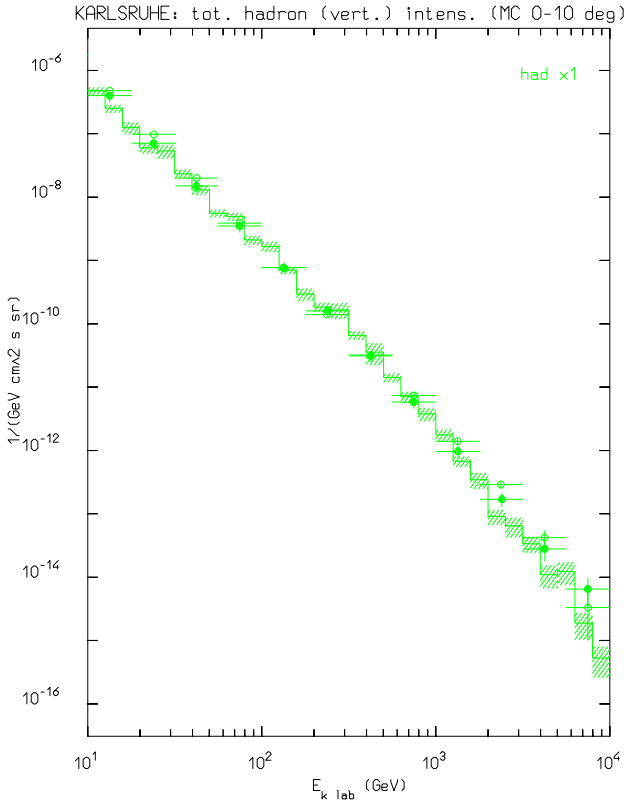

Neutron flux at top of the Zugspitze (left) for dry and wet conditions, and hadron flux (right) measured with the KASKADE experiment. Data from and from H.H Mielke et al. JPG 20, 637 (1994), H. Kornmayer et al, JPG 21, 439 (1995).

Hadron/muon fluxes in the atmosphere: examples III

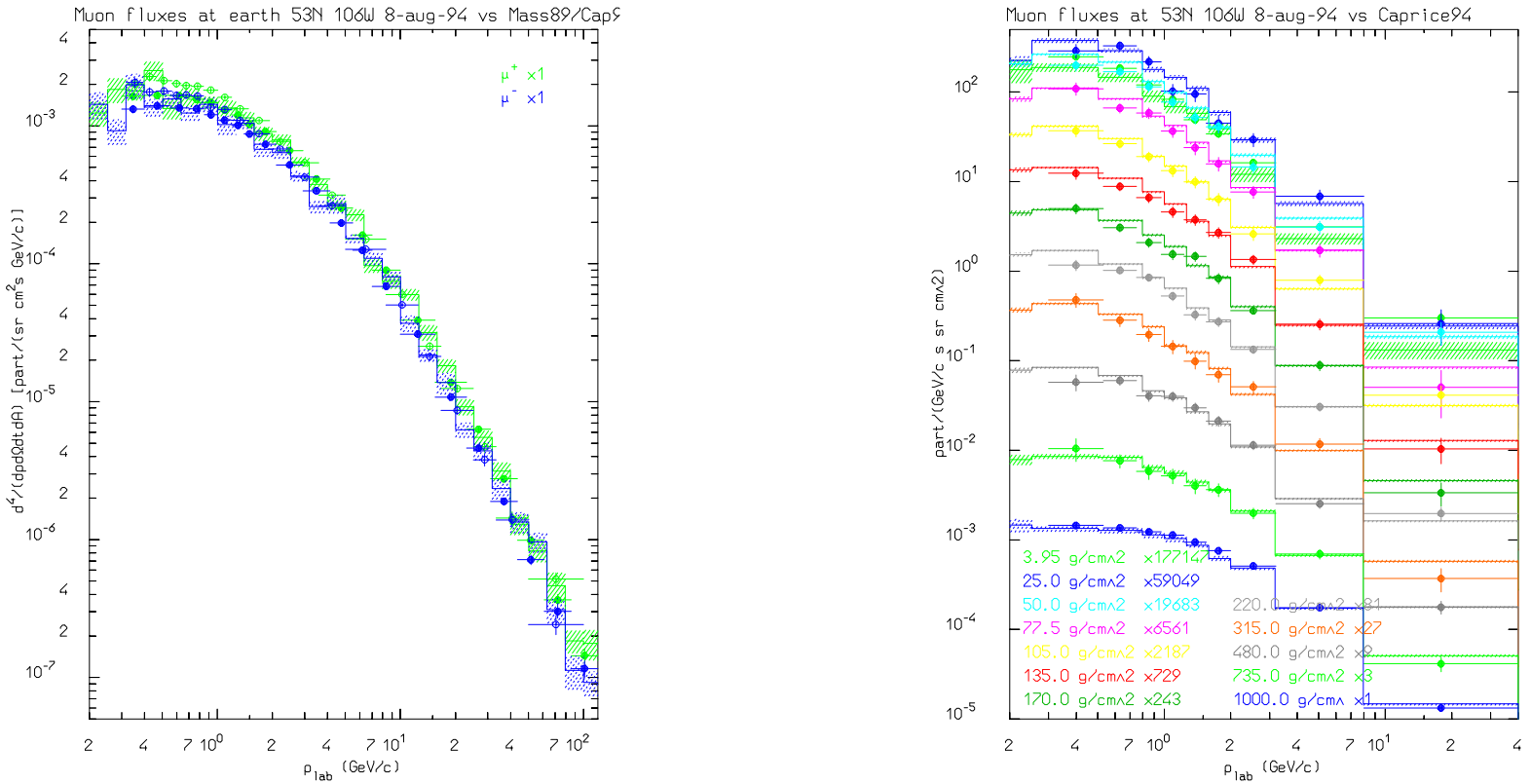

Muon fluxes at ground level (left) at 53N 106W on 8-aug-94 compared with data from Mass89 (open symbols, 1989) and from Caprice94 (full symbols). Muon fluxes at various atmospheric depths (right) on 9-aug-94, compared with Caprice94 measurements.

Hadron/muon fluxes in the atmosphere: examples IV

Poly radius (cm)	Altitude					
	0 m		4880 m		11280 m	
	EXP ($s^{-1} \pm \%$)	FLUKA ($s^{-1} \pm \%$)	EXP ($s^{-1} \pm \%$)	FLUKA ($s^{-1} \pm \%$)	EXP ($s^{-1} \pm \%$)	FLUKA ($s^{-1} \pm \%$)
0	$2.40 \cdot 10^{-2} \pm 12$	$4.15 \cdot 10^{-2} \pm 5$	0.43 ± 9	0.181 ± 1	2.61 ± 6	0.976 ± 1
4.1	$2.30 \cdot 10^{-2} \pm 12$	$2.74 \cdot 10^{-2} \pm 4$	0.570 ± 4	0.585 ± 1	3.31 ± 4	3.09 ± 1
5.6	$2.90 \cdot 10^{-2} \pm 11$	$3.27 \cdot 10^{-2} \pm 3$	0.753 ± 7	0.949 ± 1	4.5 ± 4	4.99 ± 1
7.6	$3.53 \cdot 10^{-2} \pm 10$	$3.51 \cdot 10^{-2} \pm 3$	0.860 ± 6	1.06 ± 1	5.01 ± 3	5.55 ± 1
11.6	$2.03 \cdot 10^{-2} \pm 13$	$2.71 \cdot 10^{-2} \pm 3$	0.620 ± 7	0.708 ± 1	3.35 ± 4	3.67 ± 1
22.6	$8.14 \cdot 10^{-3} \pm 13$	$1.20 \cdot 10^{-2} \pm 3$	0.177 ± 10	0.215 ± 1	1.09 ± 7	1.13 ± 1

Altitude variation of multi-sphere neutron spectrometer rates above the Narita airport (1985): comparison between experimental [8] and FLUKA results.

[8] T. Nakamura et al., Health Phys. **53** 509 (1987)

Hadron/muon fluxes in the atmosphere: examples IVbis

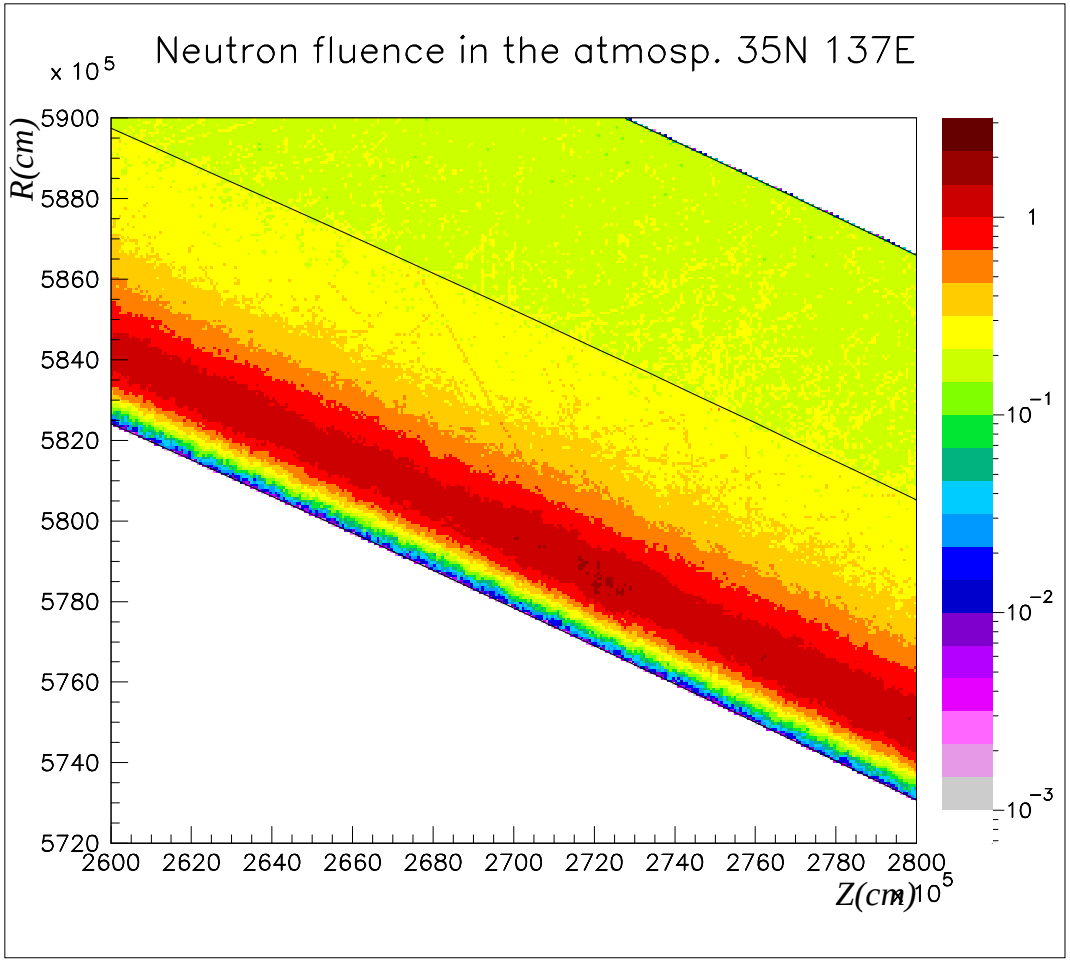

Hadron/muon fluxes in the atmosphere: examples IVtris

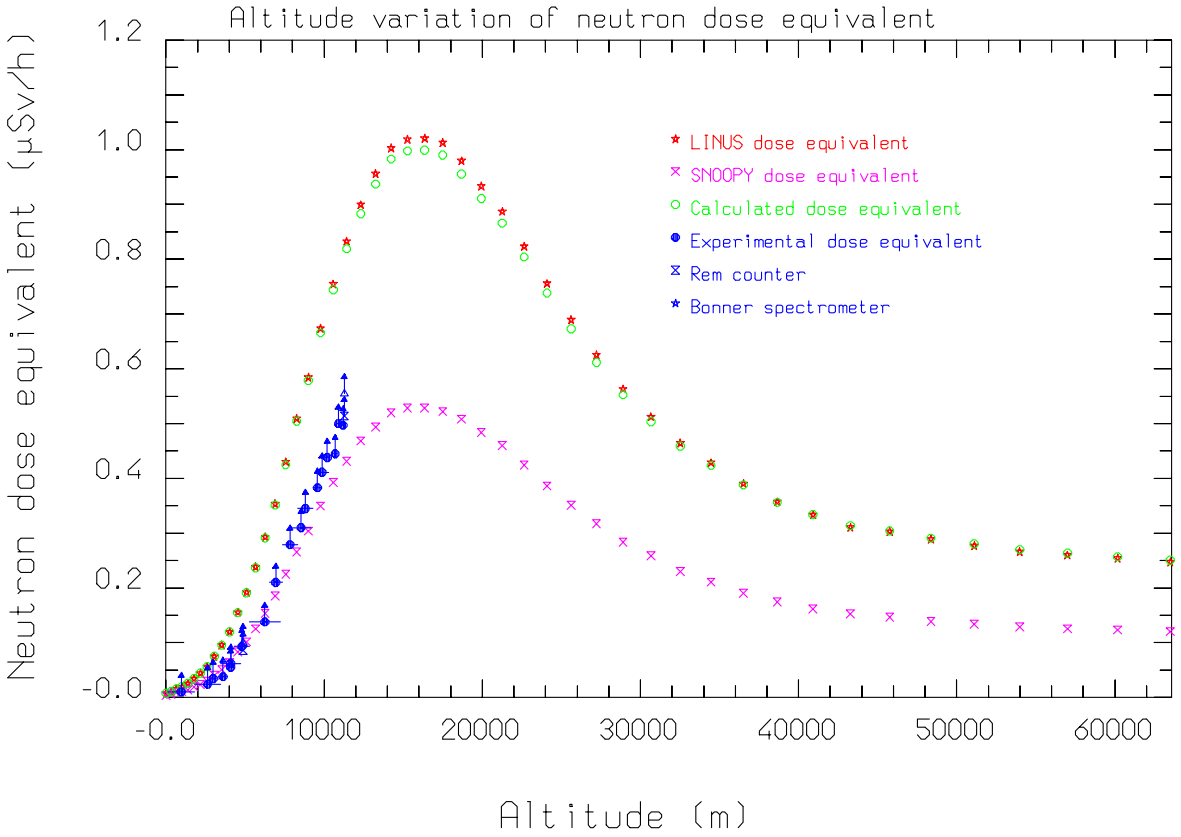

Variation with altitude of neutron dose equivalent above the Narita airport (1985). Experimental results (blue symbols) obtained with a commercial Rem Counter and the Bonner spectrometer are compared with FLUKA calculations for the overall neutron dose equivalent (green symbols) and for the response of a standard rem counter ("SNOOPY", purple) and an extended range one ("LINUS", red).

Doses to commercial flight crews (M.Pelliccioni et al, work in progress)

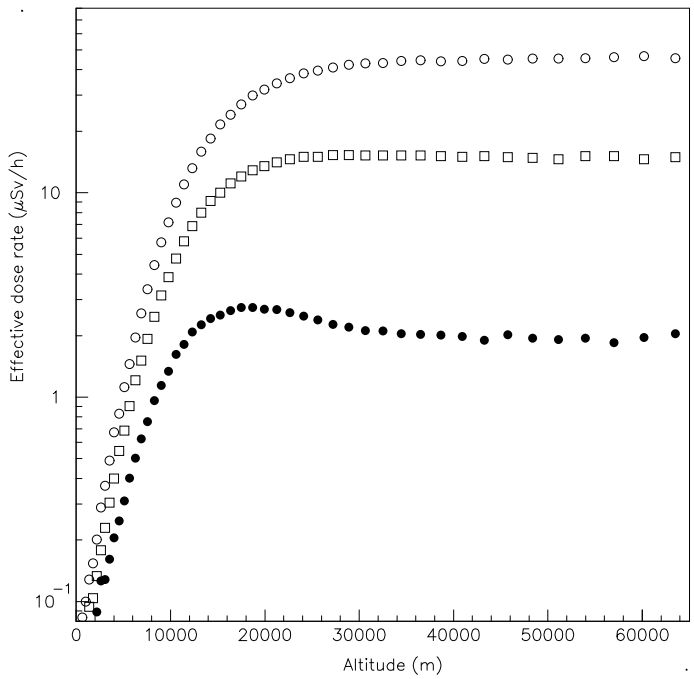

Calculated effective dose as a function of altitude for a vertical rigidity cutoff of 0.4 GV at solar minimum (open circles), and at solar maximum (open squares), and for a cutoff of 17.6 GV (black circles)

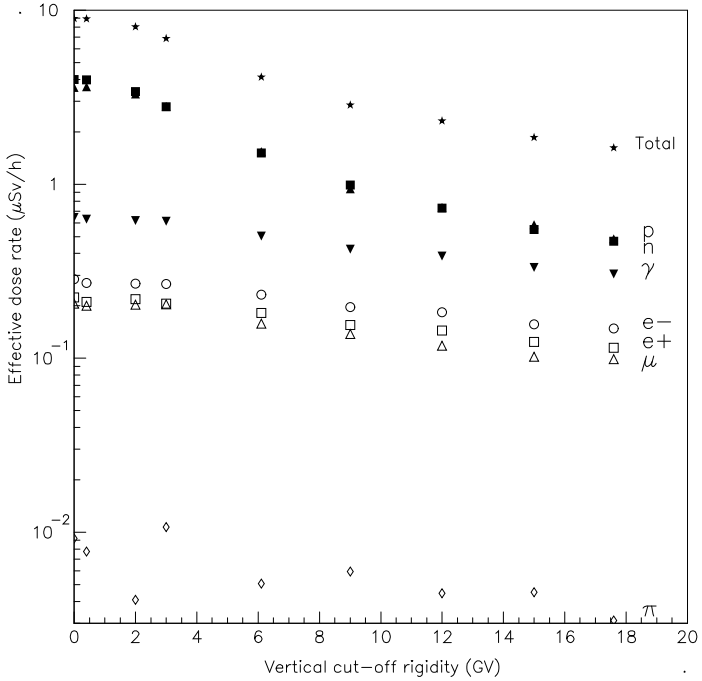

Contributions of various radiation components to the effective dose rate as a function of the vertical cut-off rigidity at solar minimum, and for an altitude of 10580 m

GCR radiation fields on the Mars surface: a first attempt

A simple model of the Mars atmosphere has been setup ($\approx 10\ g/cm^2$ of CO_2), with a terrestrial rock composition for the Mars surface (*to be improved in future calculations*)

Individual energy losses have been weighted with proper factors depending on the LET, according to the most recent recommendations for quality factors issued in ICRP60, with the same procedure used in [9] when computing fluence to dose equivalent conversion data and effective quality factors for high energy neutrons.

A 30 cm thick water layer has been used as scoring phantom. For obvious statistical reasons it had to be quite large, therefore introducing a bias in the low energy neutron spectrum. Future calculations will be done in two stages

- computing the radiation environment on the Mars surface,
- simulating on a local scale a suitable phantom into such an environment.

[9] A. Ferrari, and M. Pelliccioni, Radiat. Prot. Dos. **76**, 215 (1998)

GCR radiation fields on the Mars surface: a first attempt II

Absorbed Dose and Dose Equivalent on Mars Surface

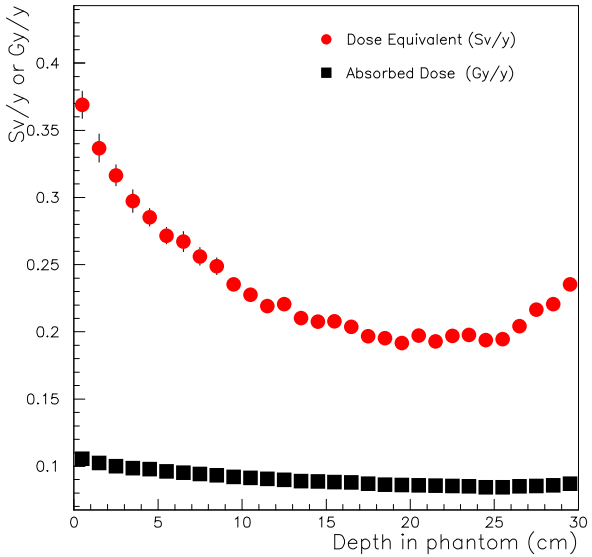

Particle Fluences in Mars Atmosphere

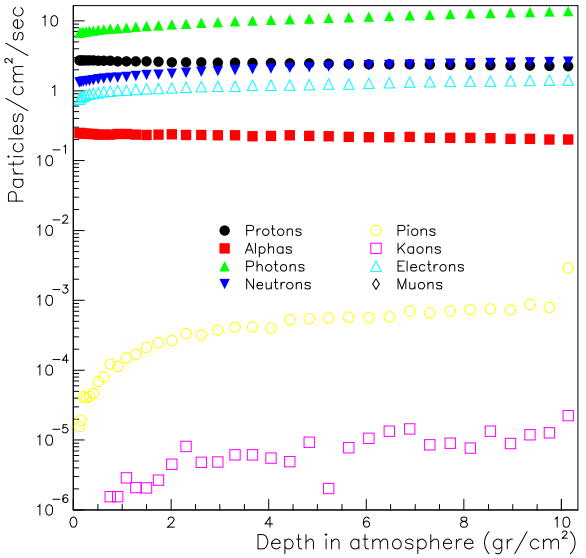

Computed Dose and Dose equivalent rates at Mars surface

Particle fluences as a function of depth in the Mars atmosphere

GCR radiation fields on the Mars surface: a first attempt III

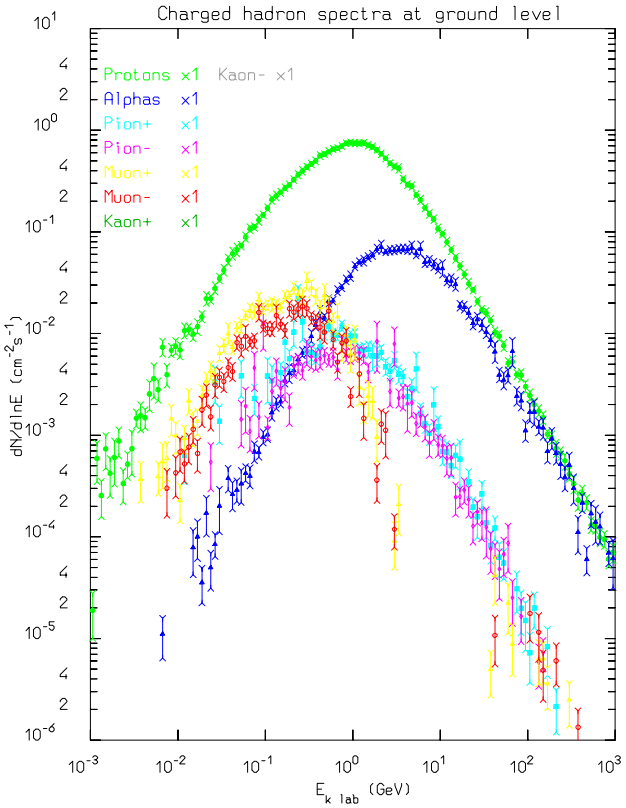

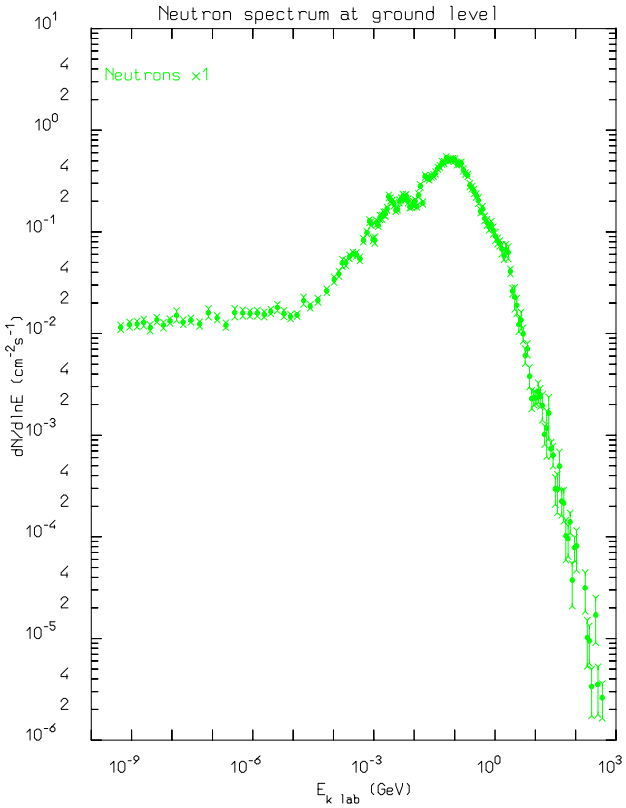

Hadron/muon (left) and neutron (right) spectra at ground level

GCR radiation fields on the Mars surface: a first attempt IV

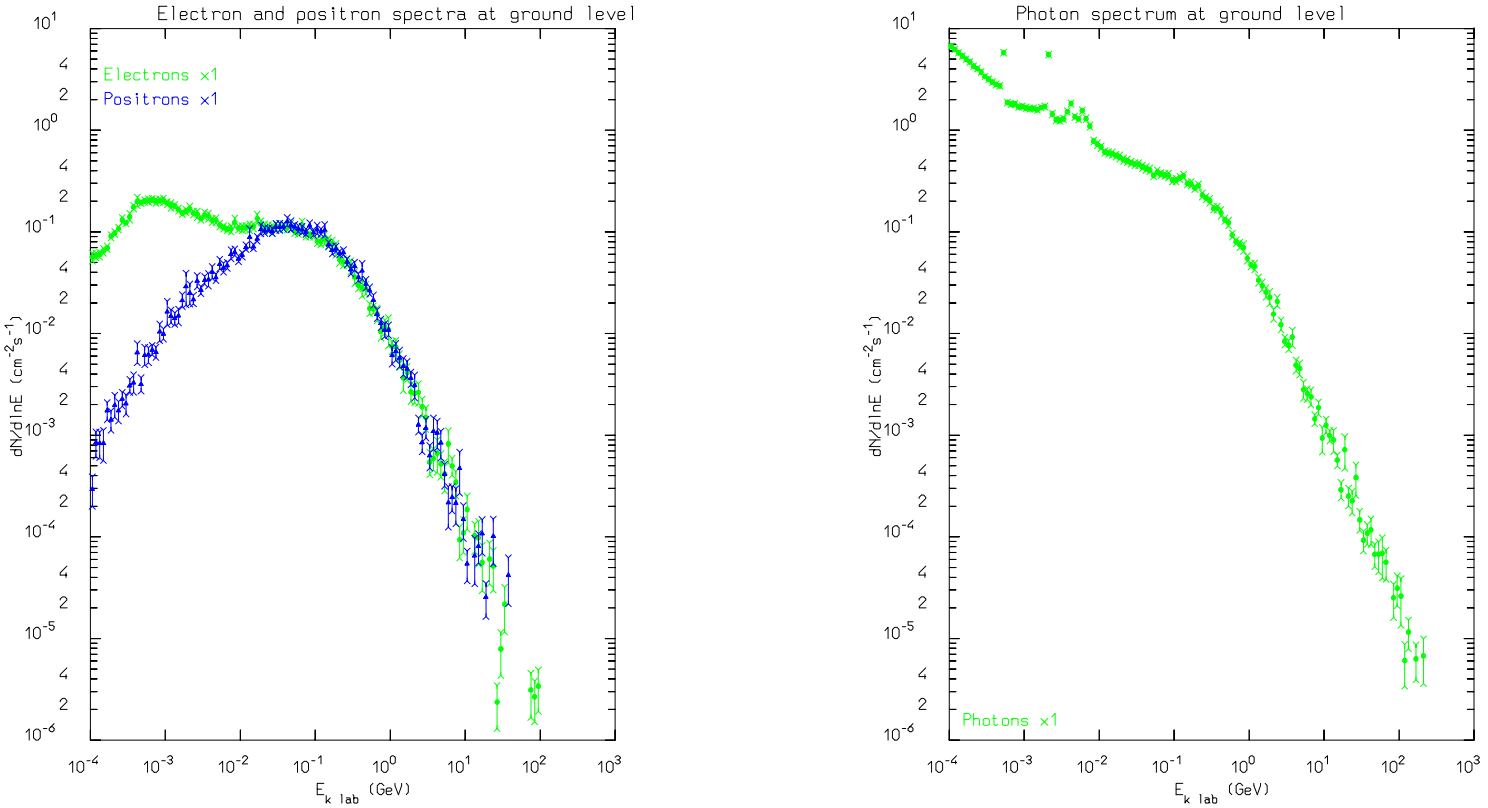

Electron/positron (left) and photon (right) spectra at ground level

The background in the ATLAS hall

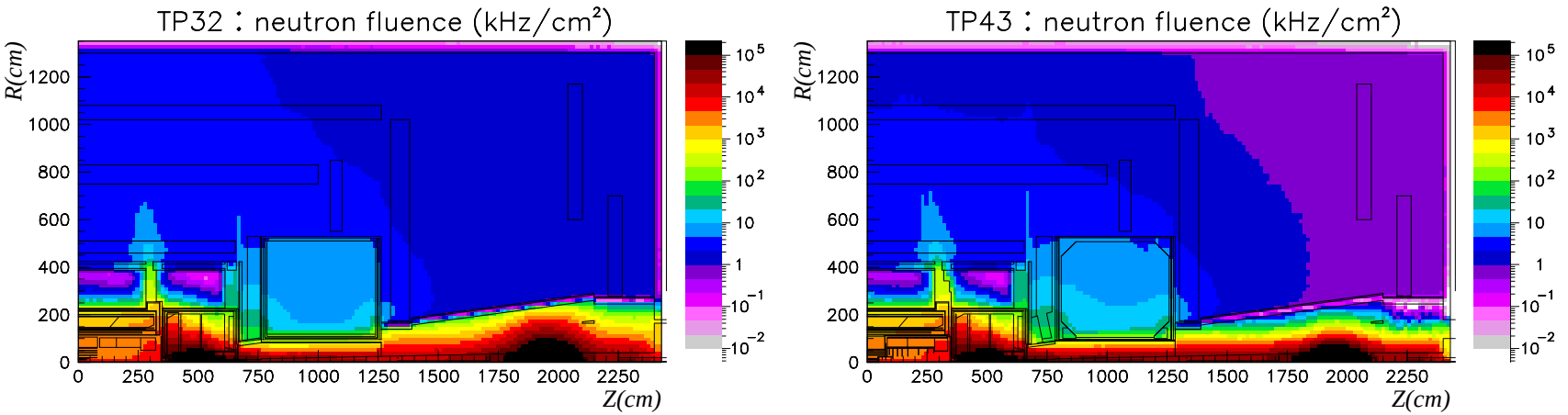

Computed neutron background in the ATLAS experiment at LHC for two different shielding configurations, one with the "shielding cone" made out of high density "pure" iron (left) and the other with a lower density, carbon rich (5% by weight) iron (right)

The background in the ATLAS hall II

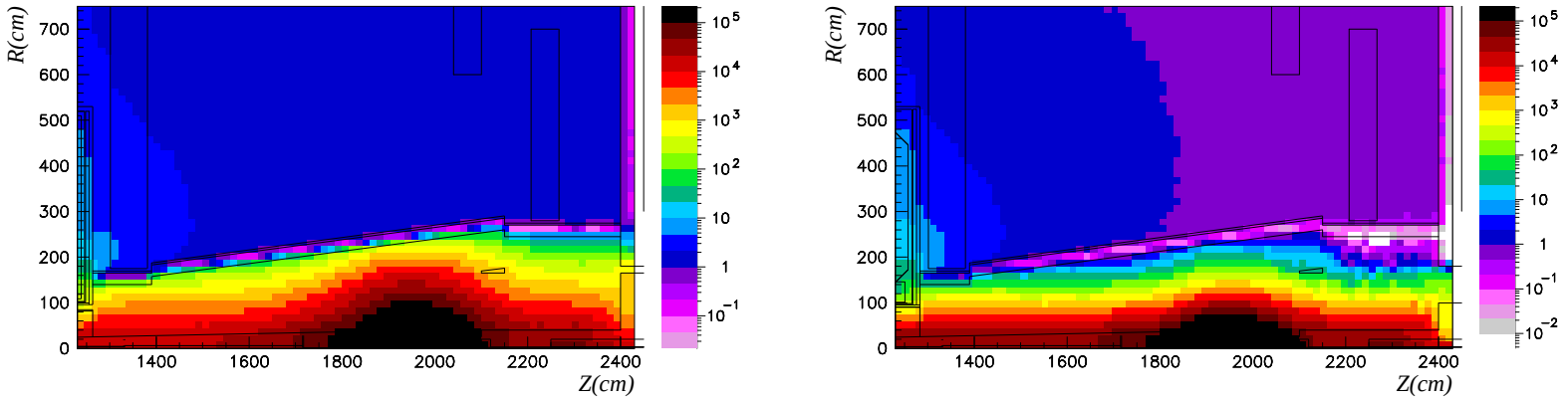

A magnification of the "shielding cone" area showing the different effectiveness of the two "iron" shielding

Shielding in the ATLAS hall

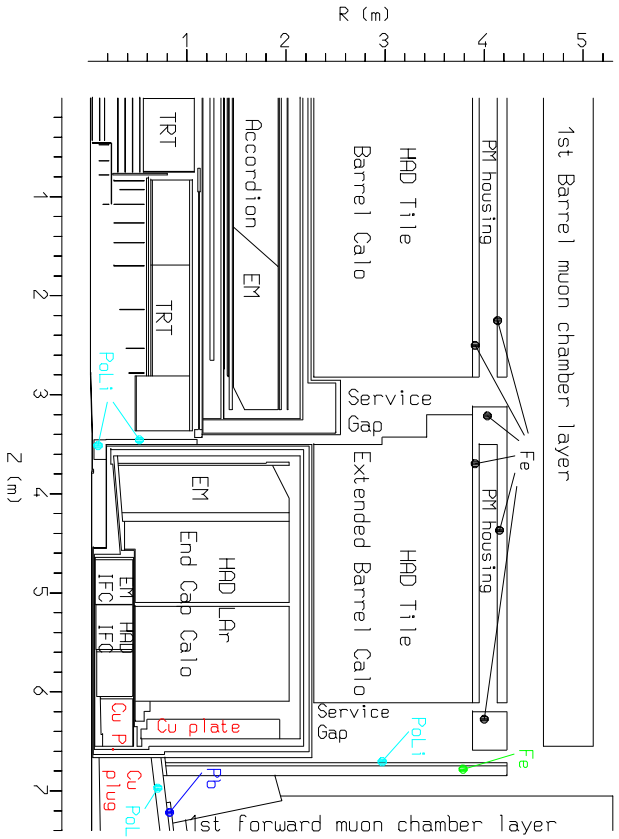

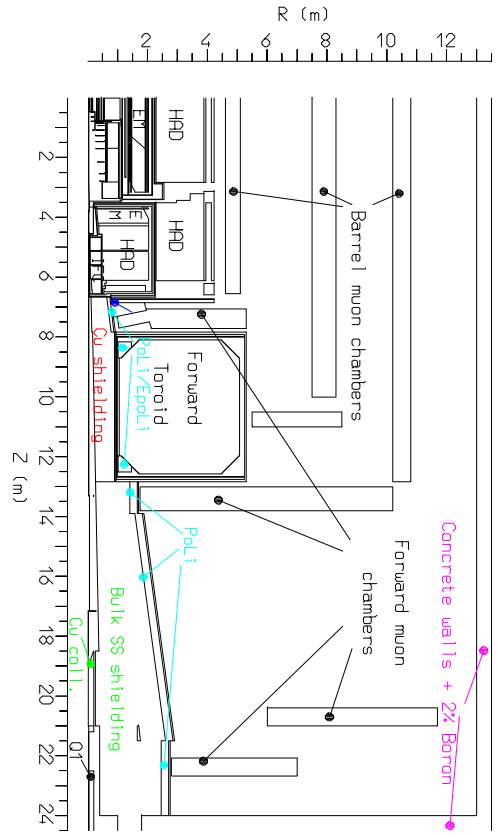

Heavy ions

Heavy ion transport and interactions are presently under development in FLUKA:

- Ionization energy losses already implemented
  - Up-to-date effective charge parametrizations
  - Energy loss straggling according to:
    - "normal" first Born approximation
    - Charge exchange effects (dominant at low energies, ad-hoc model developed for FLUKA)
    - Mott cross section and nuclear form factors (high energies)(in progress)
- Multiple scattering already implemented
- High energy A-A interactions ($E > 5 - 10\ GeV/u$): interface to DPMJET *coming soon*
- Low energy A-A interactions: extension of the PEANUT model *almost ready for tests with $\alpha's$*

  The availability of exp. data on particle production in A-A collisions in the intermediate energy range will be a crucial issue in the next future

dE/dx and straggling of heavy ions

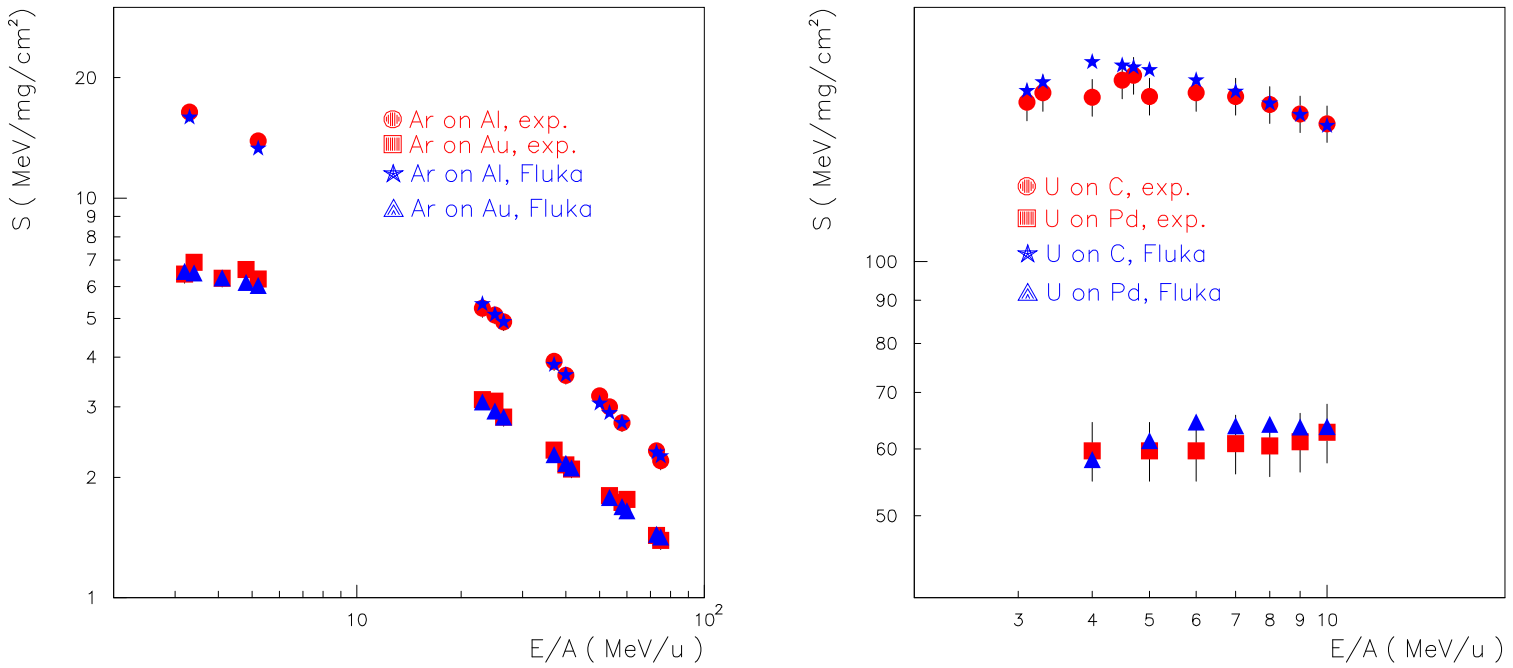

Comparison of experimental (R.Bimbot, NIM**B69** (1992) 1) (red) and FLUKA (blue) stopping powers of Argon and Uranium ions in different materials and at different energies.

dE/dx and straggling of heavy ions

Projectile	Target	thickness (mg/cm^2)	FWHM (keV) Exp		FLUKA
^{12}C	Al	0.217	74.5	±3	90
^{16}O	Al	0.110	92	±2	94
^{16}O	Al	0.246	147	±3	144
^{16}O	Al	0.457	202	±2	198
^{32}S	Al	0.315	290	±30	356
^{32}S	Al	0.990	521	±20	638
^{32}S	Au	0.053	98	±20	140
^{32}S	Au	3.492	820	±20	1092
^{127}I	Al	0.321	780	±40	735
^{127}I	Al	0.530	1000	±35	949
^{127}I	Al	0.990	1375	±50	1297
^{127}I	Au	0.053	250	±10	275
^{127}I	Au	1.186	1200	±50	1255
^{127}I	Au	3.800	2250	±90	1932

Measured (S. Ouichaoui et al. NIM B164-165 (2000) 259) and computed (FLUKA) straggling for 2 MeV/amu ^{12}C,^{16}O , ^{32}S ions and 1.467 MeV/amu ^{127}I ions

DPMJET

Authors: **R. Engel[†], J. Ranft[*], and S. Roesler[&]**
[†] Bartol, [*] Siegen University, [&] SLAC

Nucleus-Nucleus interaction code [10] *for collisions from ≈5-10 GeV/n till the highest cosmic ray energies* ($10^{18} - 10^{20}$ *eV*)

Applications of DPMJET

- Predictions for heavy ion experiments at present and future accelerators (i.e. ALICE at LHC)
- Simulations of Cosmic Ray cascades in the HEMAS-DPM code used by the MACRO Collaboration
- Simulations of Cosmic Ray cascades in the CORSIKA code (Karlsruhe)

[10] PRD 51 (1995) 64; Gran Sasso INFN/AE-97/45 (1997); hep-ph/9911232; hep-ph/9911213; hep-ph/0002137

DPMJET: examples of performances

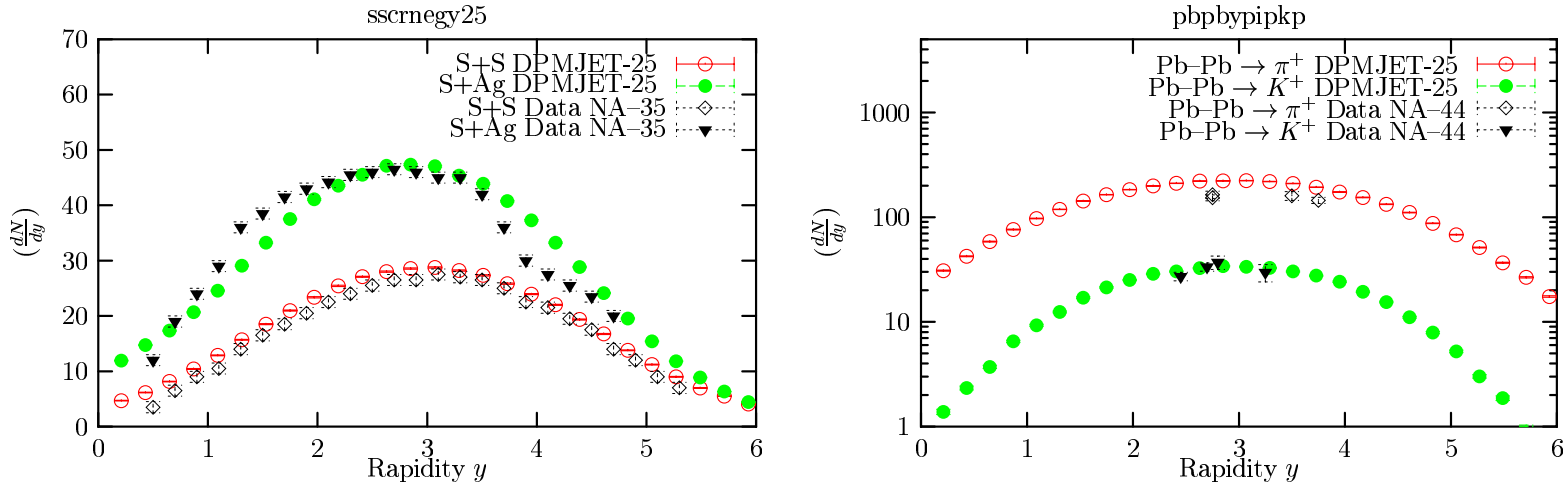

Rapidity distribution of negative particles for 158 AGeV/c S-S and S-Ag collisions (left) and of positive pions and kaons for 158 AGeV/c Pb-Pb collisions (right). Experimental data from the NA-35 and NA-44 collaborations are compared with DPMJET predictions.

Conclusions

- The physical models embedded in FLUKA have proven to be enough advanced to provide reliable estimates of particle production and propagation in a wide range of energies and problems
- The code has been already successufully used for a variety of problems related to cosmic ray propagation and interactions in the atmosphere
- Space radiation applications will benefit from the robust physics modelling and of course from the almost unlimited capabilities in geometrical description, magnetic field transport and biasing of the code
- The development of capabilities for A-A interactions comparable to those for h-A is now under progress